Politecnico di Torino

Master's Degree in Energy and Nuclear Engineering

Designing a Weather-Resilient European Energy System Considering Dunkelflaute Events

Identifying Dunkelflaute Events and Representing Them in Robust System Design

Supervisor:
Andrea Lanzini

Candidate:
Giovanni Martini

Co-Supervisor:
Antonio De Padova

External Supervisors:
Xiaoming Kan
Kamran Forghani

October 2025

Abstract

The growing deployment of wind and solar power in Europe makes electricity supply increasingly dependent on weather conditions. Ensuring security of supply during prolonged periods of low wind and solar generation, known as Dunkelflaute events, remains a key challenge. This thesis develops a detection framework to identify such events. The framework combines wind and solar capacity factors, weighted by installed capacity, and applies a variable mean-below-threshold algorithm to detect consecutive periods with weighted capacity factors below a given threshold. Multiple thresholds are used to capture both short, severe events and longer, moderate ones. Applying the detection framework to 40 years of historical weather data shows that Dunkelflaute events occur every year, though their severity and timing vary across regions and years. Wind-dominant countries, such as those in the Nordic region, show greater year-to-year variability in Dunkelflaute severity, whereas inland continental regions with poor wind conditions are more stable. A cumulative energy deficit metric with a 30% mean capacity factor threshold proved most effective for identifying Dunkelflaute events. Spatial aggregation smooths out their impacts, resulting in lower deficits at weather-zone or pan-European scales compared to the country level. For Europe as a whole, the most severe Dunkelflaute year occurred in the winter of 1996-97. Given the heterogeneous occurrence of Dunkelflaute events, we represent them at the country level, weather-zone level, using hierarchical clustering to group countries, and pan-European level within a stochastic optimization model for European renewable electricity system design. Results show that incorporating the worst Dunkelflaute years as stochastic scenarios at the weather-zone or country level provides an effective trade-off between robustness, cost, and computational efficiency. In such cases, loss of load is almost completely eliminated compared to a benchmark case based on a typical weather year, with only a 5% increase in total system cost. Considering Dunkelflaute events also influences investment decisions: solar PV capacity decreases in most cases, while wind power investments remain relatively stable. Furthermore, nuclear power emerges as the preferred backup technology under transmission-constrained scenarios, whereas neither nuclear nor hydrogen turbines are deployed when unconstrained geographical balancing through trade is allowed.

Keywords: Energy system modeling, European energy system, Dunkelflaute, Renewable energy, Weather variability, Stochastic optimization, Robust energy system design, Clustering, Capacity expansion

Contents

List of Acronyms

Below is the list of acronyms that have been used throughout this thesis, listed in alphabetical order:

CBT	Constantly Below Threshold
CFD	Capacity Factor Deficit
FMBT	Fixed-duration Mean-Below-Threshold
PSH	Pumped Storage Hydropower
PV	Photovoltaic
RES	Renewable-based Energy Sources
TC	Total Cost
VMBT	Variable-duration Mean-Below-Threshold
VRE	Variable Renewable Energy

List of Figures

List of Tables

1
Introduction

The transition toward a decarbonized energy system is one of the most pressing and politically significant global challenges of the 21st century. In response to the escalating climate crisis, countries around the world have set legally binding targets to reduce greenhouse gas emissions, with many aiming for net-zero emissions by mid-century. The energy sector plays a central role in this transition, prompting governments to adopt ambitious policies for phasing out fossil fuels and accelerating the deployment of renewable energy sources. Wind and solar photovoltaic (PV) technologies have emerged as the cornerstones of this transformation, driven by rapid cost reductions, favorable regulatory frameworks, and their modular scalability. Unlike dispatchable power plants, wind and solar power are variable renewable energy (VRE) sources whose output is directly influenced by meteorological factors and fluctuates across timescales and regions. Yet, the increasing reliance on these VRE sources introduces challenges for power system stability and security, potentially leading to periods of energy scarcity, especially during extended low-output events. This, in turn, can pose risks for supply adequacy and grid resilience. Energy system design must therefore integrate both technical modeling and climate-informed risk assessment to ensure the reliability and sustainability of future electricity systems [1, 2, 3].

The dependency of VRE power sources on meteorological conditions makes the electricity supply sensitive to variability across multiple time scales, from hourly and daily fluctuations to seasonal and even inter-annual changes. Among these, extended periods of low wind and solar output, known as Dunkelflaute events, pose a significant threat to system reliability, especially when electricity demand remains high. These events challenge the system's ability to maintain a continuous balance between supply and demand, potentially leading to loss of load or blackouts, and highlight the importance of understanding and planning for weather uncertainty in long-term energy system modeling [2].

Weather-related uncertainty in VRE generation occurs at multiple layers, each with distinct implications for power system reliability and planning. Understanding and properly modeling these uncertainties is essential, particularly in the context of ambitious policy goals such as achieving climate neutrality, phasing out fossil fuels, and increasing the share of renewables in the energy mix. The European Union's climate targets, for instance, necessitate high system flexibility and robustness under increasingly uncertain weather patterns [6, 7].

Addressing these challenges, recent studies have increasingly focused on measuring and characterizing Dunkelflaute events, meaning periods of low wind and solar generation, due to their implications for power system reliability [18, 19]. Analyses include quantifying their duration, frequency, and severity, typically using historical and reanalysis weather data to identify periods of low wind and solar availability in specific regions such as the United Kingdom, Ireland, Germany, and the North Sea [11, 16]. Other studies have extended this analysis to broader spatial scales, including pan-European and global assessments, to examine how Dunkelflaute events behave across interconnected systems [20, 21] or incorporated synthetic time series and climate model projections to explore the potential impact of future climate conditions on the frequency and intensity of these events [19, 22, 23]. Methods to detect and evaluate VRE droughts include threshold-based methods, moving averages using a fixed or a variable time period over which the data is averaged, and deviation-based indices like the *Climatological Renewable Energy Deviation Index* (CREDI) [1, 5]. Studies focusing on the planning of future energy systems typically rely on average historical years, representative weather years or synthetic weather data, but these approaches often obscure the severity or frequency of critical low-output periods. Additionally, measurement and detection criteria of Dunkelflaute events differ widely some use absolute thresholds (e.g., capacity factors below a certain level), others use relative or percentile-based criteria, which makes comparisons across studies difficult and hinders generalizable conclusions.

Modeling weather uncertainty is challenging for Europe, a region marked by substantial geographical and meteorological heterogeneity. Past modeling efforts frequently treat Europe as a homogeneous system, applying a single weather year across all countries to represent average or extreme conditions. Yet, local variations in wind and solar availability mean that an event defined as extreme at the continental level may not align with the realities in individual member states. Consequently, system configurations based solely on continental-scale extremes may offer a false sense of security, potentially underestimating national or regional vulnerabilities to supply shortfalls during Dunkelflaute events. As a result, a more nuanced, spatially resolved treatment of weather extremes is needed to ensure resilient energy systems aligned with decarbonization targets.

From an optimization perspective, various approaches have been employed in the literature for energy system design, with the most common methods being deterministic, robust, and stochastic optimization. The first one solves a single "expected" scenario, treating all inputs as exactly known, therefore ignoring variability and uncertainties, but simply focusing on a single-scenario optimum. It is simple to formulate and solve, and computationally fast, but there is no explicit hedge against rare, high-impact events, leading to systems that might perform poorly in reality. Robust optimization, on the other hand, addresses input uncertainties by defining an uncertainty set for parameters and finding solutions optimized against the worst-case conditions within this set. The main objective is therefore to minimize the worst-case cost. It has the advantage of providing guaranteed feasibility under any realization in the uncertainty set, but it can lead to overconservative solutions; indeed, consid-

ering a very unlikely worst-case scenario may significantly increase costs. Lastly, stochastic optimization uses a probabilistic approach: it models uncertainty through a discrete set of scenarios, each with an associated probability of realization. The goal is to minimize the expected (risk-adjusted) cost over all scenarios. This method explicitly accounts for multiple possible futures, finding a balance between cost and the probability of scenarios. The main drawbacks of this method are associated with the difficulty of generating scenarios and assigning probabilities. Moreover, it is computationally demanding, as the model size increases proportionally with the number of scenarios.

Most studies on long-term energy system analyses for planning purposes have addressed weather uncertainty in a broad sense, either by considering intra-annual variability [65, 53], or by examining the impact of weather-year selection on energy system costs and the supply mix [45, 66], thereby capturing inter-annual variability. To the best of our knowledge, only a few studies have explicitly investigated the implications of Dunkelflaute events or other extreme weather periods for energy system planning [67, 68, 2, 46]. However, most of these studies rely on deterministic approaches, which do not constitute true decision-making under uncertainty. Ruhnau and Qvist [67] investigated storage requirements in a fully renewable European power system, showing that rare but prolonged renewable droughts can drastically increase the need for long-duration storage. Similarly, Höltinger et al. [68] found, in the context of a fully renewable Swedish power system, that extreme events can push the system to its operational limits, highlighting the need for complementary dispatchable capacity or storage solutions. Kittel et al. [2] characterized the spatial and temporal patterns of renewable droughts, concluding that such events are widespread and can cause substantial supply shortages, and emphasizing the value of long-term storage and interconnection in mitigating their impacts. Additionally, Forghani et al. [46] incorporated multiple weather scenarios into a stochastic optimization model for Northern Europe, finding that accounting for weather uncertainty leads to higher investments in firm capacity and increases total system costs.

Methodologically, the literature on modeling weather uncertainty also differs in terms of spatial scope. Optimization may focus on a single country, a European subregion, or the entire continent. In the latter case, Europe can either be treated as a single cluster, with one weather year representing the worst Dunkelflaute event for the entire Europe [45], or modeled with regional differentiation in Dunkelflaute occurrence [2], using a country-level or subregion-level representation of Dunkelflaute events. Finally, in addition to the initial optimization of the energy system (involving both capacity expansion and dispatch decisions), a subsequent simulation phase can be performed to assess the robustness of the system. In this step, the optimized system with fixed installed capacity is subjected to dispatch-only simulations using varying weather input data. This allows for the evaluation of the reliability and adaptability of the solutions.

1.1 Research Aim

To address the gaps and challenges outlined above, this study advances the characterization and modeling of Dunkelflaute events in renewable electricity systems. We evaluate and compare methodologies for detecting and measuring Dunkelflaute events at three spatial scales: country, weather zone (groups of countries with similar weather patterns), and Europe-wide. We then analyze how representing Dunkelflaute events at these different scales influences both the robustness and cost of renewable electricity systems. This enables us to quantify the trade-off between model robustness and the complexity of incorporating detailed Dunkelflaute event data into energy system modeling. Moreover, a stochastic optimization approach is employed to enhance the robustness of the energy system design. Specifically, we aim to answer the following research questions:

1. Which detection methods and criteria are most effective for identifying and quantifying Dunkelflaute events, and how do the results vary across country, weather-zone, and Europe-wide scales?
2. How can Dunkelflaute events be most effectively represented in robust European electricity system design, given their heterogeneous occurrence across time and space?
3. What are the impacts of Dunkelflaute events on long-term energy system costs and design, and which technologies are most critical for enhancing robustness under stress?

To address these questions, we first develop a framework for ranking weather years using meteorological data from 1979 to 2019. Multiple methods are applied to detect Dunkelflaute events, using metrics specifically designed to capture low-output periods for wind and solar generation. These events are identified at three spatial scales: individual countries, weather zones, and the entire European continent. Based on these classifications, we employ a greenfield capacity expansion model to simulate investment and operational decisions in the energy system. This framework enables us to compare cost-optimal system configurations across different representations of Dunkelflaute events and to evaluate the resulting impacts on system robustness and cost.

The work is structured as follows. Chapter 2 presents the background from the literature relevant to this work. The concepts and methods applied in the study are introduced, along with the literature that forms the foundation for the analysis. Chapter 3 describes the methodology used to identify extreme weather events, rank historical weather years, and explains the energy system model employed in the analysis. Chapter 4 provides the results of the weather-year ranking and presents findings from the model outcomes regarding system robustness and costs. These results are further discussed in Chapter 5. Finally, Chapter 6 concludes the thesis with a summary of key findings and suggestions for future research.

2
Background

This section includes an overview of variable renewable energy (VRE) generation and the associated uncertainties. In this context, different temporal categories from intraday, over seasonal, and intra-annual weather variability are introduced, as well as methods that are used to identify and quantify Dunkelflaute events are explained. After that, the main optimization approaches used in the context of energy system modeling (i.e., deterministic, robust, and stochastic optimization) are introduced. Finally, a literature review on Dunkelflaute events and weather uncertainty in energy system modeling is presented, together with research gaps addressed in this study.

2.1 Variable Renewable Energy and Weather Dependencies

Power systems based on VRE sources, such as wind and solar PV, are subject to several forms of uncertainty due to the weather-dependent nature of their generation. These uncertainties manifest on various temporal and spatial scales and include short- and medium-term fluctuations, seasonal or inter-annual variability. Their occurrence is linked to changing meteorological conditions, such as wind speed, solar irradiance, cloud cover, and atmospheric pressure systems [1, 10]. As the share of wind and solar power in the generation mix increases, the exposure of the electricity system to weather-dependent supply variability becomes more important. This constitutes a structural uncertainty in the operation of VRE-dominated systems, as supply may deviate from demand over both short and longer periods. This work focuses on a specific type of variability, which is the occurrence of extended periods of low VRE generation, known as *Dunkelflaute* events.

The following sub-sections introduce the concept of *Dunkelflaute* events in more detail, outline approaches for their quantification, and review relevant methods used in the literature. This provides the theoretical foundation for the subsequent modeling and analysis of VRE drought periods within the context of energy system modeling and simulation.

2.1.1 Variable Renewable Energy

The share of renewables in energy production has grown, driven by declining costs of solar, wind, and related technologies, along with greater accessibility. Improvements in efficiency and storage, combined with policy support through subsidies, tax incen-

tives, and renewable targets, also have an impact on the increasing share [9].

Renewable energy sources can be divided into variable and non-variable types. Renewables such as hydropower with reservoirs, biomass, or geothermal energy can be dispatched more flexibly and are less dependent on immediate weather patterns. The key feature of VRE is that it cannot be fully controlled or predicted precisely in real time, because wind speeds and solar irradiation naturally change over minutes, hours, days, and seasons. This variability creates challenges for balancing electricity supply and demand, as VRE output may not always align with when energy is needed. These weather-driven fluctuations are not only short-term but also occur across different time scales, from intraday changes to seasonal and even annual variations. As a result, understanding the weather dependencies of solar and wind energy is essential for designing a reliable and resilient energy system.

Common solutions to address variability in renewable energy include battery storage, hydrogen storage, or the use of dispatchable sources such as natural gas or nuclear power. However, these options also come with drawbacks: batteries and hydrogen storage can be costly and face efficiency challenges [35], gas and other fossil-based sources produce greenhouse gas emissions, and nuclear power generates waste and faces public concerns about safety and acceptance [36].

2.1.2 Intraday Variation

Intraday variation refers to changes in the availability of renewable energy within a single day. For solar PV, this pattern is highly regular. Solar energy is only available during daylight hours, with zero generation at night. This results in a clear daily cycle where production starts in the morning, peaks around midday, and drops to zero after sunset. This predictable unavailability during nighttime hours makes solar power heavily dependent on complementary sources or storage to meet evening and nighttime electricity demand. Wind energy, in contrast, also experiences intraday fluctuations, but these are less regular and more difficult to forecast. As a result, while solar variability follows a fixed daily pattern, wind introduces an additional, less predictable layer of short-term variability into the energy system [33].

2.1.3 Seasonal Variation

Seasonal variation refers to the typical annual patterns in wind and solar power generation. Solar output is generally highest in summer and lowest in winter. Wind patterns, however, vary by region. In some areas of Europe, both wind and solar generation can be low during winter, leading to potential supply challenges. In contrast, regions with higher wind capacity factors, such as northern and western Europe, typically see increased wind generation during winter months compared to summer. These seasonal effects are important because they can lead to critical shortages when electricity demand is also high. Studies have used long-term weather data to compare current output to historical averages. This helps identify unusual

seasonal patterns and better prepare energy systems for them [42].

2.1.4 Intra-Annual Variation

Intra-annual variation includes changes in renewable generation that happen throughout the year but are not strictly seasonal. These include multi-week or multi-month periods with below-average generation. Such events can have a big impact on system planning, especially when they happen outside of expected seasonal trends. Some methods identify these events by measuring how much the generation deviates from average values over time. This approach helps highlight long periods of low availability that may not be obvious when looking at daily or weekly data alone [34].

2.1.5 Variable Renewable Energy Drought Periods - Dunkelflaute Events

Dunkelflaute events are meteorologically driven periods during which wind and solar power generation simultaneously fall to low levels for an extended duration. The term, originating from German energy discourse, translates to “dark doldrums” and refers to the coincidence of overcast skies (limited solar irradiance) and weak wind conditions (low wind speeds), typically resulting from persistent high-pressure systems [1, 10].

Technically, Dunkelflaute events can be defined as periods when the capacity factor of one or more renewable technologies falls below a fixed threshold for a certain period of time. This threshold-based definition relies on either absolute or relative measures of energy generation, such as production output or capacity factors, and may be applied to single technologies or to the combined output of wind and solar generation. For example, Li et al. [10] define Dunkelflaute events as periods when wind and solar capacity factors both fall below 20 percent in hourly data, and they only consider events lasting longer than 24 hours to capture systemically relevant occurrences. This approach reflects a technology-aggregated definition, where simultaneous deficits in wind and solar generation are required to qualify as a Dunkelflaute [10]. Additionally, Kittel and Schill propose a more flexible and robust framework that uses multiple thresholds and variable time windows for the capacity factor data. This method makes it possible to detect when the data falls below certain levels for longer durations and to combine consecutive low-generation phases into one extended Dunkelflaute event instead of treating them as separate occurrences [1].

The definition of Dunkelflaute events also depends on spatial aggregation and temporal resolution. Some studies focus on national-scale assessments, while others consider transnational or even pan-European perspectives. For example, aggregated data may mask localized variability but better reflect system-level impacts in interconnected grids. Temporal resolution determines the level of detail at which variability is captured and directly influences the identified duration and frequency of events. Higher temporal resolutions detect short-term fluctuations, while lower resolutions emphasize longer, persistent periods. To account for persistence while reducing

noise, rolling means can be applied to smooth the data over time. This allows for a consistent identification of Dunkelflaute events aligned with system-relevant timescales [1].

Meteorological drivers of Dunkelflaute events hinge on a persistent setup that produces both “dark” and “windless” conditions simultaneously. In Central and Northern Europe, Dunkelflaute events occur mostly during late autumn and winter months, particularly November through January, due to shorter daylight hours, reduced solar angles, and seasonal meteorological patterns favoring anticyclonic conditions. These events can extend from a few hours to several consecutive days and may cover broad geographical areas. This seasonal reduction in irradiance compounds the impact of Dunkelflaute events on PV output. During November-January, the availability typically can fall to 20–40% of summer values [43]. Additionally, periods of low wind generation can cause system stress as well. During high-pressure conditions, mean wind speeds can drop below the cut-in threshold of 3–4 m/s for many turbines, causing output to collapse. By contrast, offshore wind farms experience smoother sea-surface roughness and more stable marine boundary layers, which elevate mean wind speeds by roughly 20–50% compared to inland sites and reduce diurnal variability. However, even these higher baseline speeds can be markedly suppressed under expansive high-pressure systems, leading to region-wide low-wind events in winter [44]. Spatial correlation analyses have shown that while Dunkelflaute events can affect multiple countries, complete simultaneity across all of Europe is uncommon [1].

2.2 Optimization Approaches in Energy System Modeling

In energy system modeling, an optimization approach is a mathematical framework used to find the "best" system design or operation strategy by minimizing (or maximizing) an objective function (typically the total system cost) subject to constraints such as demand balance, capacity limits, and generation availability. This section provides a description of the three main optimization approaches used in the context of energy system modeling. Deterministic, robust, and stochastic optimizations are analyzed, describing what each approach is, how it works conceptually, its advantages and limitations, and its relevance to weather-resilient energy system modeling.

2.2.1 Deterministic Optimization

In energy system modeling, deterministic optimization is the traditional approach exploited, which provides a clear solution pathway. The deterministic approach is an optimization model in which all inputs, such as demand time series, profiles of renewable capacity factors, and technology costs, are assumed to be known with certainty. It is formulated as a single-scenario mathematical model. The main advantage of this approach is its simplicity and ease of use, being computationally efficient and straightforward to implement: its single-scenario models can be solved quickly, even with high temporal and spatial resolution. However, its main limitation

lies in its assumption of ignoring uncertainty. In fact, in reality, some parameters of the energy system are subject to uncertainty, such as the capacity factors of renewable technologies, which are highly dependent on weather conditions. By using a single set of "typical" input values, deterministic models often return solutions that might not perform optimally under real-world conditions. In weather-resilient energy system modeling, deterministic optimization represents a useful baseline, revealing the least-cost system configuration under assumed conditions. However, this often leads to an underestimation of system needs, such as reserve capacity or energy storage [53].

2.2.2 Robust Optimization

One solution to address uncertainty is to exploit a robust optimization model. It represents a conservative approach in which the input parameters are not treated as certain but vary within an uncertainty set. The aim is to obtain a cost-effective solution that performs adequately in every realization of these uncertainties. A robust model is typically formulated as a min-max problem, where the objective is to minimize the maximum possible cost across all realizations of input values within the uncertainty set. The main advantage of robust optimization is the reliability of its solutions, as they remain effective even under adverse scenarios. However, this can lead to overly conservative outcomes, resulting in oversized and expensive system designs (capacities that exceed realistic needs), in order to hedge against worst-case scenarios that might have a very low probability of occurring. Another limitation relates to the design of the uncertainty set definition since the choice of set bounds can strongly influence the results. This approach is highly relevant for long-term energy system modeling, especially when the uncertainty or associated risks of the input data cannot be quantified. However, because of its excessively conservative and costly solutions, a probabilistic approach, such as stochastic optimization, is often preferred.

2.2.3 Stochastic Optimization

Scenario-based stochastic optimization is a widely applied stochastic optimization approach adopted in the literature for addressing weather-related uncertainties [47, 48, 49]. This approach accounts for uncertainty by modeling it in a probabilistic framework: possible realizations of uncertain parameters (such as wind and solar capacity factors) are represented by a set of scenarios, each associated with a probability of occurrence. The goal is to obtain a solution that minimizes (or maximizes) the expected value of the objective function across all scenarios, balancing the system's performance across all possible conditions. In the energy systems context, a common methodology is the two-stage stochastic optimization, which works as follows:

- In the first stage, investment or commitment decisions are made before uncertainty is realized.
- In the second stage, operational decisions, such as dispatch and storage use, are optimized for each scenario.

Stochastic optimization offers a middle ground between deterministic and robust approaches, hedging against parameter uncertainty while avoiding the over-conservatism of the robust approach. Therefore, it returns a solution that reflects a trade-off between cost and risk of extreme scenarios. The main limitation of this approach comes with the definition of these scenarios, due to the need for reliable data records and probability distributions. In addition, the computational requirements are significant, as the model size increases exponentially with the number of scenarios.

2.3 Literature Review on Dunkelflaute Events and Weather Uncertainty in Energy System Modeling

A wide range of studies has examined Dunkelflaute events from different regional, methodological, and technological perspectives. Early research focused on analyzing wind droughts in the United Kingdom [11, 12, 13, 14], Ireland [15], the North Sea [16], and Germany [18], often using historical or reanalysis weather data to quantify their duration, frequency, and severity. More recent work has broadened this scope across Europe [20, 21, 22, 23] and globally [19], accounting for future climate scenarios and synthetic data series to project how these events may evolve.

In parallel, research has advanced in developing methods to detect and evaluate VRE droughts, including threshold-based approaches [1, 18], moving averages, and deviation-based indices such as the *CREDI* metric [31, 32]. These methodological developments reflect ongoing efforts to standardize and compare drought detection across contexts such as geographic regions or levels of renewable energy penetration. Several studies also emphasize the role of long-duration storage and geographic balancing to mitigate the impacts of Dunkelflaute events on the system [17, 24, 25, 29, 30].

Another part of the literature focuses on positive residual load events, where electricity demand exceeds the combined generation from VRE sources, often during low-wind and low-solar periods. These events are critical for energy system reliability, as they reveal mismatches between VRE supply and demand. Raynaud et al. [37] analyze such imbalances in the European context, identifying energy supply droughts as systemic risks and comparing them with energy production droughts. Rinaldi et al. [38] use machine learning methods to map the relationship between weather data, renewable power generation, and electric load, proposing a diversified energy system with storage as a mitigation strategy. Mayer et al. [39] employ a macro-scale electricity model to study the impact of Dunkelflaute events during periods of high electricity demand, showing that these events can deplete energy storage, increase reliance on dispatchable backup generation, and raise the need for electricity imports. Otero et al. [40] characterize Dunkelflaute events with concurrent low renewable output and high demand across 27 European countries, while Allen and Otero [41] develop standardized indices integrating both VRE availability and demand conditions to provide a comprehensive drought metric.
Table 2.1 provides an overview of key studies addressing the characteristics, detec-

tion methods, and mitigation strategies related to variable renewable energy droughts.

For long-term energy system modeling, different approaches have been adopted in the literature to address weather-related uncertainties. They mainly differ in the optimization method used, the representation of weather uncertainty, the geographical scope, and the analysis of system robustness via simulations. A few papers will be analyzed as examples, and a schematic summary of the different methodologies is shown in Table 2.2.

Gotske et al. [45] adopted a deterministic optimization approach for designing a robust European energy system. They used 62 years of weather data to investigate the impacts of varying solar and wind capacity factors, hydropower inflows, heating demand, and heat pump coefficient of performance. First, a greenfield joint capacity and dispatch optimization was performed for each weather year, yielding 62 alternative capacity layouts. Subsequently, with capacities fixed, the dispatch of each layout was simulated across the remaining 61 weather years (excluding the one used for the joint capacity and dispatch optimization) to analyze the robustness against inter-annual weather variations. The loss of load was the parameter used to assess the robustness of the system, and the results highlighted the importance of considering inter-annual weather variability for energy systems planning, which led to a variation of $\pm 10\%$ in total system cost.

Kittel et al. [2] analyzed the European energy system, modeling it on a country-level scale. They implemented a dispatch and capacity expansion model with a deterministic approach, focusing on the interaction between VRE droughts (i.e., Dunkelflaute) and long-duration electricity storage needs. The 36 historical weather years examined were divided into summer-to-summer planning horizons (July 1 to June 30) rather than into conventional calendar year periods (January 1 to December 31). This is because winter droughts are generally more impactful than summer droughts. This study demonstrated a positive correlation between the most extreme renewable droughts and the long-duration storage needs of a given country. It also showed that geographical balancing (that is, sharing electricity generation across interconnected countries) reduces this storage need, though it cannot fully eliminate it.

In Seljom et al. [8]'s work, the long-term energy model was optimized with a stochastic modeling approach, focusing exclusively on the Norwegian energy system. The primary objective of this study is to compare six different scenario-generation methods, each producing a set of discrete scenarios derived from the same weather dataset. These scenarios, represented as 24-hour typical days, were then used as inputs in a two-stage stochastic programming framework. Seasonal independence was considered, with separate representative days selected for each season. A key limitation of this approach is that dividing the year into time slices may not sufficiently capture the typical intra-annual weather variability. The study showed that the adopted scenario-generation method significantly influences the quality and stability of energy system model results, and also affects the number of scenarios required to achieve stable and reliable model outcomes.

Table 2.1: Summary of Literature on Dunkelflaute and VRE Drought Analysis.

Author(s)	**Main Topic**	**Contribution / Focus**
Kittel & Schill [1]	Assessment of methods to detect Dunkelflaute events	Defined, classified, and evaluated multiple methods to measure Dunkelflaute events in Europe
Cannon et al. [11]	Wind droughts (UK)	Analyzed frequency and intensity of wind droughts in Great Britain using long-term reanalysis data
Potisomporn & Vogel; Potisomporn et al. [12, 13]	Wind droughts (UK)	Assessed spatial/temporal characteristics of offshore wind and validated ERA5 data for low-wind events
Abdelaziz et al. [14]	Wind droughts (UK)	Evaluated offshore wind drought trends under climate change scenarios
Leahy & McKeogh; Patlakas et al.; Ohlendorf & Schill [15, 16, 18]	Wind droughts (Ireland, North Sea, Germany)	Investigated persistence and frequency of low wind events and implications for system variability
Antonini et al. [19]	Wind droughts (Global)	Identified globally reliable wind power sites based on climatological drought risk
Hu et al.; Breyer et al.; Kaspar et al. [23, 24, 25]	Variable renewable energy droughts	Studied climate scenarios and shortfall risk for VRE in European contexts
Mockert et al.; Mayer et al.; Ohba et al. [26, 27, 28]	Variable renewable energy droughts	Linked meteorological regimes and future projections to VRE drought patterns
Rinaldi et al.; Gangopadhyay et al. [29, 30]	Wind-solar droughts / mitigation	Emphasized hybrid systems and storage to reduce the impact of renewable droughts
Raynaud et al. [37]	Positive residual load events	Explored energy supply droughts and mismatches between VRE generation and demand in Europe
Rinaldi et al. [38]	Positive residual load events	Analyzed gaps between VRE supply and electricity demand during Dunkelflaute conditions
Mayer et al. [39]	Positive residual load events	Studied Dunkelflaute occurrences during periods of high electricity demand

Forghani et al. [46] aimed to model a robust energy system under weather uncertainty and nuclear power outages for Northern Europe. They proposed a mathematical model that combines a scenario-based stochastic optimization approach (for weather uncertainties) with an adjustable robust optimization approach (for nuclear failure uncertainties). Regarding the stochastic model, a few weather years were selected as scenarios to represent different weather conditions. After obtaining the model's results, simulations were run to evaluate the quality of the solutions, assessing the system's robustness through the analysis of the loss of load value. Considering only the weather uncertainty, the model's solution returned a reduction of 50% of the loss of load compared to the deterministic solution, and an annual savings of 0.11%.

Table 2.2: Summary of literature on the analysis of weather uncertainty in energy system modeling.

Article	**Modeling Approach**	**Methodology**	**Weather Uncertainty Analysis**	**Geographical Scope**
Gotske et al. [45]	Deterministic	Optimization & simulation	Inter-annual variability	Europe
Kittel et al. [2]	Deterministic	Only optimization	Inter-annual and Intra-annual variability, Dunkelflaute events	Europe, country-level scale
Seljom et al. [8]	Stochastic	Only optimization	Inter-annual and Intra-annual variability	Norway
Forghani et al. [46]	Stochastic	Optimization & simulation	Inter-annual variability, Dunkelflaute events	Northern Europe

2.4 Research Gaps

In the context of energy system modeling under weather uncertainty, the main literature gaps concern how weather-related uncertainty is accounted for and the type of optimization approach employed. Most studies focus on intra-annual variability [65, 53], which refers to fluctuations in weather conditions within a single year, or inter-annual variability [45, 66], which considers variations in weather conditions between different years. However, as highlighted by Kittel et al. [2], renewable droughts (i.e., Dunkelflaute events) can cause significant supply shortages and are particularly impactful for future energy systems with high shares of VRE. Among the few studies that explicitly consider Dunkelflaute events in energy system optimization, the majority adopt a deterministic approach (e.g., [67, 68, 2]), thereby neglecting weather uncertainty in the optimization process.

In the Dunkelflaute analysis, several methods are applied and compared, but there is no clear standard for how to measure or detect these events [4]. Methods such as Constant-Below-Threshold, Fixed-Mean-Below-Threshold, and the Sequent-Peak-Algorithm are used in the literature [4], as well as definitions of Dunkelflaute events vary depending on whether they are based on demand or supply perspectives[37].

To address this research gap, the present study incorporates weather uncertainty into the energy system design by adopting a stochastic optimization approach. The analysis focuses specifically on Dunkelflaute events, which are more consequential for system performance compared to general inter-annual or intra-annual variability or periods of below-average renewable generation. This thesis uses a variable-mean-below-threshold method in combination with percentage-based thresholds to develop a more robust approach for Dunkelflaute event detection, defined as VRE-droughts for periods with low resource availability of multiple VRE technologies. In addition, the study includes a simulation phase, in which the energy systems resulting from the optimization are tested under a variety of weather conditions to assess their robustness against weather variability.

3
Methodology

This thesis is the result of joint work with *Tom Schröder* from TU Berlin, carried out at Chalmers University of Technology (Gothenburg). Tom Schröder conducted the analysis of meteorological data and developed the *Dunkelflaute* detection and measurement framework, providing the results reported in Sections 3.1 and 3.2. Section 3.1 first introduces the dataset and then describes the procedures for detecting and quantifying *Dunkelflaute* events, as well as the approach to the clustering of countries based on capacity-factor correlations. Section 3.2 shows the ranking of weather years based on capacity factor data, analyzed at three spatial levels: individual countries, weather zones, and the entire set of European countries treated as a single zone. Subsequently, Section 3.3 outlines the modeling and analysis workflow developed in the thesis, while Section 3.4 describes the mathematical model adopted. The case study is introduced in Section 3.5, and the different modeling approaches together with the transmission grid scenarios are discussed in Sections 3.6 and 3.7 , respectively. Finally, Section 3.8 presents the identification of the typical weather year for Europe.

3.1 Weather Data Analysis

The following section presents the methodological framework used to identify and characterize *Dunkelflaute* events as a basis for incorporating weather uncertainties into the energy system model. It begins with a description of the underlying dataset and the preparation of capacity factor time series for onshore wind, offshore wind, and solar PV. The methodology for defining thresholds and detecting *Dunkelflaute* events is then presented, followed by the criteria used to rank event severity. Additionally, a clustering analysis is conducted to group weather zones based on their generation patterns, enabling regional assessments of VRE drought characteristics. Finally, the methodological basis for the pan-European network analysis is introduced.

3.1.1 The Dataset

The experiments in this study are based on a publicly available dataset of hourly capacity factor time series retrieved from the Copernicus Climate Data Store [72]. The dataset covers the period from 1979 to 2019 and includes three key renewable energy technologies: onshore wind, offshore wind, and solar PV. Capacity factor values represent the ratio of actual to maximum possible generation in each hour, providing a normalized and comparable measure of renewable energy availability.

The spatial scope includes 28 European countries, enabling regionally disaggregated assessments of variability and drought conditions across the continent. These data are used to analyze renewable energy droughts, as well as their spatial and temporal correlations.

3.1.2 Combining Onshore, Offshore, and Solar PV Data

To analyze the aggregate behavior of VRE generation, the capacity factor data for onshore wind, offshore wind, and solar PV were combined into a single time series for each country. This combination was performed using a weighted average approach, where the individual technology capacity factors were weighted by their respective shares of installed capacity. The installed capacity shares were derived from the output of an energy system optimization model configured for an average weather year (analysis described in Appendix B).

The result is an hourly capacity factor that reflects the actual contribution of each technology to the generation mix, based on its relative capacities. This approach ensures that the combined time series captures the variability with regard to the share of each technology. If a country has a larger share of solar capacity compared to offshore wind, the solar profile will have a proportionally higher influence on the combined capacity factor. This method enables consistent comparisons of energy drought events and residual load dynamics across countries.

3.1.3 Defining Thresholds for Determining Dunkelflaute Events

This subsection describes the method used to define thresholds for identifying periods of low renewable generation. A threshold needs to be implemented to find periods in which the capacity factor falls below a certain value to be classified as a potential *Dunkelflaute*. Two alternative approaches are compared: thresholds based on percentiles of the capacity factor data (*median-* or *percentile-based*), and thresholds defined as a percentage of the mean capacity factor (*mean-based*).

In the *percentile-based* method, the threshold represents the capacity factor levels below which the system operates for a given proportion of time. The 10th percentile, for example, marks conditions that occur in only the lowest 10% of observations. The 20th percentile provides a less restrictive but still significant threshold, while the median is the 50th percentile and can be a reference point for typical capacity factor levels. Using percentiles allows for the identification of low-generation periods without being influenced by observations of higher capacity factors.

In the *mean-based* method, the threshold is calculated as a fixed percentage (e.g., 20%, 40%, 60%) of the mean capacity factor value. This value reflects the long-term average availability and responds to both high-output and low-output periods across the entire time series. Unlike *percentile-based* thresholds, which are influenced only by the lower part of the distribution, *mean-based* thresholds are sensitive to the

full range of generation levels. They are less affected by systematic zero-production periods (such as night-time for solar PV), but more influenced by occasional periods of very high availability, which raise the mean value and, in turn, the threshold.

For countries with a high share of solar generation, availability curves typically show extended periods of zero capacity factor due to night-time hours without solar production. In contrast, countries dominated by wind generation exhibit fewer zero-output periods, and their median and mean capacity factors tend to be closer. The analysis compares how the choice of threshold definition influences the identification of *Dunkelflaute* events across different country profiles.

Figure 3.1 illustrates the availability duration curve for Spain, based on 41 years of hourly weighted capacity factor data. Spain's generation mix includes a high share of solar PV, resulting in an availability profile with a pronounced segment of zero-output periods due to the absence of solar production at night. The figure compares *mean-based* and *percentile-based* thresholds applied to this distribution. *Mean-based* thresholds (Mean, 20% of Mean) are influenced by the full range of capacity factor values, while *percentile-based* thresholds (Median, 10th Percentile) are determined by the lower part of the availability distribution. The differences in these threshold levels highlight how the characteristics of the generation profiles affect threshold selection and, consequently, the identification of *Dunkelflaute* events.

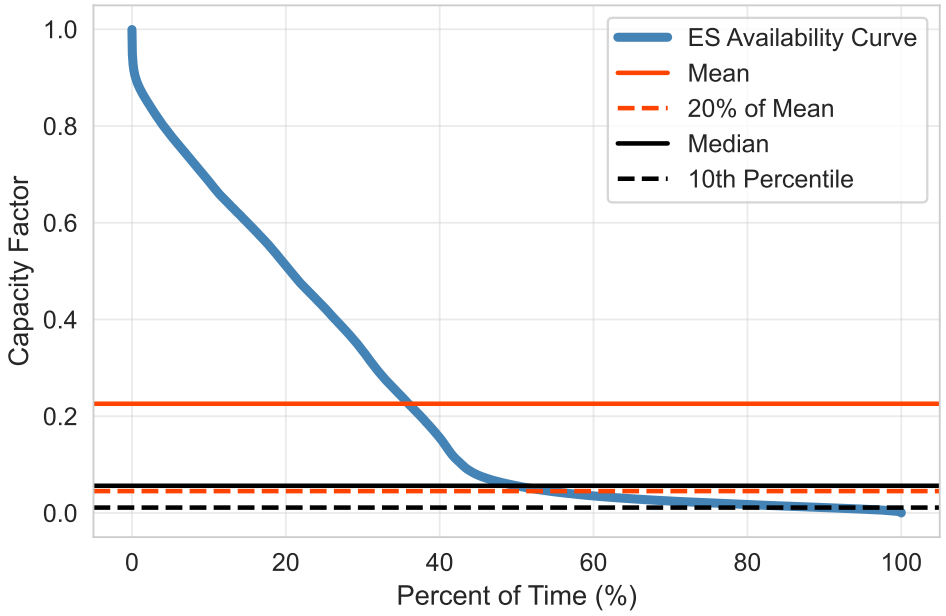

Figure 3.1: Availability curve for hourly data over 41 years using weighted capacity factor data from Spain with *median-* and *mean-based* thresholds.

Figure 3.2, instead, shows the availability duration curve for Sweden, based on 41 years of hourly weighted capacity factor data. In contrast to Spain (Figure 3.1), the Swedish generation mix is dominated by wind energy, resulting in an availability

profile with very few zero-output periods. The curve exhibits a smoother decline compared to the more segmented profile observed for solar-dominated countries. In this case, the mean and median capacity factors are relatively close, reflecting the more continuous nature of wind generation. The impact of the generation profile on threshold selection and the resulting classification of *Dunkelflaute* events can be observed clearly when comparing the Swedish and Spanish cases.

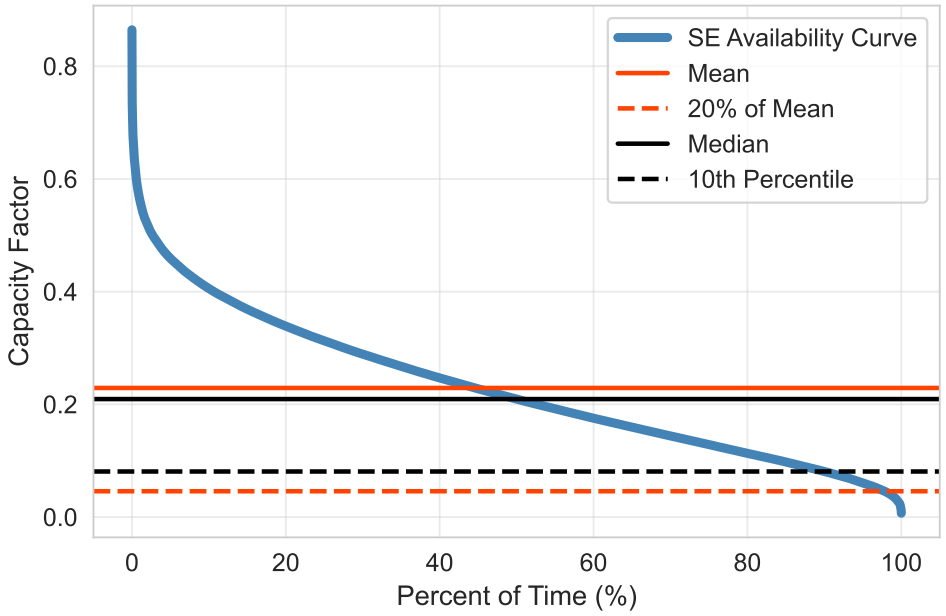

Figure 3.2: Availability curve for hourly data over 41 years using weighted capacity factor data from Sweden with *median-* and *mean-based* thresholds.

The comparison of availability curves for Spain and Sweden illustrates how the choice of threshold definition influences the identification of *Dunkelflaute* events. For wind-dominated countries such as Sweden, where mean and median capacity factors are relatively similar, *mean-based* and *percentile-based* thresholds lead to comparable results. In contrast, for solar-dominated systems such as Spain, systematic zero-production periods lead to larger differences between the two approaches.

Based on these findings, this study applies *mean-based* thresholds to ensure consistency across countries with different generation profiles. Thresholds are defined as percentages of the mean capacity factor, with multiple levels (e.g., 20%, 40%, and 60% of the mean) used to capture a range of low-generation conditions. The selection of threshold values has a direct influence on the number, duration, and severity of detected *Dunkelflaute* events. Using several threshold levels here allows for a more robust assessment of system behavior under varying degrees of renewable scarcity and avoids bias toward any single threshold definition.

3.1.4 Dunkelflaute Detection Methodology

Quantifying *Dunkelflaute* events involves the identification and classification of periods with low availability of VRE generation. Methodologically, this requires setting conditions under which a period qualifies as a "drought event", typically using capacity factor time series derived from modeled or observed VRE output. The aim is to capture the frequency, duration, and severity of such events using robust and transparent criteria. A range of methods exists, differing primarily in how the drought threshold is defined and over what time horizon it is applied.

3.1.4.1 Fixed-Mean-Below-Threshold (FMBT)

One commonly used approach applies a fixed threshold to the availability factor time series. Events are defined as periods in which the VRE capacity factor remains continuously below a static value (e.g., 10% or 20%) for a defined number of time steps. This method, often referred to as the *Constantly-Below-Threshold* (CBT) method, identifies droughts based on strict exceedance criteria and produces a countable set of discrete events. These methods are straightforward to implement and interpret, but are sensitive to threshold selection and may overestimate event frequency by segmenting longer, compound events into multiple shorter ones.

An alternative within this category is the *Fixed-duration Mean-Below-Threshold* (FMBT) approach, which defines a drought event as a period where the moving average of the availability factor over a specified window remains below a fixed threshold. This approach smooths short-term fluctuations and allows for temporary exceedance during overall low-generation phases. However, the results depend on the chosen averaging interval, and drought events may overlap depending on this parameterization.

Metrics that can be used to describe the characteristics of *Dunkelflaute* include the event duration (i.e., the number of consecutive time steps during which the moving average remains below the threshold), event frequency (the number of identified events within a given analysis period), and the energy deficit, which quantifies the cumulative shortfall of VRE availability compared to the threshold during the event. This deficit can be calculated using either the smoothed time series or, alternatively, the original availability data over the identified event period. Each of these metrics provides insight into different aspects of the system stress associated with VRE droughts. Duration and frequency reflect operational challenges, while the energy deficit indicates the scale of flexibility or backup capacity needed to compensate for the shortfall.

Figure 3.3 illustrates capacity factor data for an example *Dunkelflaute* event, analyzed using the FMBT method. A 3-day rolling mean has been applied to smooth the raw capacity factor time series, and a threshold set at 60% of the long-term mean capacity factor is used to define the event. The yellow-shaded area between the threshold line and the smoothed capacity factor curve represents the deficit area, a metric quantifying the cumulative shortfall in VRE availability during the event.

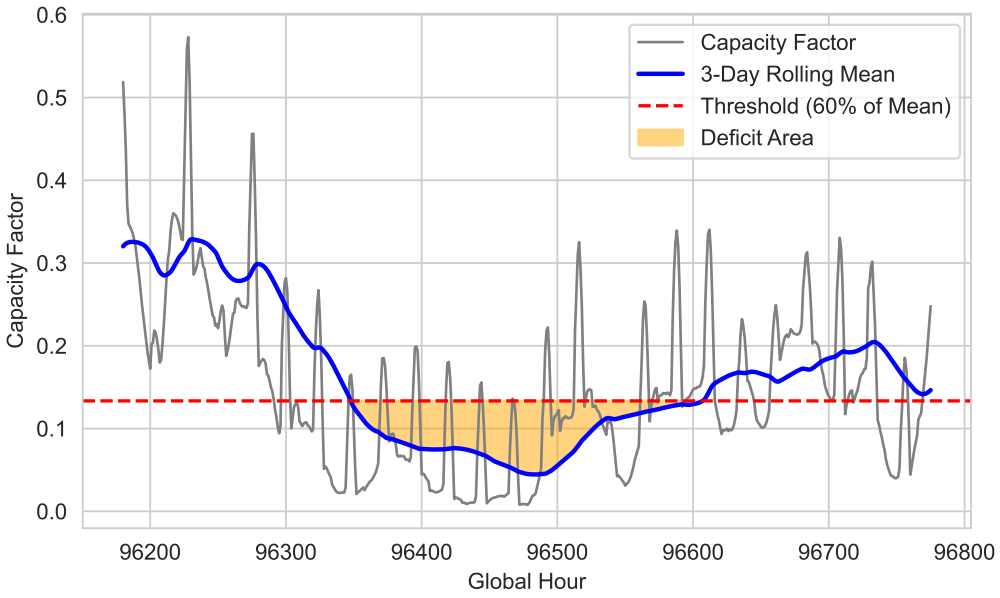

Figure 3.3: Capacity Factor Data for an example *Dunkelflaute* event using a fixed-duration Mean of 3 days and a Threshold of 60% of the Mean of the Raw Capacity Factor data.

3.1.4.2 Variable-Mean-Below-Threshold (VMBT)

To address the limitations of the FMBT method, the *Variable-duration Mean-Below-Threshold* (VMBT) method offers a more dynamic approach to identify *Dunkelflaute* events. In the fixed-duration case, the choice of the rolling mean window is arbitrary and can result in fragmented or missed events if the averaging period does not align with the structure of the actual period with low capacity factor values. VMBT overcomes this by iteratively applying moving averages of varying durations and identifying events as soon as the rolling mean touches or falls below a predefined threshold. The averaging window is progressively shortened, and each detected event is excluded from subsequent iterations, ensuring that all events are identified without overlap. The VMBT method allows a detection of *Dunkelflaute* events of varying length, regardless of whether they are short and intense or long and moderate

To characterize the identified events, several metrics can be used. Duration measures the length of the rolling mean window at the iteration in which the event is detected, corresponding to the time span from the start to the endpoint of the rolling mean time period at which the event is detected. Deficit measures the cumulative difference of raw capacity factor values to the threshold within the *Dunkelflaute* event. It is calculated by summing the differences between the threshold and the raw capacity factor values, but only for those time steps where the capacity factor is below the threshold. This metric reflects the energy volume that would need to be compensated by system flexibility. Frequency simply counts the number of events identified over the analysis period, offering insight into how often such low-generation periods occur. Together, these metrics can provide a robust representation of *Dunkelflaute* characteristics.

3.1.5 Dunkelflaute Ranking Criteria

To evaluate and compare the severity of *Dunkelflaute* conditions across different years, a ranking framework is established based on metrics derived from the VMBT-detected events. This ranking aims to characterize each year according to the intensity and impact of low renewable resource availability, based purely on weather-driven capacity factor data.

This work considers two complementary ranking criteria:

- Annual Cumulative Capacity-Factor-Deficit (**Cumulative CFD**): A measure of the capacity factor deficit across all detected *Dunkelflaute* events within a given year. After identifying the *Dunkelflaute* events by their start and end timestamps, the area under the hourly capacity factor curve that lies below a predefined threshold is calculated. This is done by summing the differences between the threshold and the actual capacity factor values for all timestamps where the capacity factor is below the threshold. In the next step, the deficits from all identified periods within the considered year are aggregated to determine the total capacity factor deficit.

- Highest Single-Event Capacity-Factor-Deficit (**Single-Event CFD**): This metric calculates the largest capacity factor deficit observed during any single *Dunkelflaute* event within a given year. For each year, all *Dunkelflaute* events are identified based on their start and end timestamps. The capacity factor deficit for each event is calculated as the area between the capacity factor curve and a defined threshold, considering only the timestamps where the capacity factor falls below that threshold. Among all events, the one with the highest deficit is selected and used for comparison across years.

Both metrics are computed using weighted capacity factor time series and can be applied at various spatial scales (e.g., national, regional, or continental). By ranking years according to these criteria, the analysis enables a comparative assessment of weather-driven stress on renewable generation across different historical periods.

Figure 3.4 illustrates the two ways of quantifying a country's capacity factor deficit over a period of one year (here, Germany from July 1996 to July 1997). On both plots, the horizontal axis denotes time, and the vertical axis shows the capacity factor values. In the top panel, the yellow-shaded area between the capacity factor curve and the chosen threshold represents the cumulative annual deficit by which the capacity factor falls below a certain threshold over the entire year. In the bottom panel, the yellow-shaded area represents the total deficit over the single continuous period with the greatest deficit within the year.

3.1.6 Clustering Weather Zones

To reduce spatial complexity while preserving key patterns in weather-driven renewable generation, countries are grouped into weather zones using *hierarchical clustering*. This clustering is based on the similarity of hourly capacity factor time

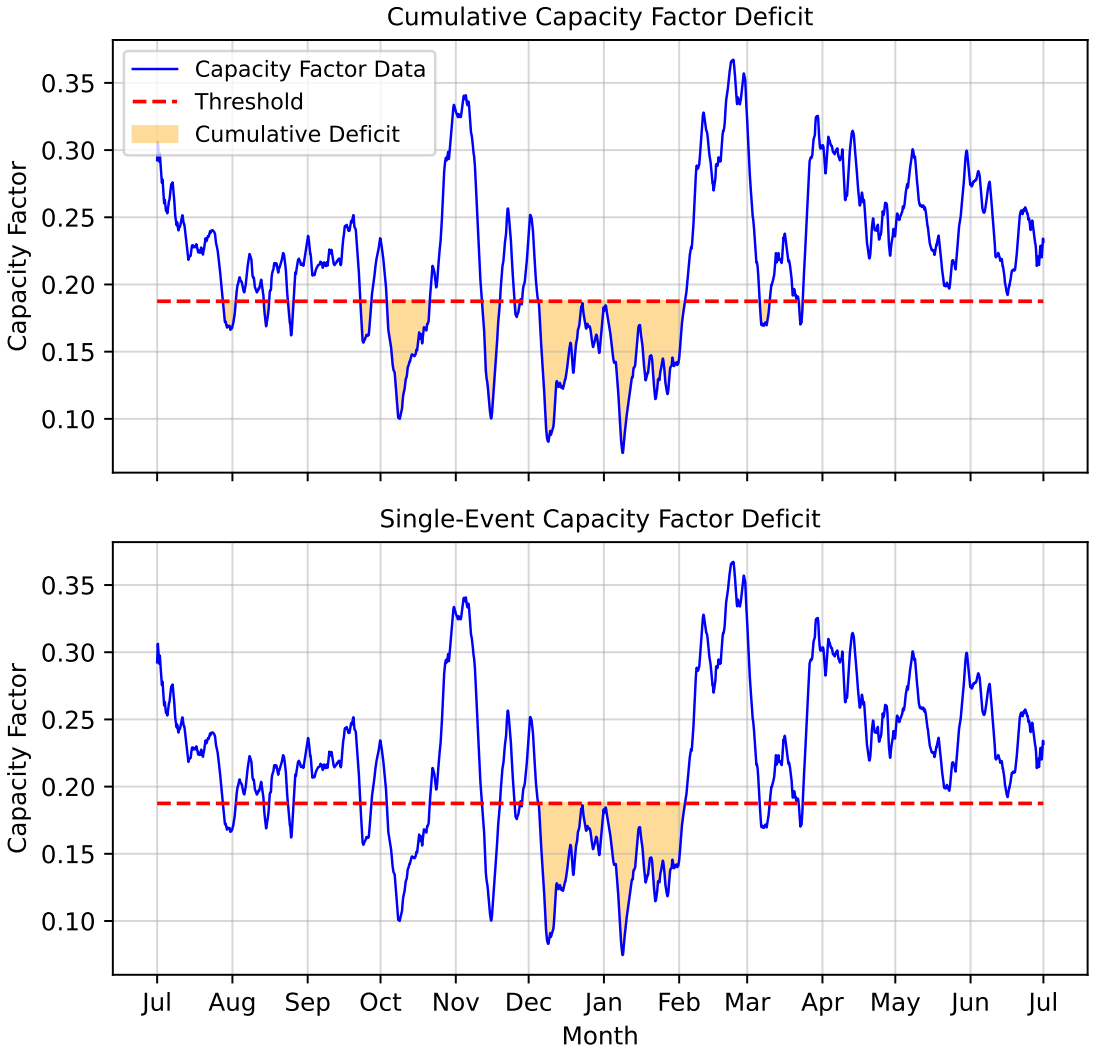

Figure 3.4: Yearly and single-period cumulative capacity factor deficits for a year from July to July. Top: The total deficit below the threshold accumulated over the full year (*Cumulative CFD*). Bottom: The total deficit during the single continuous interval with the greatest deficit (*Single-Event CFD*).

series for wind, solar, and offshore wind, with each technology weighted according to its contribution to the overall renewable generation mix. The resulting weather zones serve as the basis for aggregated analysis in later parts of the study.
One part of the clustering process is a correlation analysis of the capacity factor time series for each technology. For wind, solar, and offshore wind, separate *Pearson correlation* matrices are computed using hourly capacity factor data across all countries. These matrices capture the degree of correlation in capacity factor data patterns between countries.

To construct these matrices, the Pearson correlation coefficient is calculated for each pair of countries based on their respective hourly capacity factor time series. The Pearson correlation measures the linear relationship between two time series and yields a value between -1 and 1, where 1 indicates perfect positive correlation, -1 indicates perfect negative correlation, and 0 indicates no linear correlation. Each matrix is symmetric, with dimensions equal to the number of countries considered, and each element r_{ij} represents the correlation between country i and country j for a given technology.

The resulting correlation matrices serve as the foundation for identifying spatial relationships and similarities in capacity factor behavior between countries. These insights are later used as input for clustering algorithms, which group countries with similar temporal patterns in renewable generation capacity factors.
Using the combined correlation matrix, a hierarchical clustering algorithm is applied to group countries into similar weather zones. The distance metric is defined as $1 - r$, where r is the Pearson correlation coefficient. The clustering is performed using the *complete* linkage method, which considers the maximum distance between elements of different clusters when merging them.

A dendrogram is generated from the hierarchical clustering results, and the number of clusters is selected manually based on visual inspection of the dendrogram and the trade-off between spatial resolution and model complexity. This approach enables the creation of weather zones with internally coherent renewable generation patterns.
Unlike the earlier correlation analysis, which considered wind, offshore wind, and solar separately, the clustering here is based on combined hourly capacity factor data from 1979 to 2019, weighted by the installed capacity of each technology in each country. This approach accounts for the actual contribution of each renewable source to a country's generation profile.

Figure 3.5 shows the dendrogram resulting from hierarchical clustering. The vertical axis represents the linkage distance, which measures dissimilarity between clusters; higher values indicate greater differences. Countries with more similar weighted capacity factor profiles are merged at lower linkage distances. The clustering algorithm begins with each country as an individual cluster and iteratively merges the most similar pairs until a single hierarchical structure is formed. To define meaningful regional groupings, the dendrogram is cut at a chosen level, resulting in eight distinct clusters. These clusters are visually indicated by different color-coded branches in

the figure.

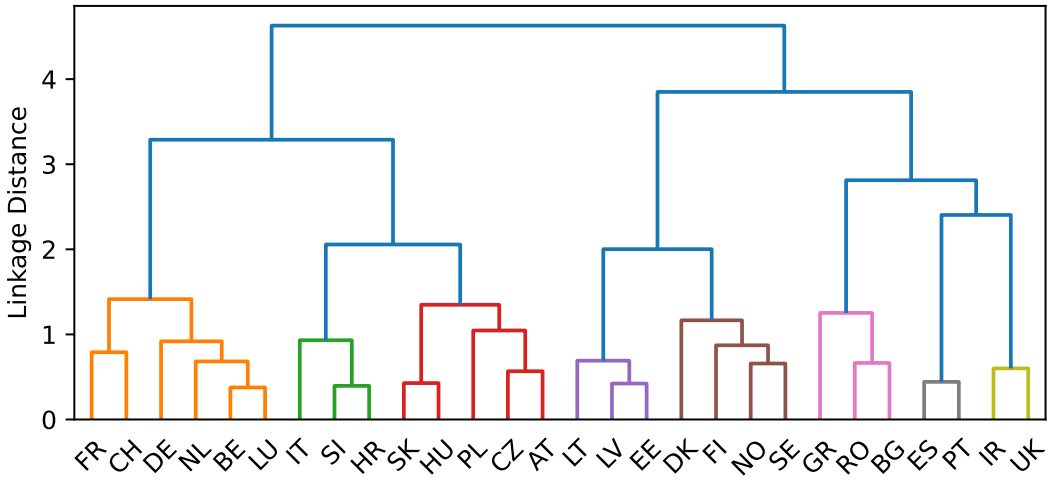

Figure 3.5: Hierarchical Cluster Dendrogram based on Combined Capacity Factor Correlations using the Pearson-Correlation-Coefficient. Distances are used as 1 - Correlation Coefficient.

Table 3.1 presents the results of the hierarchical clustering analysis, which groups countries into eight distinct clusters based on similarities in their underlying capacity factor data correlations, as seen in Figure 3.8.

Table 3.1: Identified clusters from hierarchical clustering

Cluster	Countries
1	FR, CH, DE, NL, BE, LU
2	IT, SI, HR
3	SK, HU, PL, CZ, AT
4	LT, LV, EE
5	DK, FI, NO, SE
6	GR, RO, BG
7	ES, PT
8	IR, UK

3.2 Year Ranking of Dunkelflaute Appearances

This section presents the ranking of weather years, based on the metrics defined in Section 3.1.5: *Cumulative CFD* and *Single-Event CFD*. The weather years are defined from July 1st to June 30th of the following year, consistent with the summer-to-summer time frame used throughout the study.

3.2.1 Year Ranking at Country Level

Each weather year is evaluated for every country using the *Cumulative CFD* and *Single-Event CFD* metrics. Figure 3.6 shows the ranking of weather years from 1979 to 2019 based on the *Cumulative CFD*. The cumulative deficit, calculated either over the full year or in the case of *Single-Event CFD* over the single most critical period, is averaged across thresholds from 0.2 to 0.6 in 0.1 steps and normalized by the maximum observed deficit for each country. This range of thresholds ensures robust results by capturing both very severe *Dunkelflaute* events (e.g., threshold 0.2) and less extreme but still relevant ones (e.g., threshold 0.6). Normalization enables comparison by showing how each year relates to the worst case for each country.

The results presented in Figure 3.6 show notable interannual variability, with the most severe *Dunkelflaute* years differing across countries. For example, the period from July 1995 to July 1996 shows particularly high *Cumulative CFD* values for Denmark, Germany, and the Czech Republic. Similarly, the winter of 1984–85 also stands out for this group. In more recent years, Hungary and Croatia experienced high relative deficits in 2015–16, and Slovenia and Slovakia in 2012–13. Overall, severe *Dunkelflaute* years are not concentrated in a specific period or region but are spread throughout 1979–2019, occurring irregularly across countries. For instance, for France, the year spanning 1988–89 stands out, with all other years showing no more than 70% of the *Cumulative CFD* of that year. In contrast, countries such as Austria, Slovenia, and Slovakia exhibit relatively little variability across years, with most years falling between 70% and 100% of their worst case.

Figure 3.7 shows the ranking of weather years for each analyzed country based on the *Single-Event CFD*. Compared with the *Cumulative CFD* analysis, this metric shows greater variability both over time within individual countries and between countries.
Another observation is that Belgium, the Czech Republic, Germany, Denmark, Sweden, Slovenia, and Slovakia show a concentration of years with high *Single-Event CFD* values in the mid-1990s, particularly during 1995–96, 1996–97, and 1997–98. Central European countries located within or near mountain regions, such as Slovenia, Slovakia, Austria, and Switzerland, show relatively little variability in their year rankings compared with other countries. In contrast, countries with higher shares of onshore wind and offshore wind, including Sweden, Finland, Norway, Romania, and France, display greater year-to-year variability, indicating stronger fluctuations in their exposure to extreme low-wind periods.

The country-level analysis shows identifiable differences between countries with high shares of onshore and offshore wind and those in Central Europe with limited wind and a greater reliance on solar energy. For example, Austria, Switzerland, Slovakia, and Slovenia all show relatively low variability in the highest *Cumulative CFD* observed for any single event within a year, consistent with the earlier metric of total annual *Cumulative CFD*. In contrast, larger countries such as France, Sweden, Spain, and Romania display greater variability, with more years falling below 35% of the maximum annual deficit. Both metrics (*Cumulative CFD* and *Single-Event*

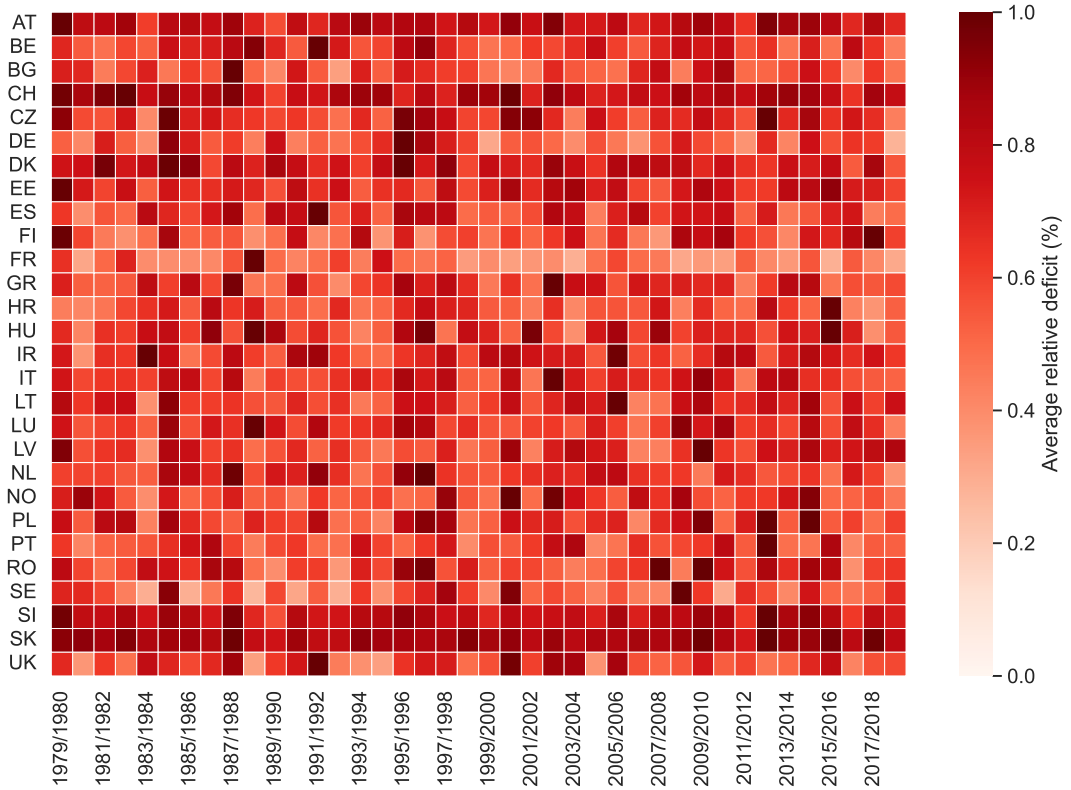

Figure 3.6: Year ranking of single countries based on cumulative capacity factor deficit, averaged over thresholds 0.2, 0.3, 0.4, 0.5, 0.6, and normalized by the highest deficit of each country.

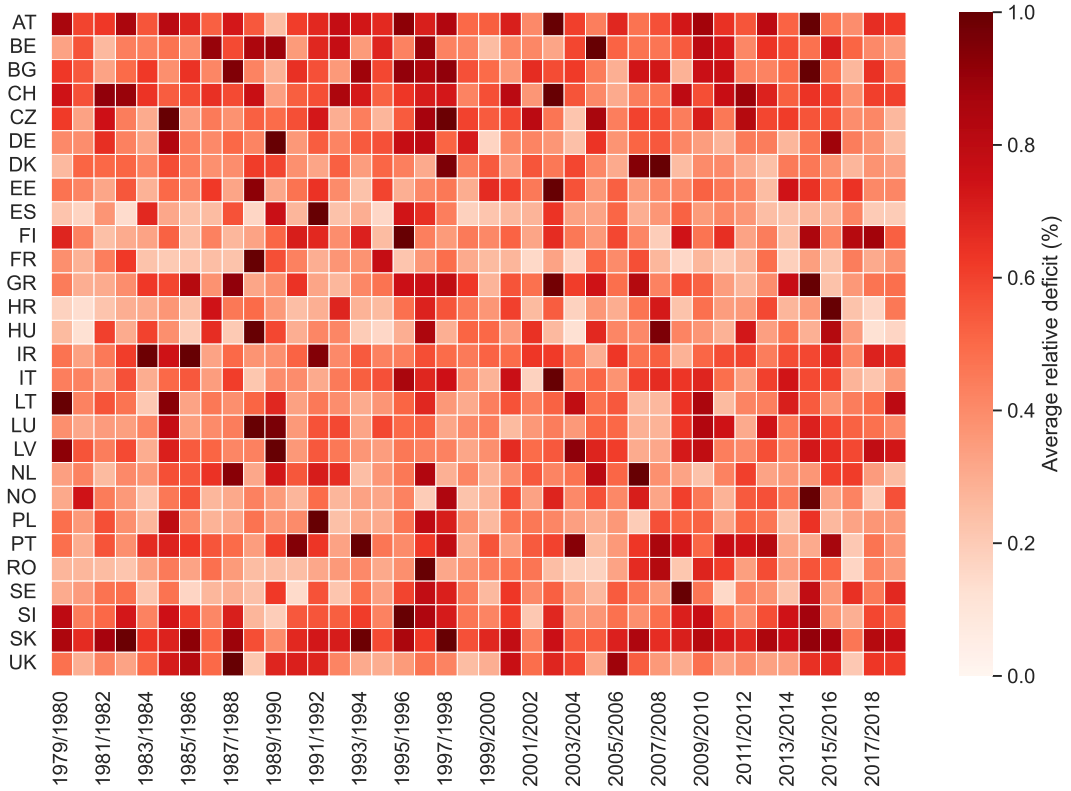

Figure 3.7: Year ranking of countries based on the single event with the highest capacity factor deficit, averaged over thresholds 0.2, 0.3, 0.4, 0.5, 0.6, and normalized by the highest deficit of each country.

CFD) reveal substantial variability within individual countries and across different countries. This variability is particularly pronounced when examining the single worst event, reflecting the irregular occurrence and distribution of extreme periods. For example, strong year-level correlations are observed in countries such as the Czech Republic, Germany, and Denmark in 1984-85 and 1995-96, or in Slovenia and Slovakia in 1987-88 and 2012-13. However, these patterns do not hold when examining the single worst period within each year. Overall, with the *Single-Event CFD* metric, many more years show values below 30% of the peak year compared with the analysis based on the *Cumulative CFD*.

3.2.2 Year Ranking at Weather Zone Level

Following the country-level analysis of weather variability, this section presents the results for weather zones, defined as the clusters of countries derived from the hierarchical clustering described in Section 3.1.6, based on correlations in their capacity factors.

This section examines the correlation of hourly capacity factors for wind, solar, and offshore wind across all EU countries using Pearson correlation coefficients. The analysis provides a preliminary step for identifying clusters within the capacity factor data, with each cluster representing a distinct weather zone. Correlations between solar, onshore wind, and offshore wind technologies are provided in the Appendix (Section A). Figure 3.8 shows the Pearson correlation coefficients of weighted capacity factors for these technologies across all studied countries.

Several regional groupings stand out: the Nordic countries of Norway, Sweden, and Finland share strong correlations in their capacity factor profiles, while Denmark shows noticeably weaker links to its northern neighbors, with its highest correlation being with Norway. In the British Isles, Ireland's capacity factors correlate mainly with the UK and remain low with the rest of Europe, whereas the UK itself exhibits slightly stronger correlations with the Benelux countries. The Benelux–Central Europe cluster, comprising the Netherlands, Belgium, Luxembourg, and Germany, displays uniformly high inter-correlations, although France shows relatively lower correlation values both within that group and across the continent. In the Baltic region, Latvia, Estonia, and Lithuania form a distinct cluster. This pattern is also observed among several Central and Eastern European countries. Generally, Western European and coastal nations exhibit lower correlations than more central, continental countries. Finally, Spain and Portugal form a tightly linked Iberian pair that is more loosely connected to the broader European network.

Based on the hierarchical clustering results described in Section 3.1.6, countries are grouped into clusters, and the weighted capacity factor data are averaged for each hour. For this calculation, the metrics are first computed individually for each threshold, and then averaged across the five analyzed thresholds. Using the aggregated cluster-level data, the *Dunkelflaute* event detection and year-ranking analysis are applied using the same two metrics as before: the *Cumulative CFD* and the *Single-Event CFD*.

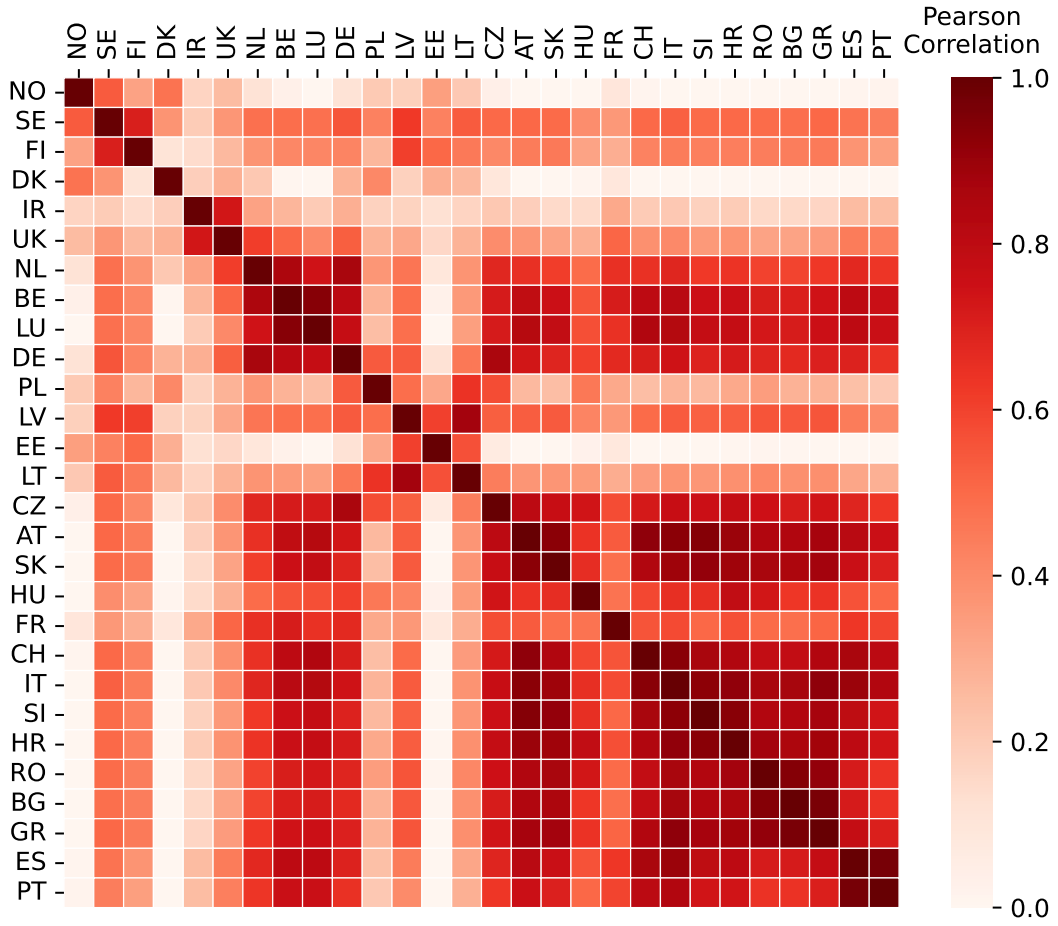

Figure 3.8: Weighted Capacity Factor Correlation Matrix for EU Countries, based on hourly data over one year.

Figure 3.9 (a) presents the year rankings for each cluster based on the *Cumulative CFD*. The analysis is performed across multiple threshold values: 0.25, 0.3, 0.4, 0.5, and 0.6 times the mean capacity factor of each cluster. In contrast to the country-level analysis, the threshold of 0.2 is not included here. This change is due to the smoothing effect introduced by averaging capacity factor values across all countries within each cluster. At this level of aggregation, no *Dunkelflaute* events are detected using a 0.2 threshold. For each threshold, the deficits are normalized by the maximum annual deficit observed within the cluster. The figure shows the average deficit for each year as a percentage of the maximum, allowing for a consistent comparison across clusters. The results indicate that, similar to the country-level analysis, the year rankings vary notably across clusters. In particular, Clusters 3 and 5 show higher variability in year-to-year *Cumulative CFD*, indicating more fluctuation in their *Dunkelflaute* severity over time. In contrast, other clusters, especially Clusters 2, 4, and 7, show less variability, with most years having cumulative deficits that lie relatively close to their respective maximum values. One year that stands out at the cluster level is 1996–97, which exhibits a high *Cumulative CFD* for most clusters, particularly Clusters 1, 2, and 3, while Cluster 5 is less affected. Interestingly, in the single-country analysis, 1995–96 showed higher deficits for most countries.

At the cluster level, however, 1996–97 appears more severe, highlighting that the timing and intensity of *Dunkelflaute* events depend on how the system is defined. Aggregating countries smooths some of the short-term or localized extremes observed at the national level, which can shift the identification of the worst years. Consequently, a year that is severe for an individual country may not stand out when countries are analyzed as part of a regional cluster, depending on how generation patterns interact across the group.

When analyzing the metric of the highest capacity factor deficit for the single most severe *Dunkelflaute* event within each year (*Single-Event CFD*), Figure 3.9 (b) shows that the spread of values across years is greater than for the annual *Cumulative CFD* metric discussed previously. This indicates that extreme single events are more variable in both timing and intensity across the clusters.

There is also notable variation between clusters in terms of which years exhibit the highest *Single-Event CFD*. The periods 1995-96 and 1996-97 show particularly high deficits for Clusters 2, 6, and 7. In contrast, the year 1989-90 records high deficits for Clusters 1, 4, and 7. Meanwhile, 1988-89 stands out for its relatively low CFD across several clusters, including Clusters 2, 3, 5, 6, 7, and 8. Overall, the results show a wide distribution of peak *Dunkelflaute* years, highlighting the high variability of these events across both time and regions.

When examining results for individual thresholds, especially higher ones, the year 1996-97 also emerges with a higher *Single-Event CFD* in Cluster 1. At lower thresholds, however, other years become more prominent in terms of the most severe single *Dunkelflaute* event.

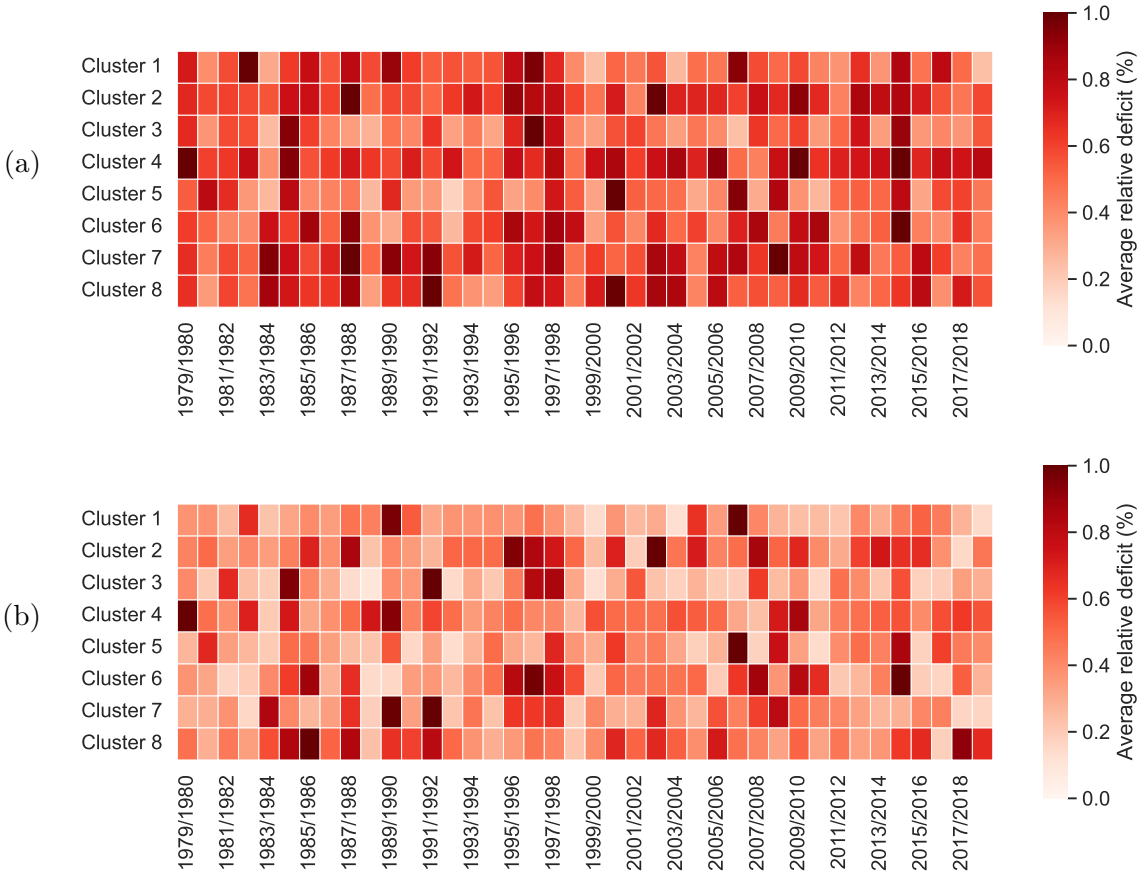

Figure 3.9: **(a)** Year ranking of clustered countries based on *Cumulative CFD*, averaged over thresholds 0.25, 0.3, 0.4, 0.5, 0.6, and normalized by the highest deficit of each cluster. **(b)** Year ranking of clustered countries based on *Single-Event CFD*, averaged over thresholds 0.25, 0.3, 0.4, 0.5, 0.6, and normalized by the highest deficit of each cluster.

3.2.3 Year Ranking at European Level

The results of the *Dunkelflaute* analysis are illustrated here for an aggregated zone that represents all European countries. The hourly capacity factor data from each country is weighted by its total installed capacity, creating a Europe-wide average profile. Using this aggregated dataset, the same analysis methods applied previously to individual countries and clusters are used.

The results for the *Cumulative CFD*, calculated in relation to this aggregated European system, are shown in Figure 3.10 (a). Among all years analyzed, 1996-97 stands out as having the highest *Cumulative CFD* when averaged across the selected thresholds of 0.35, 0.4, 0.5, and 0.6. This finding is consistent with previous studies in the literature [1], showing the significance of this year as a low-generation period at the European scale.

The year 1996-97 also stands out in the *Single-Event CFD* analysis, as shown in Figure 3.10 (b). In this case, another relevant year is 1989-90, with a similar value of average *Single-Event CFD*. When considering thresholds individually, the higher thresholds of 0.6 and 0.5 identify 1989-90 as the most critical period, whereas at lower thresholds of 0.4 and 0.35, 1996-97 corresponds to the most severe *Dunkelflaute* event. These results demonstrate that the identification of critical years depends on the threshold applied, reflecting differences in both the severity and duration of low renewable generation events.

3.3 Modeling and Analysis Workflow

Figure 3.11 presents the workflow followed in this thesis, including data preparation, model setup, optimization process, and results analysis.
The analysis begins with a dataset comprising historical hourly capacity factors for wind and solar energy over a 40-year period, spanning from July 1, 1979, to June 30, 2019. This dataset is then divided into 40 consecutive summer-to-summer periods, each with a duration of one year, ranging from 1979-80 to 2018-19. Based on these weather data, we identify *Dunkelflaute* events and perform a clustering of countries into weather zones. Subsequently, four cases, representing four different modeling approaches (described in Section 3.6), are considered for the system optimization, running a greenfield capacity expansion model for each of them. The resulting energy systems are then evaluated through simulations over the full dataset of 40 historical weather years to assess the long-term performance and reliability of each solution. Finally, the system costs and capacity mixes obtained from each Case are compared against one another and against a benchmark case based on a typical weather year.

3.4 Mathematical Model

The mathematical model used in this work is built upon the *Weather Uncertainty model* proposed by Forghani et al. [46], with some modifications. The entire model

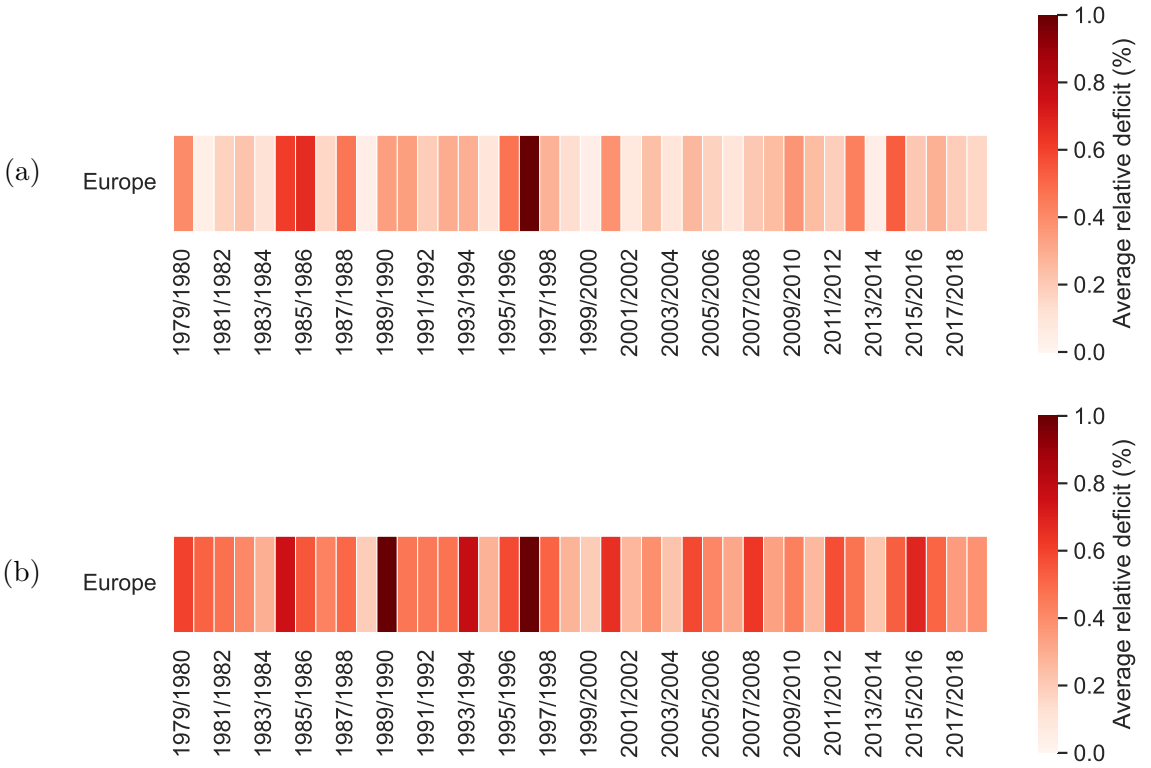

Figure 3.10: **(a)** Year ranking of one European cluster based on *Cumulative CFD*, averaged over thresholds 0.35, 0.4, 0.5, 0.6, and normalized by the highest deficit of each cluster.
(b) Year ranking of one European cluster based on *Single-Event CFD*, averaged over thresholds 0.35, 0.4, 0.5, 0.6, and normalized by the highest deficit of each cluster.

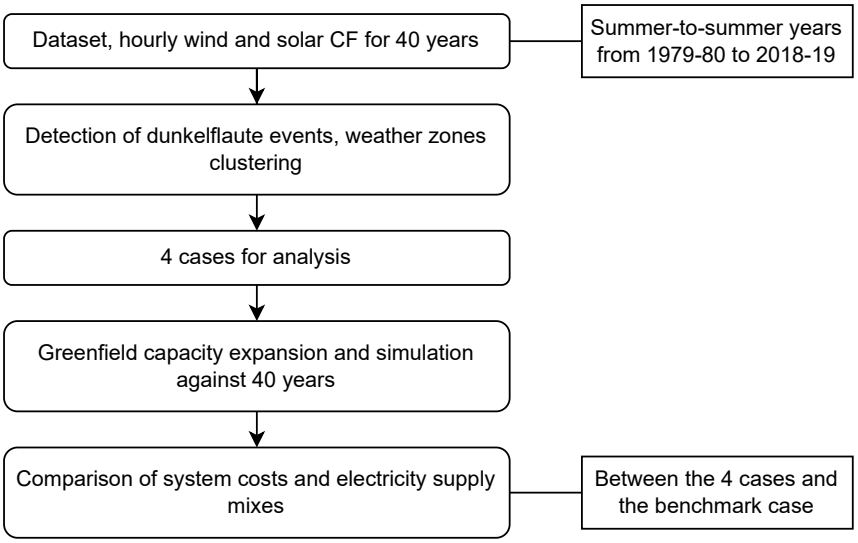

Figure 3.11: Overview of the methodological framework.

is divided into two frameworks, described in the following sections: the *Stochastic Optimization Model* and the *Simulation Model*. The model is implemented in the Julia programming language, and all optimization problems are solved using the Gurobi® Optimizer [64], with the barrier solver selected as the default.

3.4.1 Stochastic Optimization Model

The first is a greenfield cost optimization model for capacity investments and the dispatch of electricity generation, transmission, and storage. This framework optimizes decisions for both capacity expansion (generation and storage technologies, and transmission infrastructure) and operations (electricity generation, storage operation, and load shedding) across multiple scenarios. This type of mathematical model is typically used in long-term energy planning to determine the optimal mix of generation capacities and transmission layouts, guiding strategic investment decisions. The term "greenfield" refers to the model's assumption of no pre-existing infrastructure, starting from scratch, aiming for the optimal design of a completely new system. The only exception is related to the hydropower capacity. This type of technology is strongly bound to geographical conditions, and it is assumed that its potential capacity is already largely fully exploited. Therefore, in the model, the hydropower investments are fixed to the values taken from "ENTSO-E & ENTSOG TYNDP 2024 Scenarios" [50]. This is achieved by setting the hydropower investment costs to zero (see Appendix G) and capping the installed capacities at the specified values. Regarding the transmission investments, the constraints change depending on the transmission grid scenario adopted, as will be explained in Section 3.7.

To deal with the unserved load, the model allows load shedding. However, the shed load must not exceed 5% of the electricity load (at each timestep), and it is penalized in the objective function by a parameter called load shedding cost.

The main features of the model are described below.

Input:

- Wind and solar capacity factor hourly time series (for 40 weather years);
- Electricity demand hourly time series (for a single year);
- Hydropower inflow hourly time series (for a single year);
- Hydropower storage potential for each country;
- Cost and performance characteristics of the generation and storage technologies;
- Capacity potential of each technology for each country;
- Transmission network cost, valid links between countries, and maximum grid capacities (depending on the transmission grid scenario);
- Fuel prices (i.e., gas and nuclear);
- Policy constraint (i.e., carbon cap).

Optimization (objective function):

- Minimize the total cost of the system.

Outputs:

- System costs;

- Optimal mix of generation and energy storage technologies;
- Optimal configuration of the transmission network.

The in-depth description of the mathematical model, with its full list of parameters, decision variables, and constraints, is reported in Appendix C and D.

It should be noted that, for electricity demand, a single-year time series is used (corresponding to the summer-to-summer year 2022-23 [51]), rather than varying the load profile according to the weather year considered. This modeling choice is justified by the primary objective of this work, which is to investigate the influence of weather variability on system configuration, particularly through variations in solar and wind capacity factors. Therefore, even though the load may be affected by weather conditions, maintaining a consistent demand profile across all weather years allows for a clearer isolation and interpretation of the effects of renewable resource variability on system optimization outcomes.

3.4.2 Simulation Model

The *Simulation Model* is employed to evaluate the performance of the electricity system over a single selected weather year, using the installed capacities and transmission infrastructure resulting from the *Stochastic Optimization Model*. It is a deterministic optimization model that simulates system operations (specifically, electricity generation, storage operation, and load shedding) for a specific weather year under fixed capacity assumptions. This allows for a detailed assessment of how a given system configuration responds to different weather conditions.

While the model shares the same input structure as the *Stochastic Optimization Model*, it additionally requires the installed generation, storage, and transmission capacities as inputs. The objective remains the minimization of the total system cost. However, the metric "loss of load" is introduced to quantify unmet electricity demand (beyond load shedding) under the assumed system setup. This metric is penalized in the objective function by a "loss of load penalty" parameter (set at 100000 €/MWh), which significantly impacts the final total cost. As will be discussed later, the load-loss value provides valuable insights into the robustness and reliability of the energy system. Finally, the model provides detailed results on system performance and costs.

A comprehensive description of the model structure is provided in Appendix E.

3.5 Case Study

The generation technologies included in the system are the following:

- Solar Photovoltaics, both utility-scale and rooftop;
- Wind turbines, including onshore and offshore installations;
- Hydrogen gas turbines;
- Hydropower, comprising reservoir, run-of-river, and pumped storage;
- Nuclear power;
- Natural gas turbines.

On the storage side, the model incorporates batteries, hydrogen storage tanks, and hydropower reservoirs, the latter of which are modeled using historical water inflow data [50]. Regarding energy consumption, the model focuses exclusively on electricity demand, while other sectors (e.g., heating, transport, industry) are excluded to maintain a manageable level of complexity and computational feasibility. A schematic of the electricity system and the interactions between the technologies is shown in Figure 3.12.

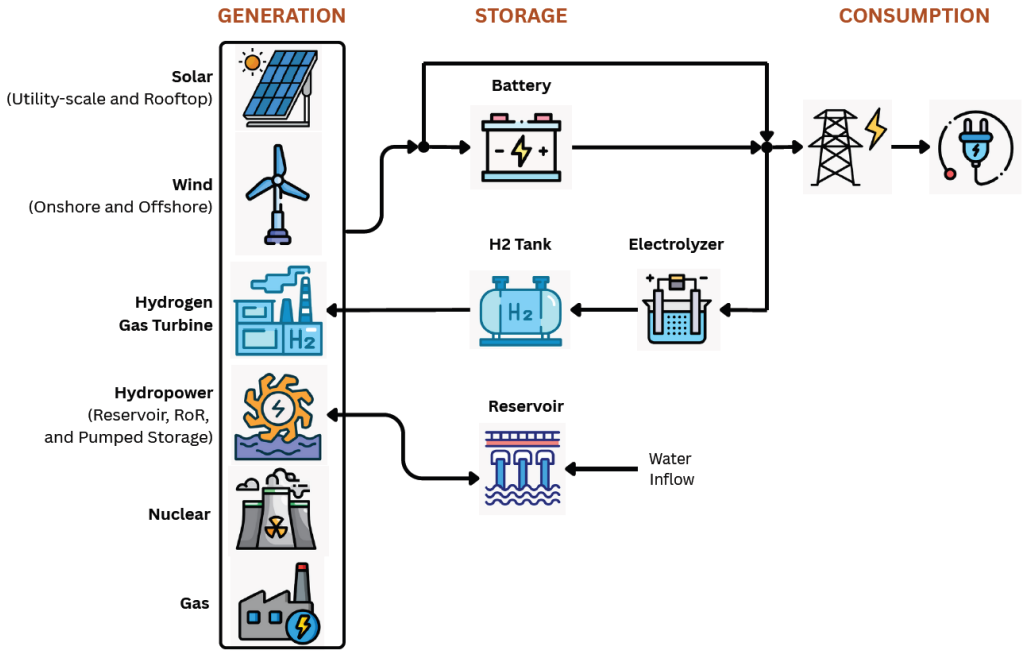

Figure 3.12: Schematic of the electricity system and technologies interactions.

Compared to the original model developed by Forghani et al. [46], several modifications and extensions were introduced in this work. Notably, additional technologies were implemented, including rooftop solar, offshore wind, hydrogen gas turbines (along with electrolyzers and hydrogen storage tanks), run-of-river hydropower, and pumped storage hydropower. Another key difference lies in the adopted carbon pricing tool. In the original model, a carbon tax was incorporated into the objective function to penalize CO_2 emissions. In contrast, this work adopts a carbon cap approach by imposing a direct constraint on total emissions. In particular, total CO_2 emissions must remain below 10 gCO_2 per kWh of satisfied load (i.e., total demand minus total load shedding). This specific limit on carbon intensity can be used to effectively represent a clean or near-zero emission power sector. A carbon cap is particularly valuable in scenarios aiming to meet stringent climate targets (such as 1.5°C or 2°C pathways), as it ensures a hard limit on emissions, which a carbon tax alone may not guarantee. Finally, the geographical scope of the model has been significantly expanded. While the original study focused solely on northern Europe, the current work comprises a broader set of countries, covering most of the European continent. The model now includes 28 nodes that represent all countries in the European Union (except the Republic of Cyprus and Malta), as well as the

United Kingdom, Norway, and Switzerland.

The model adopts a time step of 7 hours, resulting in approximately 1250 time steps per year. This time resolution provides a practical compromise between modeling accuracy and computational efficiency, as suggested in Forghani et al. [46]. All input hourly time series (i.e., electricity demand, wind and solar CF, and hydropower inflows) are defined over summer-to-summer periods to more effectively capture the most critical *Dunkelflaute* events. Since the most severe weather periods typically occur during the winter months [2], adopting a summer-to-summer timeframe ensures that these events are fully captured within a single analysis period. This approach avoids the risk of splitting them across two separate years, which could otherwise compromise the accuracy of the system performance evaluation.

3.6 Modeling Approaches

In this study, four distinct modeling approaches (referred to as "cases") are analyzed to evaluate the impact of different methodological choices on system design and performance. These cases are ultimately compared against a benchmark case. A summary of the key characteristics of the four cases, along with the benchmark, is provided in Table 3.2.

Table 3.2: Overview of the four modeling approaches (cases) considered, along with the benchmark case

Case	Modeling Approach	Optimization Method	No. Scenarios
1	Worst weather year for Europe	Deterministic optimization	1
2	Worst weather year for each weather zone	Stochastic optimization	At most 8
3	Worst weather year for each country	Stochastic optimization	At most 28
4	40 weather year scenarios	Stochastic optimization	40
Benchmark	Typical weather year for Europe	Deterministic optimization	1

Case 1 applies a deterministic optimization approach, in which the system is optimized using wind and solar capacity factors corresponding to the worst weather year for Europe. Case 2 adopts a stochastic optimization approach, incorporating the worst weather year for each weather zone. As there are eight identified weather zones, the model includes up to eight scenarios. If multiple zones share the same worst year, the total number of scenarios is reduced accordingly. Case 3 extends the stochastic approach to a finer spatial resolution by considering the worst weather year for each country, resulting in up to 28 scenarios (one per country). Case 4 represents a fully stochastic approach, accounting for all 40 weather years, each treated as an independent scenario. The benchmark case, on the other hand, employs a deterministic optimization using wind and solar capacity factors from a typical weather year for Europe, providing a point of reference for evaluating the alternative modeling strategies.

It is worth noting that deterministic optimization refers to a specific case of the *Stochastic Optimization Model*, in which a single scenario with unitary probability is used. Moreover, within the stochastic approach, equal probabilities are assigned to all scenarios due to the difficulty of accurately estimating a representative probability distribution for each weather year.

3.7 Transmission Grid Scenarios

In order to understand and quantify the influence of the geographical balancing effect, three transmission grid scenarios are evaluated, namely:

- 2025 Reference Grid (or 2025 Grid);
- 2040 Reference Grid (or 2040 Grid);
- Unconstrained Grid.

In all of the above-mentioned scenarios, the transmission network capacities are optimized by the model. However, they differ in whether a limit is imposed on the interconnections between countries. In particular, the first two scenarios include upper bounds on the transmission line capacities, based on the 2025 and 2040 reference grids, respectively. These data are taken from Ember's Europe Electricity Interconnection Data Tool [52]. The third scenario, referred to as "Unconstrained Grid", represents a system without transmission capacity limits.

3.8 Typical Weather Year for Europe

To identify the typical weather year for Europe, a ranking of weather years is performed based on the total cost (TC) of the resulting energy systems. This typical year is required in Section 4.2, as it serves as the reference year for evaluating the deterministic benchmark case (see Section 3.6). All available weather years are individually analyzed by performing a deterministic optimization for each year, evaluating the total system costs. The typical weather year is determined as the one for which the resulting total system cost is closest to the average value obtained across all single-year deterministic optimizations. In addition, to support the weather data analysis, the worst weather year is also identified. Given the model setup, where the only input varying across years is the time series of wind and solar capacity factors, a higher system cost reflects a lower availability of renewable resources, often due to extended *Dunkelflaute* events or generally below-average wind and solar generation. Consequently, the year associated with the highest total system cost is expected to be identified as the worst weather year. This sensitivity analysis is conducted for each transmission grid scenario (see Section 3.7), resulting in distinct outcomes depending on the grid configuration.

The TC year ranking related to the 2025 Reference Grid is shown in Figure 3.13. The typical weather year for Europe is identified as 1997-98, which returns a total system cost of €104.8 billion, the value closest to the average across all deterministic optimizations (equal to €104.6 billion). The worst weather scenario corresponds to

the summer-to-summer year 1996-97, yielding an energy system with a total cost of €111.3 billion.

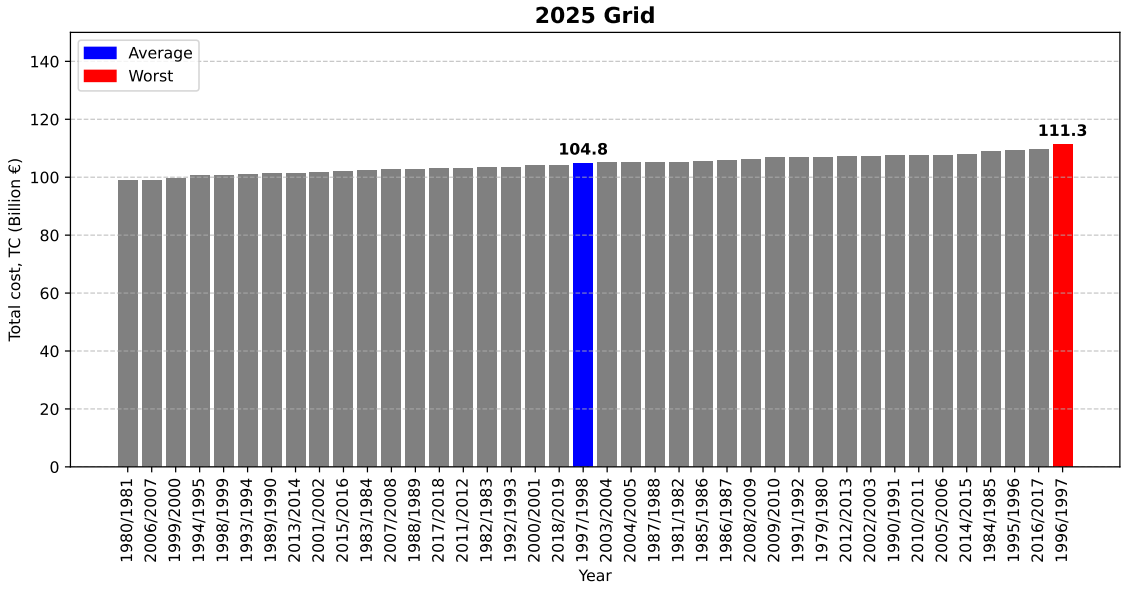

Figure 3.13: Ranked total system costs (in billion of €) resulting from deterministic optimization for each of the 40 weather years, under the 2025 Reference Grid scenario.

Considering the 2040 Reference Grid, the total cost bar chart of the 40 years is illustrated in Figure 3.14. The ranking is similar to that of the 2025 grid's scenario, with 1996-97 as the worst year (TC equal to €105.7 billion). In this case, the average scenario is represented by the year 2000-01, with a system total cost of €99.2 billion.

Analyzing the transmission grid scenario without limits on transmission capacity (Unconstrained Grid) reveals more changes in the weather year ranking, as shown in Figure 3.15. The worst weather year is 1995-96, which leads to an energy system characterized by a total cost of €94.7 billion. The typical weather year, instead, is 2004-05 with a system total cost of €89.3 billion. Notably, the year 2004-05 consistently yields a total system cost that is among the closest to the average across all three transmission grid scenarios. For this reason, it is selected as the typical weather year.

The total cost values clearly indicate that optimized systems without constraints on transmission grid capacities are significantly less costly than those with imposed upper limits. This behavior highlights the critical role and advantages of cross-border interconnections.

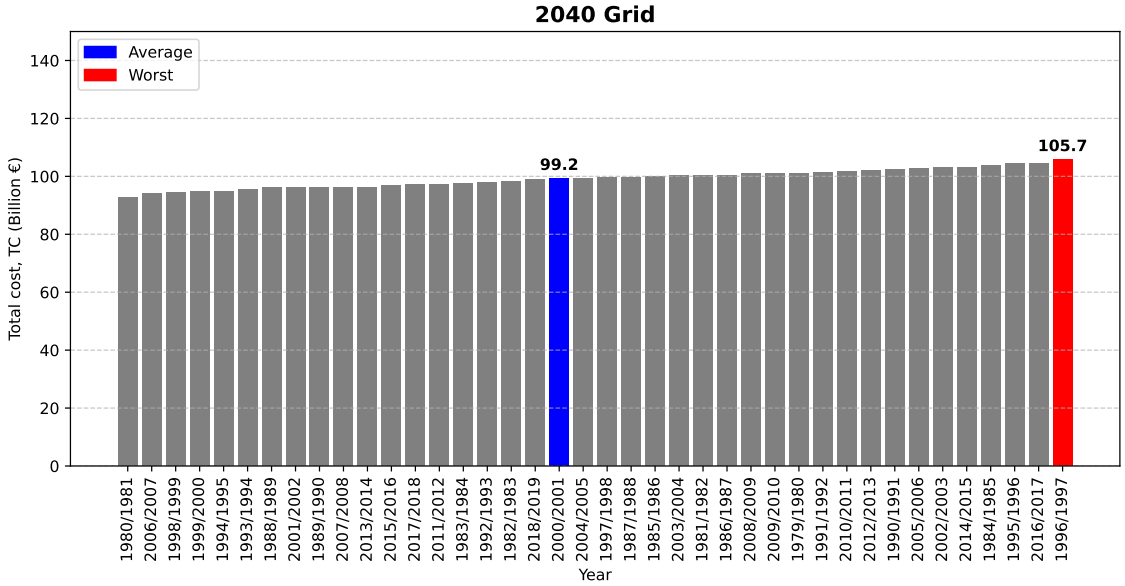

Figure 3.14: Ranked total system costs (in billion of €) resulting from deterministic optimization for each of the 40 weather years, under the 2040 Reference Grid scenario.

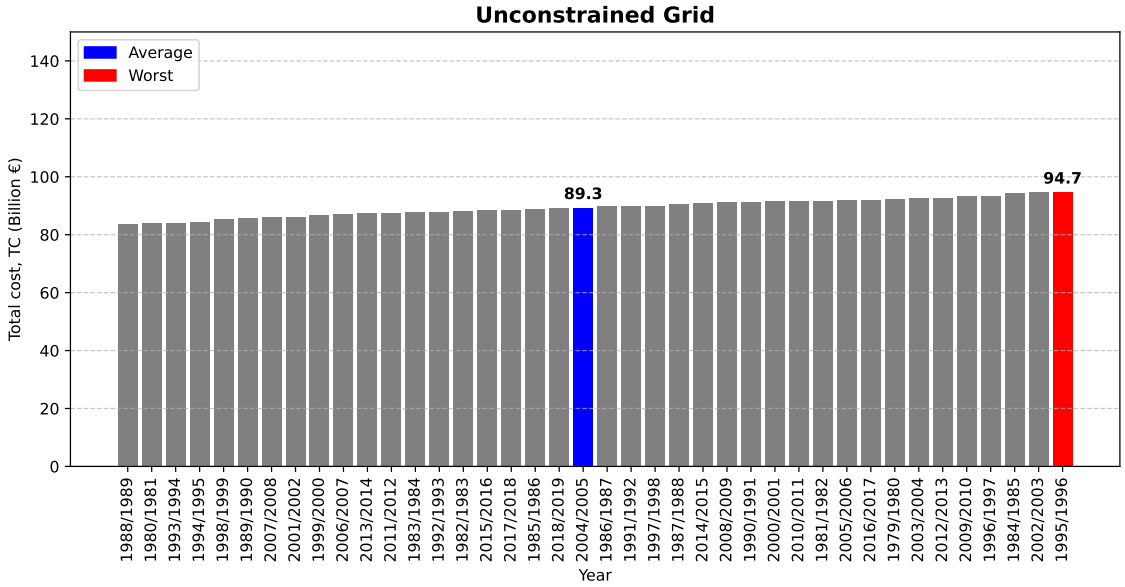

Figure 3.15: Ranked total system costs (in billion of €) resulting from deterministic optimization for each of the 40 weather years, under the Unconstrained Grid scenario.

4

Results

Building on Chapter 3, which introduced the approaches for ranking weather years and detecting Dunkelflaute events, this section presents the results of applying these methods to the energy system modeling. In Section 4.1, the selection of a suitable metric-threshold approach for detecting the worst weather years is introduced. Finally, in Section 4.2, the results of the energy system model for the analyzed cases are presented under the three transmission grid scenarios, along with comparisons of system costs and capacity mixes.

4.1 Selection of the Metric-Threshold Approach for Detecting the Worst Weather Years

The optimization cases analyzed in this work (presented in Section 3.6) require identifying the worst weather years at three spatial levels: European, weather zone, and country level. The worst year for Europe will be used in a deterministic optimization (Case 1), while the worst years for the weather zones and the countries (Cases 2 and 3) will be incorporated as scenarios in the *Stochastic Optimization Model* (Section 3.4.1) with the aim of improving the robustness of the energy system design. To select the most critical weather years, several approaches are compared for detecting periods of low variable renewable energy (VRE) generation within a year. We analyze two distinct metrics for detecting Dunkelflaute events: the *Cumulative CFD* and the *Single-Event CFD* (described in Section 3.1.5). Since both metrics rely on a threshold value, multiple thresholds are considered in the analysis. As a result, the identification of the worst weather years varies depending on the combination of metric and threshold applied. The ultimate objective of this section is to identify the combination of metric and threshold that yields the most extreme weather years in terms of unfavorable conditions for wind and solar generation.

To evaluate each combination and select the most relevant one, we examine the resulting total system cost (TC) obtained from the energy system optimization using the selected weather years. A higher system TC indicates that the selected years have a greater impact on system design and cost, thus representing more critical conditions. Therefore, the most accurate and relevant Dunkelflaute detection approach, defined as a specific combination of metric and threshold, is considered to be the one that results in the highest system TC. The transmission grid scenario chosen for this step, as a common basis, is the 2025 Reference Grid (see Section 3.7).

The analysis of Europe as a single cluster leads to the results provided in Table 4.1. The worst years were identified from the weather data analysis (in Section 3.2.3), whereas the total cost value (TC) is given by optimizing the energy system for the selected year. For both metrics, the threshold value was varied from 0.35 to 0.6 of the mean VRE capacity factor. The minimum threshold was set to 0.35 as no extreme events were detected below this value. Conversely, the maximum threshold was set at 0.6, since higher values failed to capture Dunkelflaute events and instead only identified periods of moderately below-average VRE generation.

As will be shown later, the minimum threshold tends to decrease when considering smaller spatial clusters, such as weather zones or individual countries. This behavior highlights the relevance of the balancing effect across countries within larger clusters, which helps smooth out periods of low availability of renewable energy through geographical diversification.

At the European level, most combinations of metric and threshold yielded 1996-97 as the worst year, resulting in the same system TC, which also corresponds to the highest observed TC. Consequently, it is not possible to distinguish which combination is most effective for identifying extreme weather years at the continental scale. However, it is important to note that the *Single-Event CFD* metric with thresholds above 0.4 (i.e., 0.5 or 0.6) were the only combinations that failed to capture the year associated with the highest TC. Therefore, these options are not considered valid approaches for detecting Dunkelflatue periods.

Table 4.1: Worst weather years and corresponding total system costs (TC) based on different combinations of metrics and thresholds at the European level. The ranking is based on TC. The highest TC is highlighted in orange, and the corresponding year is highlighted in yellow.

Metric	Threshold	Worst Year	TC (M€)	Ranking
Cumulative CFD	0.35	1996-97	111262	1
	0.4	1996-97	111262	1
	0.5	1996-97	111262	1
	0.6	1996-97	111262	1
Single-Event CFD	0.35	1996-97	111262	1
	0.4	1996-97	111262	1
	0.5	1989-90	101328	2
	0.6	1989-90	101328	2

Concerning the weather zone level, the threshold varies from 0.25 to 0.6. For each combination of metric and threshold, the weather data analysis yielded the worst year for each cluster (weather zone), resulting in eight years. These years are reported in Table 4.2, and are used as scenarios for stochastic optimization, leading to a model with at most eight scenarios. The number of scenarios can be lower if different clusters share the same worst year. For example, Table 4.2 shows that the *Cumu-*

lative CFD-0.25 combination yields 7 scenarios, whereas the *Single-Event CFD*-0.6 combination yields only 6 scenarios. By running the stochastic optimization for each group of worst years, we then obtain the total system cost for each combination of metric and threshold, reported in Table 4.2.

As mentioned above, the highest TC is used as the selection criterion, as it identifies the most effective approach (metric and threshold) to detect adverse weather conditions. The highest value is highlighted in the table and corresponds to the *Cumulative CFD* metric with a threshold of 0.3.

Table 4.2: Worst weather years and corresponding total system costs (TC) identified for each weather zone using different combinations of metrics and thresholds. The ranking is based on TC. The highest TC is highlighted in orange, and the corresponding set of years is highlighted in yellow.

Metric	Cumulative CFD					Single-Event CFD				
Threshold	0.25	0.3	0.4	0.5	0.6	0.25	0.3	0.4	0.5	0.6
Cluster 1	2006-07	1982-83	1996-97	1995-96	1995-96	2006-07	2006-07	2006-07	2004-05	2004-05
Cluster 2	2002-03	2002-03	1987-88	1984-85	1984-85	2002-03	1992-93	1997-98	2002-03	2013-14
Cluster 3	1997-98	1996-97	2012-13	1984-85	1982-83	1981-82	1991-92	1991-92	1984-85	1996-97
Cluster 4	2014-15	2014-15	1979-80	1997-98	2000-01	2009-10	1989-90	1978-79	1988-89	1988-89
Cluster 5	2006-07	2016-17	1980-81	1984-85	1984-85	2006-07	2016-17	1997-98	2014-15	2006-07
Cluster 6	1985-86	1987-88	1987-88	1987-88	1987-88	1985-86	2009-10	1996-97	2014-15	1996-97
Cluster 7	2008-09	1991-92	1996-97	2003-04	1986-87	2002-03	1991-92	1991-92	1989-90	1996-97
Cluster 8	1991-92	1991-92	2000-01	2000-01	2000-01	1985-86	1985-86	2017-18	2018-19	2002-03
TC (M€)	107320	110280	109995	108859	108844	106750	108243	109745	108060	109480
Ranking	9	1	2	5	5	10	7	3	8	4

The same steps were performed at the country level, selecting the worst years for each country from the weather data analysis and using them as scenarios for the stochastic optimization. In this case, since the model includes 28 countries, each metric-threshold combination results in a set of 28 worst weather years (one for each country), leading to a maximum of 28 scenarios (as previously discussed in the weather zone level analysis). Table 4.3 presents the worst years identified for each country across all metric-threshold combinations, along with the corresponding total system costs obtained from the optimization results.

Even at the country level, the highest system's total cost results from the optimization based on the years identified using the *Cumulative CFD* metric with a threshold of 0.3. This combination is therefore selected for identifying extreme weather events for the subsequent analysis (Section 4.2).
It is also noteworthy that, in both cases - at the weather zone and country levels - the second-highest total system cost is associated with the *Cumulative CFD* with a threshold of 0.4. As a result, the optimal threshold lies between 0.3 and 0.4, depending on the spatial scale of the cluster. In general, for larger clusters, a threshold of 0.4 is more appropriate due to the smoothing effect of geographic aggregation, while for smaller clusters, a threshold of 0.3 provides a more accurate identification of extreme conditions.

Table 4.3: Worst weather years and corresponding total system costs (TC) identified for each country using different combinations of metrics and thresholds. The ranking is based on TC. The highest TC is highlighted in orange, and the corresponding set of years is highlighted in yellow.

Metric	Cumulative CFD					Single-Event CFD				
Threshold	0.2	0.3	0.4	0.5	0.6	0.2	0.3	0.4	0.5	0.6
NO	2000-01	2000-01	2000-01	1980-81	1980-81	2014-15	2014-15	1997-98	1980-81	2008-09
SE	2008-09	2000-01	1984-85	1984-85	1997-98	1996-97	2008-09	2008-09	2008-09	1997-98
FI	2017-18	1979-80	1979-80	1979-80	1979-80	2016-17	2017-18	1995-96	1995-96	1995-96
DK	1981-82	1984-85	1995-96	1995-96	1985-86	2007-08	2007-08	2006-07	2006-07	1997-98
IE	1991-92	2005-06	1983-84	1983-84	1983-84	1985-86	1991-92	1985-86	1983-84	2018-19
UK	1987-88	1991-92	2000-01	2000-01	2000-01	2005-06	2005-06	1987-88	2018-19	2002-03
NL	1996-97	1995-96	1995-96	1995-96	1996-97	2006-07	2006-07	2006-07	1987-88	2004-05
BE	1991-92	1996-97	1991-92	1991-92	1995-96	1989-90	1986-87	2004-05	2009-10	1988-89
LU	1988-89	1988-89	1988-89	1984-85	1984-85	1989-90	1989-90	1989-90	1988-89	1988-89
DE	1984-85	1995-96	1995-96	1995-96	1995-96	1989-90	1989-90	1989-90	1984-85	1996-97
PL	2009-10	1996-97	2012-13	2012-13	2012-13	1991-92	1991-92	1991-92	1991-92	1996-97
LV	2009-10	1979-80	2000-01	2000-01	2000-01	1989-90	1989-90	1989-90	2017-18	2008-09
EE	1979-80	1979-80	1979-80	2015-16	1979-80	1986-87	1988-89	1988-89	2002-03	1999-00
LT	2005-06	2005-06	1984-85	2005-06	2005-06	1979-80	1979-80	1979-80	1984-85	1984-85
CZ	1984-85	2012-13	2012-13	2000-01	2000-01	1984-85	1997-98	1997-98	1984-85	1996-97
AT	2002-03	2002-03	2012-13	2012-13	1979-80	1997-98	2014-15	1995-96	2002-03	2002-03
SK	2009-10	2015-16	2017-18	2012-13	1979-80	1997-98	1993-94	2012-13	1987-88	2012-13
HU	2001-02	2015-16	2015-16	1988-89	1989-90	2007-08	1988-89	1988-89	1988-89	1996-97
FR	1988-89	1988-89	1979-80	1987-88	1988-89	1988-89	1994-95	1988-89	1989-90	1988-89
CH	2002-03	1982-83	1982-83	2000-01	1982-83	1991-92	2002-03	1981-82	2002-03	2002-03
IT	2002-03	2002-03	1985-86	1984-85	1984-85	1997-98	2002-03	2014-15	2002-03	1987-88
SI	2012-13	2012-13	2012-13	1979-80	1979-80	2014-15	1995-96	1995-96	2013-14	1979-80
HR	1997-98	2015-16	2015-16	2015-16	2015-16	2000-01	1992-93	2015-16	2015-16	2015-16
RO	2007-08	2009-10	1987-88	1987-88	1995-96	1996-97	1996-97	2007-08	1996-97	1996-97
BG	2010-11	1987-88	1987-88	1987-88	1987-88	1993-94	2009-10	2014-15	2014-15	1996-97
GR	2002-03	1997-98	1987-88	1983-84	1983-84	1985-86	2014-15	2014-15	2014-15	1995-96
ES	1991-92	1987-88	1996-97	2003-04	1979-80	1995-96	1989-90	1991-92	1989-90	1996-97
PT	2012-13	2012-13	2012-13	2003-04	1987-88	2015-16	2007-08	1990-91	1983-84	2003-04
TC (M€)	109346	109818	109654	108617	109424	109391	109191	108451	109232	109608
Ranking	6	1	2	9	4	5	8	10	7	3

4.2 Energy System Model Results

The four cases described in Section 3.6 are evaluated using the selected approach for identifying the worst years, namely, the *Cumulative CFD* metric with a threshold of 30% of the mean VRE capacity factor. For each Case, the capacity expansion model is run under the given scenario assumptions, yielding a system with optimal investment decisions. The resulting system, with fixed investment capacities, is then simulated across 40 historical weather years. Each simulation returns, among other results, the total system cost (Simulation TC) and the corresponding loss of load value.

4.2.1 Robustness Evaluation Criteria

The main criterion used to assess the robustness of each system configuration is the average Loss of Load across all 40 simulated weather years. Loss of load is introduced in the *Simulation Model* as a metric to represent situations in which the system is unable to meet electricity demand, even through load shedding. This metric indicates a risk of service interruptions, such as brownouts or blackouts [46].
In the event that two or more capacity mixes exhibit similar average load-loss values, the evaluation proceeds by considering the following secondary metrics:

- The average total cost across all simulations (Average Simulation TC)
- The highest total cost among all simulations (Worst-Case Simulation TC)

In particular, if the average total costs are also similar, the final selection is based on the minimum worst-case total cost. Specifically, when energy systems show comparable average load-loss and Average Simulation TC, the solution with the lower worst-case simulation TC is preferred, even if it comes at the expense of a slightly higher Average Simulation TC.

4.2.2 Model Results for the 2025 Reference Grid

Firstly, the 2025 Reference Grid scenario is analyzed. To identify the worst weather year in Europe (Case 1), the weather data analysis, based on the *Cumulative CFD* metric with a threshold of 0.3, yields the summer-to-summer period 1996-97 as the most unfavorable year (see Table 4.1). This selection is consistent across all transmission grid scenarios. Regarding the weather zone level (Case 2), the eight worst years resulting from the weather data analysis are highlighted in Table 4.2. Since the year 1991-92 is present twice, the stochastic optimization will eventually include seven different scenarios. For Case 3 (i.e., "worst weather year for each country"), although there are 28 countries, the number of distinct scenarios is 15, since some countries share the same worst weather years. Finally, the results for the four cases are presented in Table 4.4.
The "Optimization TC" column reports the total system cost obtained from the capacity expansion optimization using the *Stochastic Optimization Model*. The subsequent three columns present performance metrics derived from the 40 deterministic simulations performed using the *Simulation Model*: the average total cost across all simulations, the worst-case total cost, and the average loss of load.

Table 4.4: Optimization and simulation results for the analyzed cases under the 2025 Reference Grid scenario.

Case	Modeling Approach	No. Scenarios	Optimization TC (M€)	Average Simulation TC (M€)	Worst-Case Simulation TC (M€)	Average Load-Loss (TWh)
1	Worst weather year for Europe (1996-97)	1	111262	110804	115234	0.0104
2	Worst weather year for each weather zone	7	110280	110000	115627	0.0055
3	Worst weather year for each country	15	109818	108983	120188	0.0002
4	40 weather year scenarios	40	108882	108882	123337	0
Benchmark	Typical weather year for Europe	1	105097	145385	1067438	0.2526

As the number of scenarios included in the optimization increases, the following outcomes are observed.

- The Optimization TC and the Average Simulation TC decrease.
- The Worst-Case Simulation TC increases.
- The Average Load-Loss decreases.

Examining the results of the benchmark case, it is evident that neglecting weather uncertainty during system optimization, by relying solely on average weather conditions, leads to a lower total system cost (Optimization TC). This outcome is primarily driven by reduced upfront investments and fixed costs, as will be demonstrated in Table 4.5. However, this cost reduction comes at the expense of system robustness. The benchmark case exhibits a significantly higher Average Simulation TC when evaluated across all possible weather conditions, as well as an extremely high Worst-Case Simulation TC. These outcomes are largely attributed to substantial levels of load-loss and load shedding, indicating frequent instances of unmet demand.
Excluding the benchmark case, Case 4, which includes 40 scenarios, yields the lowest Optimization TC among the four analyzed cases. Specifically, rather than focusing on a single worst-case scenario, stochastic optimization distributes system investments across a broad range of weather conditions. This diversification allows the model to identify a cost-efficient capacity mix that performs well across all scenarios. By incorporating a larger number of scenarios, the model accounts for a wider range of variability. As a result, the total system cost of Case 4 is lower than that of the deterministic model based on the worst-case weather year (Case 1) and also lower than those of the other cases with fewer scenarios (Cases 2 and 3).

As discussed in Section 4.2.1, the Average Load-Loss and the Average Simulation TC are key parameters considered to evaluate the robustness of the energy system. These metrics indicate that the system is sufficiently robust to meet demand in different weather conditions, without resulting in extremely high costs. Analyzing these metrics, we can assume that the most robust energy system is the one resulting from the stochastic optimization with 40 scenarios (Case 4). However, Case 4 leads to the highest Worst-Case Simulation TC. This outcome can be attributed to the

following considerations:

- The optimization model is designed to minimize the overall system total cost (Optimization TC), rather than the worst-case simulation cost across the 40 weather-year simulations.
- Although no loss of load occurs in Case 4, the system relies more heavily on load shedding compared to the other solutions. In fact, it exhibits the highest amount of shedded load among the four evaluated cases, as shown later in Table 4.5. Since load shedding is penalized through an additional cost term in the objective function, this finally contributes to a higher worst-case simulation cost.

The highest shedded load can be explained by examining the installed capacities of Case 4 (shown in Figure 4.1). This case results in the lowest level of installed dispatchable capacity (Gas and Nuclear), heavily relying on renewable technologies and battery storage. On the other hand, since the model in this case has access to the full set of weather conditions information (40 scenarios), the resulting capacity mix is optimized to be just sufficient to avoid loss of load, explaining its greater reliance on load shedding.

The different systems' costs derived from the 40 simulations (average values), for each case, are shown in Table 4.5. Another comparison is made with the total installed capacity, for both generation and storage technologies, to investigate the differences in capacity mixes between the various approaches, and the values are reported in Appendix H (Table H.1). The four analyzed cases are compared to the benchmark case, which corresponds to the deterministic optimization based on a typical weather year (i.e., with average weather conditions). As discussed in Section 3.8, the typical weather year chosen for Europe, for all transmission grid scenarios, is the summer-to-summer period 2004-05. Figure 4.1 presents a graphical representation of the relative difference in system costs and installed capacities of the solutions from each analyzed case compared to that of the benchmark case.

Table 4.5: Comparison of average system costs (in M€), based on the results from 40 simulations, across the different cases under the 2025 Reference Grid scenario.

Average System Costs (M€) - 2025 Grid					
Cost	**Benchmark**	**Case 1**	**Case 2**	**Case 3**	**Case 4**
Investment and Fixed Cost	96810.4	101485.0	101604.6	101203.8	100976.6
Operational Cost	7774.4	8183.6	7747.0	7389.7	7270.6
Loss of Load	25255.7	1036.7	551.1	15.1	0
Load Shedding	15544.6	98.8	97.5	374.6	635.1

Regarding the capacity mix, when contrasted with the benchmark case, the following trends are observed in the four cases:

- Lower installed gas capacity across all cases.
- Similar wind capacity, with only marginal deviations.
- Reduced investments in PV technologies, although this difference gradually decreases from Case 1 to Case 4.

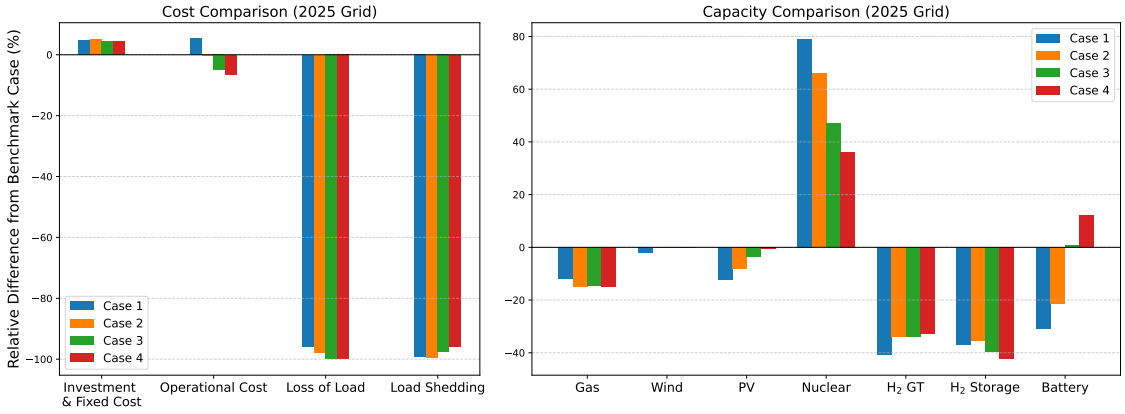

Figure 4.1: Relative differences (%) in system costs (on the left) and installed capacities (on the right) for the four analyzed cases compared to the benchmark case, under the 2025 Reference Grid scenario.

- Significantly higher nuclear capacity; the difference progressively reduces from Case 1 to Case 4.
- Lower investments in hydrogen technologies and battery storage, with the exception of:
  - Case 3, which shows a minimal increase in battery capacity.
  - Case 4, where battery investments increase by almost 15%.

4.2.3 Model Results for the 2040 Reference Grid

The results for all the examined cases with the 2040 Reference Grid are reported in Table 4.6. The outcomes exhibit the same trends compared to those of the 2025 Reference Grid, but in this case, the worst-case simulation TC does not show a clear behavior based on the number of scenarios.

Table 4.6: Optimization and simulation results for the analyzed cases under the 2040 Reference Grid scenario.

Case	Modeling Approach	No. Scenarios	Optimization TC (M€)	Average Simulation TC (M€)	Worst-Case Simulation TC (M€)	Average Load-Loss (TWh)
1	Worst weather year for Europe (1996-97)	1	105711	104394	112415	0.0023
2	Worst weather year for each weather zone	7	104761	104023	108345	0.0014
3	Worst weather year for each country	15	104316	103597	110381	0
4	40 weather year scenarios	40	103492	103492	115863	0
Benchmark	Typical weather year for Europe	1	99409	147671	1199083	0.284

The cost comparison, resulting from the simulations' results, is summarized in Table 4.7, and the different capacity mixes are presented in Appendix H (Table H.2). Figure

4.2 shows the percentage differences in the costs and capacity mixes of the four cases compared to those of the benchmark case.
Concerning the relative differences in installed capacity, the 2040 Grid scenario exhibits general trends consistent with those observed in the 2025 Grid case. The only distinction regards nuclear capacity, with an even more pronounced relative increase occurring at the expense of hydrogen technologies. However, it is noteworthy that, despite this increase in relative difference, the absolute differences in installed capacities are similar to those observed in the 2025 Grid scenario (see Tables H.1 and H.2).

Table 4.7: Comparison of average system costs (in M€), based on the results from 40 simulations, across the different cases under the 2040 Reference Grid scenario.

Average System Costs (M€) - 2040 Grid					
Cost	**Benchmark**	**Case 1**	**Case 2**	**Case 3**	**Case 4**
Investment and Fixed Cost	92048.4	97061.2	97421.4	97384.4	96716.4
Operational Cost	6594.0	6889.4	6355.0	6028.0	6004.3
Loss of Load	28404.8	233.1	139.4	0	0
Load Shedding	20624.0	210.1	107.6	184.9	771.3

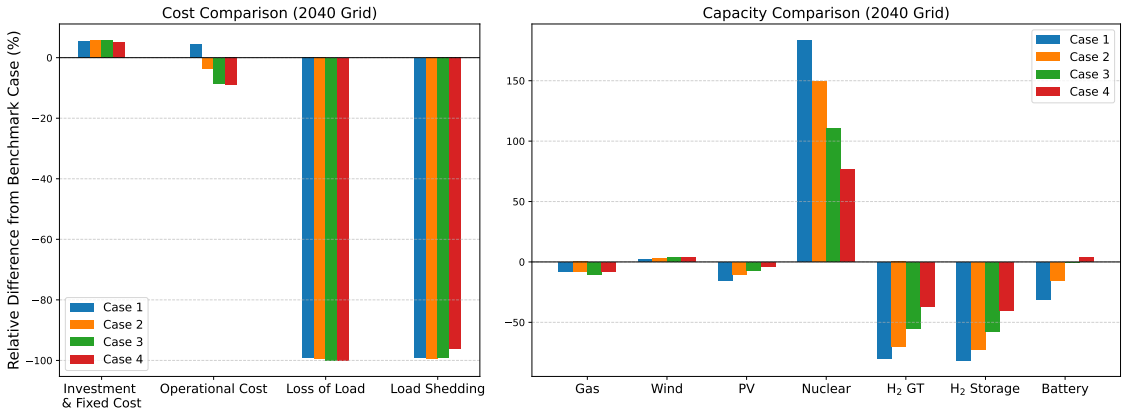

Figure 4.2: Relative differences (%) in system costs (on the left) and installed capacities (on the right) for the four analyzed cases compared to the benchmark case, under the 2040 Reference Grid scenario.

4.2.4 Model Results for the Unconstrained Grid

Moving to the model setup without limits on transmission capacity (i.e., Unconstrained Grid scenario), the optimization results, reported in Table 4.8, confirm that increasing the number of scenarios generally leads to a reduction in the Average Simulation TC. However, in this analysis, the Optimization TC and the Worst-Case Simulation TC do not exhibit a clear trend, with the latter which tends to decrease, in opposition to what is observed in the 2025 Reference Grid scenario. This divergence is primarily due to differences in capacity mix decisions, as explained later in

this section. Within this scenario, the advantages of stochastic optimization over deterministic optimization become particularly evident. Specifically, Cases 2, 3, and 4, which rely on stochastic optimization, exhibit zero loss of load and significantly lower Average Simulation TC compared to Case 1, which is based on deterministic optimization. Interestingly, Case 2 is characterized by a slightly lower Average Simulation TC compared to Case 3, deviating from the trend observed in the other transmission grid scenarios. The implications of this finding will be examined in the Discussion chapter (Section 5.1).
Comparing the results of the different transmission grid scenarios, it is evident that, overall, a scenario without constraints on transmission capacities results in lower total system costs and reduced load-loss.

Table 4.8: Optimization and simulation results for the analyzed cases under the Unconstrained Grid scenario.

Case	Modeling Approach	No. Scenarios	Optimization TC (M€)	Average Simulation TC (M€)	Worst-Case Simulation TC (M€)	Average Load-Loss (TWh)
1	Worst weather year for Europe (1996-97)	1	93458	103840	160356	0.0079
2	Worst weather year for each weather zone	7	94081	93954	115341	0
3	Worst weather year for each country	15	94485	93965	95971	0
4	40 weather year scenarios	40	93786	93786	108699	0
Benchmark	Typical weather year for Europe	1	89310	156951	921562	0.3852

In this transmission grid scenario as well, the same set of comparisons is carried out, focusing on system costs and installed capacities. The results are summarized in Tables 4.9 and H.3 (reported in Appendix H), respectively, and are graphically illustrated in Figure 4.3.
Regarding the system costs comparison, overall, a similar trend is observed in all three transmission grid scenarios. Specifically, compared to the benchmark case, the four analyzed cases present higher investment and fixed cost, a lower operational cost (except for Case 1 in both the 2025 Grid and 2040 Grid scenarios), and a considerably lower loss of load and load shedding.

Table 4.9: Comparison of average system costs (in M€), based on the results from 40 simulations, across the different cases under the Unconstrained Grid scenario.

Average System Costs (M€) - Unconstrained Grid					
Cost	**Benchmark**	**Case 1**	**Case 2**	**Case 3**	**Case 4**
Investment and Fixed Cost	82638.1	86675.6	88709.6	89540.4	88850.2
Operational Cost	5916.3	5551.8	4633.2	4392.4	4560.6
Loss of Load	38516.5	793.3	0	0	0
Load Shedding	29879.7	10818.9	611.4	32.6	375.6

In the Unconstrained Grid scenario, investments in the transmission network are also included in the installed capacity comparison. In the previous transmission grid scenarios, the grid infrastructure was constrained by an upper bound, leading the model to optimize the system by exploiting all the admissible interconnection capacity in every modeling approach. Specifically, the total installed transmission capacity reached approximately 110 GW in the 2025 Grid scenario, and nearly 160 GW in the 2040 Grid scenario. In contrast, the current scenario imposes no such limitations, allowing the model to freely determine the optimal level of transmission expansion.
The Unconstrained Grid scenario analysis leads to considerably different results compared to the previous transmission grid scenarios. No investments in nuclear power or hydrogen technologies are observed in all cases, and regarding the comparison with the benchmark case, the following trends are observed:

- Higher gas turbine capacity is installed in all cases.
- Slightly higher wind and solar capacities, both rising by approximately 10%, with the exception of Case 1, where a reduction in PV capacity is observed.
- Significantly higher investments in battery storage, except in Case 1, which shows a decrease of nearly 20%.
- Slightly lower investments in transmission capacity, with reductions remaining below 10% compared to the benchmark. Once again, Case 1 diverges from the trend, exhibiting increased transmission capacity relative to the benchmark.

It is evident that Case 1 results in different investment decisions compared to the other cases. In particular, it places greater reliance on the transmission grid and gas turbines, leading to lower investments in solar photovoltaic and battery storage.

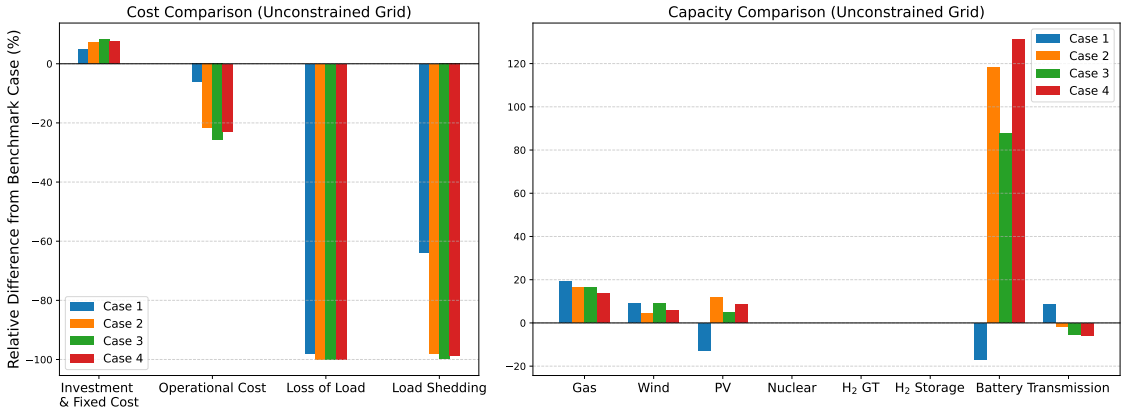

Figure 4.3: Relative differences (%) in system costs (on the left) and installed capacities (on the right) for the four analyzed cases compared to the benchmark case, under the 2040 Reference Grid scenario.

4.2.5 Summary of the Model Results

This section summarizes the results from the energy system model, highlighting the major findings. The main focus is on the impact of considering Dunkelflaute events in the system optimization and how the modeling approach influences the system

design, therefore assessing the key differences between the four analyzed cases. A schematic summary is depicted in Table 4.10.

Table 4.10: Summary of model results for the four optimization cases. For each case, the table presents the modeling approach, computational intensity, loss of load and average simulation TC, along with the main technology enhancing robustness against Dunkelflaute events.

Case	**1**	**2**	**3**	**4**
Modeling Approach	Deterministic optimization (worst year for Europe, 1996-97)	Stochastic optimization (worst year per weather zone)	Stochastic optimization (worst year per country)	Stochastic optimization (full dataset, 40 years)
Computational Intensity	Low	Medium	High	Very High
Loss of Load	High	Low	Negligible	Zero
Avg. Simulation TC	High	Medium	Low	Lowest
Robustness Tech. (Constrained Grids[a])	Nuclear power	Nuclear power	Nuclear power	Nuclear power
Robustness Tech. (Unconstrained Grid)	Gas turbines + Transmission grid	Battery storage	Battery storage	Battery storage

[a] Constrained Grids: 2025 and 2040 Grid.

The average values of loss of load and simulation total cost decrease from Case 1 to Case 4, reflecting a gradual improvement in system robustness. However, this robustness gain comes at the expense of computational complexity, which grows significantly with the number of stochastic scenarios. Case 4 achieves the most robust outcome, with zero average loss of load and the lowest simulation cost across all transmission grid scenarios, but it also requires the highest computational effort.
A more balanced compromise is obtained in Case 2 and 3, where stochastic optimization with the worst years at the weather zone or country level substantially reduces load-loss and simulation costs compared to the benchmark, while keeping computational requirements manageable.

In terms of capacity mix, the constrained grid scenarios (2025 and 2040 Grid) highlight nuclear powers as the key technology for enhancing robustness against Dunkelflaute events. In particular, Case 1, which optimizes for the worst European weather year, results in the highest nuclear capacity and the lowest VRE, hydrogen, and battery investments among all cases. In contrast, in the Unconstrained Grid scenario, nuclear power and hydrogen disappear entirely (see Section 4.2.4), with robustness instead ensured primarily by battery storage, supported by modest contributions from gas and VRE. The only exception is Case 1, which relies heavily on transmission capacity and gas turbines, drastically reducing solar PV and battery investments.

5
Discussion

Having presented weather data analysis and year rankings across three spatial scales, followed by corresponding energy system modeling results, this Discussion section interprets and situates these findings in relation to the research questions. First, results are explained in relation to the research questions, highlighting how the findings address the study objectives. Next, the employed methodologies are critically evaluated, discussing their strengths, potential biases, and suitability for the research goals. Following this, the limitations in the methods and the interpretation of results are acknowledged.

5.1 Interpretation and Critical Analysis of Results

The choice of Dunkelflaute detection metric and threshold significantly influences the identification and ranking of Dunkelflaute events. Mean-based thresholds provide consistent criteria across countries, clusters, and spatial scales, while effectively capturing year-to-year variability in Dunkelflaute occurrence. Percentile-based thresholds were not used because, in countries with high installed solar PV capacity, night-time hours with zero generation dominate the hourly datasets. This results in very low threshold values that would easily overlook consequential Dunkelflaute events.

The results also underscore the importance of combining wind, solar, and offshore wind capacity factors, weighted by their respective installed capacities. This method not only captures the renewable production potential across technologies but also reflects the system's dependency on, and sensitivity to, variations in weather patterns and capacity distributions. Moreover, using a summer-to-summer analysis period from the beginning of July to the end of June in the following year ensures that each period contains a complete winter season. This approach means that year rankings are consistently driven by winter conditions across all metrics, avoiding the issue in a calendar-year approach where a severe winter Dunkelflaute could be split between two years. When applied to weighted capacity factor data, this method provides a more consistent basis for comparing the severity and frequency of Dunkelflaute events between years, as each period captures the full extent of consecutive winter stresses.

As for the specific detection method, applying variable period lengths by using the algorithm of VMBT ensures that both short intense and long moderate Dunkelflaute

events are detected. A fixed-duration approach would not allow for combining longer-lasting drought periods with short peaks of capacity factor values lying within a Dunkelflaute event. Even though, to analyze general patterns of the lengths of a Dunkelflaute event, the FMBT method can be helpful.

At the country level, both the *Cumulative CFD* and the *Single-Event CFD* exhibit wide spreads across the 1979-2019 time frame. The single-event metric shows more evident year-to-year differences compared to the *Cumulative CFD*, reflecting the capture of more extreme, localized lows with higher variability across the analyzed years. But it also only shows the single worst period, not the second or third worst periods, which could have an impact on the yearly variability score as well. Countries without offshore wind resources (e.g., Austria, Slovenia, Slovakia, Switzerland) show relatively low interannual variability on both metrics, whereas nations with substantial onshore wind and offshore wind shares (e.g., Sweden, France) display larger fluctuations in their worst-case deficits. At the weather zone level, where countries are grouped by correlated capacity factor profiles, there is notable variation between weather zones in the single worst-event metric: some weather zones exhibit much larger year-to-year differences than others. Future analyses could further refine these weather zones by incorporating actual transmission capacities and testing alternative grouping schemes to improve regional definitions. In the pan-European zone, where hourly capacity factors are averaged and weighted by installed capacity across all countries, the inherent smoothing effect reduces interannual variability and dampens short-term extremes, especially at lower thresholds. Nevertheless, the year 1996-97 emerges as the most severe in terms of cumulative deficit, which is consistent with the literature[2], and fewer Dunkelflaute events are detected at stricter thresholds. This aggregated perspective highlights how spatial smoothing shifts the identification of critical years compared to more granular analyses.

The *Cumulative CFD* metric with a threshold of 30% of the mean VRE capacity factor proved to be the most effective approach to detect Dunkelflaute events (see Section 4.1). This metric-threshold combination consistently identified weather years that, when used as scenarios within the stochastic optimization, yielded the highest total system costs. Notably, the second-highest system costs were also associated with the same metric (i.e., *Cumulative CFD*) using a 40% threshold, suggesting that the effective threshold lies between 0.3 and 0.4, depending on the spatial scale. Specifically, larger geographic clusters require a slightly higher threshold due to the smoothing effect of spatial aggregation.

We modeled the future European electricity system with different approaches to represent the Dunkelflaute events. Examining the model results for the 2025 Reference Grid scenario, and applying the robustness evaluation approach described in Section 4.2.1, Case 4 (i.e., the stochastic optimization with 40 scenarios) appears to yield the most robust energy system. Specifically, it shows the lowest value of loss of load (equal to zero) and the lowest average system cost across the 40 simulations (Average Simulation TC). These outcomes are also observed under the other two transmission grid scenarios, reinforcing the robustness of this modeling approach.

However, as discussed in Section 4.2.2, in the 2025 and 2040 Grid scenarios, this capacity mix also results in the highest Worst-Case Simulation TC among the four examined cases, primarily due to the highest level of load shedding. While load shedding is technically allowed in the model, it is not a desirable system response in practice. For this reason, it is important to consider the Worst-Case Simulation TC as a decision criterion when evaluating the system's robustness. As a result, although average performance metrics provide valuable insight, complementary metrics, such as worst-case performance, can offer a more complete understanding of the system's robustness under adverse conditions. Another consideration about this modeling approach (Case 4) is that significant computational power and time are demanded, particularly if the system includes a larger number of nodes and technologies or requires a higher temporal resolution.

The primary objective of this study is not to determine a single, "perfect" modeling approach for designing a robust energy system. Instead, our aim is to demonstrate that a favorable balance between system robustness, computational efficiency, and economic performance can be achieved by employing alternative optimization strategies that are less computationally demanding than the extensive 40-year scenarios approach (Case 4). Therefore, a trade-off between minimizing load-loss and simulation costs while keeping the number of scenarios low is advisable. Consequently, adopting a stochastic optimization that incorporates the worst weather years at the weather zone or country level as scenarios (i.e., Case 2 or 3) represents a suitable choice. These approaches demonstrate clear performance improvements (in terms of load-loss and simulation costs reductions) over the deterministic optimization (Case 1), while maintaining relatively low computational demand.

More specifically, the results show that the systems obtained from Case 2 (based on the weather zone level) and Case 3 (based on the country level) show similar robustness performance, with only slight differences in system costs and load-loss values (in favor of Case 3). Notably, in the Unconstrained Grid analysis, both yield systems with zero Average Load-Loss, with Case 2 characterized by a slightly lower Average Simulation TC compared to Case 3, reversing the behavior observed in other transmission grid scenarios. These results indicate that the choice between the weather zone level and the country level optimization has a limited impact on system performance. In terms of model size and computational burden, Case 3, featuring a relatively high number of scenarios (15 in this study), requires the use of a high-performance computer, although it remains less demanding than Case 4. Case 2, by contrast, includes fewer scenarios (7 in this study) and is therefore more manageable and accessible from a computational perspective. Therefore, it can be concluded that employing an optimization model based on the weather zone level (Case 2) offers a favorable balance between system robustness, computational efficiency, and economic performance.

The model results and the comparison with the benchmark case (which optimizes the system based on average weather conditions) emphasize the importance of accounting for Dunkelflaute events in energy system optimization, highlighting the impacts of

these events on system cost and design. Considering the 2025 Reference Grid scenario, representing Dunkelflaute events at the weather-zone level (Case 2) reduces the loss of load by 97.8% compared to the benchmark (see Table 4.4). This substantial improvement comes with a slightly higher total system cost (i.e., Optimization TC), driven by higher investment costs, as shown in Table 4.5. However, the cost increase is modest, amounting to only 4.9%. Regarding the impacts of Dunkelflaute events on the capacity mix, different patterns are observed in the three transmission grid scenarios. In the constrained grid scenarios (i.e., 2025 and 2040 Reference Grid), nuclear power plays a critical role in enhancing system robustness, with its capacity increasing substantially compared to the benchmark case. In contrast, in the Unconstrained Grid scenario, nuclear power (together with hydrogen technologies) disappears entirely in all the resulting systems, due to the stronger reliance on cross-border transmission, which provides extensive spatial smoothing. Specifically, installed transmission capacity expands from approximately 110 GW in the 2025 Grid to around 440 GW in the Unconstrained Grid, corresponding to a fourfold increase in capacity. In this scenario, Dunkelflaute events are addressed with moderately higher investments in gas turbines, wind, and solar PV, with battery storage playing the dominant role, nearly doubling compared to the benchmark. Among the four modeling approaches, the only deviation in capacity mix decisions within the Unconstrained Grid occurs in Case 1 (i.e., deterministic optimization based on the worst weather year). Here, the system places greater reliance on transmission expansion to mitigate stress and enhance robustness, resulting in reduced battery storage and solar PV capacities compared to the benchmark. Dunkelflaute events are inherently linked to wind and solar. The results show that wind capacity is not significantly impacted, remaining largely unaffected, whereas solar PV investments generally decline when these events are taken into account in the optimization. This highlights a greater sensitivity of solar to prolonged low-generation periods compared to wind.

The findings (Section 4.2) also indicate that expanding transmission grids enables a better spatial balancing of weather variability, which reduces loss of load in each modeling approach and decreases the need for backup capacity, such as nuclear power, thus lowering the overall system cost.

In this study, the identification of the worst weather year in Europe is based on the weather data analysis using the *Cumulative CFD* metric, applying a threshold of 30% of the mean VRE capacity factor (see Section 4.1). An alternative method would be to rely on the TC year ranking derived from the model results [55] (as presented in Section 3.8). Both approaches generally converge on the same outcome, namely, the summer-to-summer year 1996-97, which aligns with the findings from previous studies in the literature [2, 46]. The only exception is observed in the Unconstrained Grid scenario, where the TC-based ranking from the model results (illustrated in Figure 3.15) identifies 1995-96 as the most unfavorable year. However, this type of ranking reflects only the system's operational performance and does not directly focus on the occurrence of extreme weather conditions, such as Dunkelflaute events. Therefore, this outcome is likely due to prolonged periods of below-average

VRE generation in 1995-96, rather than the presence of more severe or consequential Dunkelflaute events, which is the primary focus of this study.

5.2 Limitations of the Study

While hierarchical clustering of weighted capacity factor data provides a useful framework for defining coherent weather zones, it also depends on the chosen distance metric and linkage method; small changes in these parameters can produce different cluster boundaries. Moreover, clustering based solely on capacity factor correlations does not account for physical transmission constraints or real-world grid interconnections, which may change the relevance of the identified zones. The Dunkelflaute detection relies on fixed thresholds defined as percentages of the mean capacity factor, but these thresholds can strongly influence event detection: higher thresholds may capture only the most severe droughts, while lower thresholds may include less consequential dips. Additionally, weighting capacity factors by installed capacity emphasizes technologies with larger deployments. However, these installed capacities are derived from modeling results based on an average weather year. Therefore, they do not represent actual future capacities and can be sensitive to the selection of the average weather year used in the analysis. Together, these methodological choices and assumptions should be considered when interpreting the results and applying the findings to energy system planning.

The study relies on historical raw capacity factor data without accounting for evolving weather patterns or projected climate change, which may alter future Dunkelflaute characteristics. Hourly correlations are assessed without considering potential temporal lags between countries, potentially overlooking propagation of weather systems across regions. Finally, aggregating data at the national level masks intra-country variability; large countries (e.g., Germany, Sweden, France, Norway) may exhibit significant north–south differences in renewable generation that are not captured by this analysis.

Regarding the energy model, although it incorporates a large number of countries and technologies, it remains a simplified version compared to current state-of-the-art models. For example, it only focuses on the electricity sector and does not consider sector coupling, which plays a significant role in comprehensive energy system design. Furthermore, in the stochastic optimization approaches examined in this study, the selection of scenarios is a critical step. If the scenarios are not carefully chosen, they can lead to misleading results, which could compromise the validity of the optimization findings and the overall process.

5.3 Recommendations for Future Research

Following the results and discussions, several options for future research can be expressed. First, examining correlations between different renewable technologies or other indicators such as country size, geographic features, or topography and the

corresponding Dunkelflaute events can refine understanding of technology-specific and regional sensitivities. Moreover, incorporating temporal lags in hourly correlation analyses would capture the cross-border propagation of weather systems and improve the realism of cluster definitions. Besides, integrating evolving climate scenarios and observed trends into capacity factor datasets will enable assessment of how future changes in weather patterns could affect Dunkelflaute event frequency and severity. From the modeling perspective, future research can focus on analyzing the variability of electricity demand and water inflows (for hydropower plants) depending on weather conditions, to evaluate their relevance and impact on energy system optimization. Moreover, the energy model can be expanded by including other energy sectors, such as the heating, transport, and industry sectors. It would also be beneficial to examine other geographical areas to validate the effectiveness of the model and the proposed modeling approaches.

6

Conclusion

In this thesis, we detect, measure, and model Dunkelflaute events for future renewable-based electricity systems in Europe to strengthen system robustness and hedge against the risks posed by such events. The detection framework combines capacity factors for onshore wind, offshore wind, and solar power, weighted by installed capacity, and applies a variable mean below threshold algorithm over summer-to-summer periods to ensure complete winter coverage. Thresholds defined relative to each system's mean capacity factor enable comparability across regions, while using a range of thresholds captures both short, severe events and longer, moderate ones.

Our results show that Dunkelflaute is a persistent challenge: such events occur every year, but their magnitude and timing vary. Spatial scale strongly affects Dunkelflaute rankings: aggregation smooths extremes, with greater variability observed at the country level than in weather zones or in pan-European analysis. On- and offshore wind–dominant systems (e.g., Nordic countries) exhibit relatively high year-to-year variability in the cumulative deficit year ranking, with standard deviations ranging from 0.14 to 0.18. In contrast, inland continental regions with poor wind conditions are more stable, showing standard deviations of 0.07 to 0.10 for the same metric. The annual cumulative capacity factor deficit metric with a threshold of 30% of the mean capacity factor proved to be the most effective metric for identifying Dunkelflaute events. By modeling the future renewable European electricity system with Dunkelflaute events represented at the country, weather zone, and pan-European levels, we identify the most effective representation for designing a robust European electricity system. Our findings indicate that a balance between robustness, computational efficiency, and cost can be achieved by incorporating the worst Dunkelflaute years at the weather zone or country level as scenarios in a stochastic optimization, retaining most of the robustness benefits while significantly reducing computational effort. Specifically, representing Dunkelflaute events at the weather zone level already reduces the loss of load by 97.8% compared with the benchmark case, with only a minor cost increase of 4.9 % (values based on the 2025 Reference Grid scenario). Our results also show that Dunkelflaute events have a stronger impact on solar PV than on wind power, as reflected by the reductions in installed solar capacity for most of the cases, while wind capacity remains almost unaffected. Moreover, in scenarios with the current transmission grid or limited expansion, nuclear power emerges as the primary technology for enhancing system robustness during Dunkelflaute events. In contrast, when the transmission grid is optimally expanded, no nuclear power is deployed; instead, the system relies more heavily on cross-border trade, battery storage and gas turbine to manage periods of low renewable output. In summary, this thesis proposes a methodological framework for integrating Dunkelflaute events into

energy system modeling, thereby supporting the design of robust renewable-based electricity systems.

Bibliography

[1] Kittel, M., & Schill, W.-P. (2024). Quantifying the Dunkelflaute: An analysis of variable renewable energy droughts in Europe. DIW Berlin, TU Berlin. *Environmental Research: Energy*.

[2] Kittel, M., Roth, A., & Schill, W.-P. (2025). Coping with the Dunkelflaute: Power system implications of variable renewable energy droughts in Europe. *arXiv preprint* `arXiv:2411.17683`.

[3] van der Most, L., van der Wiel, K., Benders, R. M. J., Gerbens-Leenes, P. W., Kerkmans, P., & Bintanja, R. (2022). Extreme events in the European renewable power system: Validation of a modeling framework to estimate renewable electricity production and demand from meteorological data. *Renewable and Sustainable Energy Reviews*, *170*.

[4] Kittel, M., & Schill, W.-P. (2024). Measuring the Dunkelflaute: how (not) to analyze variable renewable energy shortage. Environ. Res.: Energy 1 035007

[5] Stoop, L. P., van der Wiel, K., Zappa, W., Haverkamp, A., Feelders, A. J., & van den Broek, M. (2024). The climatological renewable energy deviation index (credi). Environmental Research Letters, 19(3), 034021. https://doi.org/10.1088/1748-9326/acc59c

[6] Gorenstein Dedecca J., Ansarin, M., Bene, C., van Delzen, T., van Nuffel, L., Jagtenberg, H. (2025). Increasing Flexibility in the EU Energy System - Technologies and policies to enable the integration of renewable electricity sources. Publication for the Committee on Industry, Research and Energy, Policy Department for Transformation, Innovation and Health, European Parliament, Luxembourg

[7] De Felice M, Koolen D, Kanellopoulos K, Busch S, Zucker A (2023) Climate variability on Fit for 55 European power systems. PLOS ONE 18(12): e0289705.

[8] Seljom, P., Kvalbein, L., Hellemo, L., Kaut, M., & Muñoz Ortiz, M. (2021). Stochastic modelling of variable renewables in long-term energy models: Dataset, scenario generation & quality of results. *Energy*, *236*, 121470.

[9] Kost, C., Müller, P., Sepúlveda Schweiger, J., Fluri, V., & Thomsen, J. (2024, July). *Levelized cost of electricity: Renewable energy technologies*. Fraunhofer Institute for Solar Energy Systems ISE

[10] Li, B., Basu, S., Watson, S. J., & Russchenberg, H. W. J. (2021). A Brief Climatology of Dunkelflaute Events over and Surrounding the North and Baltic Sea Areas. Energies, 14(20), 6508. https://doi.org/10.3390/en14206508

[11] Cannon, D. J., Brayshaw, D. J., Methven, J., Coker, P. J., & Lenaghan, D. (2015). Using reanalysis data to quantify extreme wind power generation statistics: A 33-year case study in Great Britain. *Renewable Energy, 75*, 767–778.

[12] Potisomporn, P., & Vogel, C. R. (2022). Spatial and temporal variability characteristics of offshore wind energy in the United Kingdom. *Wind Energy, 25*(3), 537–552.

[13] Potisomporn, P., Adcock, T. A., & Vogel, C. R. (2023). Evaluating ERA5 reanalysis predictions of low wind speed events around the UK. *Energy Reports, 10*, 4781–4790.

[14] Abdelaziz, S., Sparrow, S. N., Hua, W., & Wallom, D. C. (2024). Assessing long-term future climate change impacts on extreme low wind events for offshore wind turbines in the UK exclusive economic zone. *Applied Energy, 354*, 122218.

[15] Leahy, P. G., & McKeogh, E. J. (2013). Persistence of low wind speed conditions and implications for wind power variability. *Wind Energy, 16*(4), 575–586.

[16] Patlakas, P., Galanis, G., Diamantis, D., & Kallos, G. (2017). Low wind speed events: Persistence and frequency. *Wind Energy, 20*(6), 1033–1047.

[17] Harrison-Atlas, D., Murphy, C., Schleifer, A., & Grue, N. (2022). Temporal complementarity and value of wind-PV hybrid systems across the United States. *Renewable Energy*, *201* (Part 1), 111–123.

[18] Ohlendorf, N., & Schill, W.-P. (2020). Frequency and duration of low-wind-power events in Germany. *Environmental Research Letters, 15*, 084045.

[19] Antonini, A., Virgüez, E., Ashfaq, S., Duan, L., Ruggles, T. H., & Caldeira, K. (2024). Identification of reliable locations for wind power generation through a global analysis of wind droughts. *Communications Earth & Environment, 5*(1), 103.

[20] Raynaud, D., Hingray, B., François, B., & Creutin, J. (2018). Energy droughts from variable renewable energy sources in European climates. *Renewable Energy, 125*, 578–589.

[21] Kies, A., Schyska, B. U., Bilousova, M., El Sayed, O., Jurasz, J., & Stoecker, H. (2021). Critical review of renewable generation datasets and their implications for European power system models. *Renewable and Sustainable Energy Reviews, 152*, 111614.

[22] Kapica, J., Jurasz, J., Canales, F. A., Bloomfield, H., Guezgouz, M., De Felice, M., & Zbigniew, K. (2024). The potential impact of climate change on European renewable energy droughts. *Renewable and Sustainable Energy Reviews, 189*, 114011.

[23] Hu, J., Koning, V., Bosshard, T., Harmsen, R., Crijns-Graus, W., Worrell, E., & Van Den Broek, M. (2023). Implications of a Paris-proof scenario for future supply of weather-dependent variable renewable energy in Europe. *Advances in Applied Energy, 10*, 100134.

[24] Breyer, C., Bogdanov, D., Ram, M., Khalili, S., Vartiainen, E., Moser, D., et al. (2022). Reflecting the energy transition from a European perspective and in the global context—Relevance of solar photovoltaics benchmarking two ambitious scenarios. *Progress in Photovoltaics: Research and Applications*.

[25] Kaspar, F., Borsche, M., Pfeifroth, U., Trentmann, J., Drücke, J., & Becker, P. (2019). A climatological assessment of balancing effects and shortfall risks of photovoltaics and wind energy in Germany and Europe. *Advances in Science and Research, 16*, 119–128.

[26] Mockert, F., Grams, C. M., Brown, T., & Neumann, F. (2023). Meteorological conditions during periods of low wind speed and insolation in Germany: The role of weather regimes. *Meteorological Applications, 30*, e2141.

[27] Mayer, M. J., Biró, B., Szűcs, B., & Aszódi, A. (2023). Probabilistic modeling of future electricity systems with high renewable energy penetration using machine learning. *Applied Energy, 336*, 120801.

[28] Ohba, M., Kanno, Y., & Nohara, D. (2022). Climatology of dark doldrums in Japan. *Renewable and Sustainable Energy Reviews, 155*, 111927.

[29] Rinaldi, K. Z., Dowling, J. A., Ruggles, T. H., Caldeira, K., & Lewis, N. S. (2021). Wind and solar resource droughts in California highlight the benefits of long-term storage. *Environmental Science & Technology, 55*, 6214–6226.

[30] Gangopadhyay, A., Seshadri, A., Sparks, N., & Toumi, R. (2022). The role of wind-solar hybrid plants in mitigating renewable energy droughts. *Renewable Energy, 194*, 926–937.

[31] Stoop, L. P., Antonini, A., & Patt, A. (2022). CREDI: A new index to assess the climatological renewable energy deviation in power systems. *Applied Energy, 307*, 118221.

[32] Antonini, A., Stoop, L. P., & Patt, A. (2021). The climate variability of wind and solar energy supply. *Environmental Research Letters, 16*(4), 044047.

[33] Chen, R., Lu, Z., & Qiao, Y. (2023). Long-term generation expansion planning model based on intraday and interday renewable energy uncertainty sets. SSRN.

[34] Collins, S., Deane, P., Ó Gallachóir, B., Pfenninger, S., & Staffell, I. (2018). Impacts of inter-annual wind and solar variations on the European power system. Joule, 2(10)

[35] Mitali, J., Dhinakaran, S., & Mohamad, A. A. (2022). Energy storage systems: A review. Energy Storage and Saving, 1(3)

[36] Yokoyama, M., Ohnuma, S., Osawa, H., et al. (2023). Public acceptance of nuclear waste disposal sites: A decision-making process utilising the 'veil of ignorance' concept. Humanities and Social Sciences Communications, 10, 623.

[37] Raynaud, D., Hingray, B., François, B., & Creutin, J. D. (2018). Energy droughts from variable renewable energy sources in European climates. *Renewable Energy, 125*, 578–589. https://doi.org/10.1016/j.renene.2018.02.130 using a logistic regression-based approach Meteorol. Appl.

[38] Rinaldi, K. Z., Dowling, J. A., Ruggles, T. H., Caldeira, K., & Lewis, N. S. (2021). Wind and solar resource droughts in California highlight the benefits of long-term storage and integration with the Western Interconnect. *Environmental Science & Technology, 55*(9), 6214–6226. https://doi.org/10.1021/acs.est.0c07848

[39] Mayer, M. J., Biró, B., Szűcs, B., & Aszódi, A. (2023). Probabilistic modeling of future electricity systems with high renewable energy penetration using machine learning. *Applied Energy, 336*, 120801. https://doi.org/10.1016/j.apenergy.2023.120801

[40] Otero N, Martius O, Allen S, Bloomfield H and Schaefli B 2022 Characterizing renewable energy compound events across Europe

[41] Allen S and Otero N 2023 Standardised indices to monitor energy droughts Renew. Energy

[42] International Energy Agency. (2023). Managing seasonal and interannual variability of renewables. International Energy Agency. https://www.iea.org/reports/managing-seasonal-and-interannual-variability-of-renewables

[43] Deutscher Wetterdienst, *Global, diffuse and direct radiation (monthly and annual totals and deviation maps)*, Climate Data Center, 2025. Available at: `https://www.dwd.de/EN/ourservices/solarenergy/maps_globalradiation_sum_new.html`. Accessed: July 29, 2025.

[44] Bureau of Safety and Environmental Enforcement, *Renewable energy: Offshore wind safety incidents—Looking to Europe for lessons learned*, U.S. Department of the Interior, Fact sheet, Jan. 2022. Available at: `https://www.bsee.gov/sites/bsee.gov/files/bsee-fact-sheet-renewable-energy.pdf`. Accessed: July 29, 2025.

[45] E. Goetske, G. Andresen, F. Neumann, and M. Victoria, *Designing a sector-coupled European energy system robust to 60 years of historical weather data*, *Nature Communications*, vol. 15, Dec. 2024. doi: 10.1038/s41467-024-54853-3.

[46] K. Forghani, X. Kan, L. Reichenberg, and F. Hedenus, *Modeling Robust Energy Systems Considering Weather Uncertainty and Nuclear Power Failures: A Case Study in Northern Europe*, arXiv preprint arXiv:2504.08145, 2025. https://arxiv.org/abs/2504.08145.

[47] S. Backe, M. Ahang, and A. Tomasgård, *Stable stochastic capacity expansion with variable renewables: Comparing moment matching and stratified scenario generation sampling*, *Applied Energy*, vol. 302, 2021. doi: 10.1016/j.apenergy.2021.117538.

[48] F. Bagheri, H. Dagdougui, and M. Gendreau, *Stochastic optimization and scenario generation for peak load shaving in Smart District microgrid: sizing and operation*, *Energy and Buildings*, vol. 275, p. 112426, 2022. doi: 10.1016/j.enbuild.2022.112426.

[49] [Author(s)], *Optimal capacity configuration of wind–photovoltaic–storage hybrid system using integrated optimization parametric modeling*, *Energy Reports*, vol. [volume], 2022. doi:10.1016/j.egyr.2022.024456.

[50] ENTSO-E & ENTSOG, *TYNDP 2024 Scenarios Package and Data*, TYNDP 2024 Scenarios download portal, accessed July 2025. https://2024.entsos-tyndp-scenarios.eu/download/.

[51] ENTSO-E, *ENTSO-E Transparency Platform*, European Network of Transmission System Operators for Electricity, accessed July 2025. https://transparency.entsoe.eu/.

[52] Ember, *Europe Electricity Interconnection Data Tool*, Ember – Global Energy Think Tank, accessed July 2025. https://ember-energy.org/data/europe-electricity-interconnection-data-tool/.

[53] P. Seljom, A. Tomasgard, K. B. Lindberg, G. Doorman and I. Sartori, *Short-term uncertainty in long-term energy system models: A case study of wind power in Denmark*, *Energy Economics*, vol. 49, pp. 157–166, 2015. doi: 10.1016/j.eneco.2015.02.004.

[54] P. Seljom, L. Kvalbein, L. Hellemo, M. Kaut, and M. M. Ortiz, *Stochastic modelling of variable renewables in long-term energy models: Dataset, scenario*

generation & quality of results, *Energy*, vol. 236, 2021, Art. no. 121415, doi: 10.1016/j.energy.2021.121415.

[55] A. Grochowicz, K. van Greevenbroek, and H. C. Bloomfield, *Using power system modelling outputs to identify weather-induced extreme events in highly renewable systems*, *Environmental Research Letters*, vol. 19, no. 5, p. 054038, 2024. doi: 10.1088/1748-9326/ad374a.

[56] Danish Energy Agency, *Technology data for generation of electricity and district heating*, 2025. Accessed: April 2025. Available at: https://ens.dk/en/analyses-and-statistics/technology-data-generation-electricity-and-district-heating.

[57] Danish Energy Agency, *Technology Data for Energy Storage*, 2025. Accessed: April 2025. Available at: https://ens.dk/en/analyses-and-statistics/technology-data-energy-storage.

[58] S. Hagspiel, C. Jägemann, D. Lindenberger, T. Brown, S. Cherevatskiy, and E. Tröster, *Cost-optimal power system extension under flow-based market coupling*, *Energy*, vol. 66, pp. 654–666, 2014. doi: 10.1016/j.energy.2014.01.025.

[59] W. J. Cole and A. Frazier, *Cost projections for utility-scale battery storage*, National Renewable Energy Laboratory (NREL), Golden, CO (United States), 2019.

[60] B. van Zuijlen, W. Zappa, W. Turkenburg, G. van der Schrier, and M. van den Broek, *Cost-optimal reliable power generation in a deep decarbonisation future*, *Applied Energy*, vol. 253, 2019, Art. no. 113587. doi: 10.1016/j.apenergy.2019.113587.

[61] E. Goetske, G. Andresen, F. Neumann, and M. Victoria, *Designing a sector-coupled European energy system robust to 60 years of historical weather data*, *Nature Communications*, vol. 15, 2024, Art. no. 54853. Supplementary material available at: https://ars.els-cdn.com/content/image/1-s2.0-S2542435123002660-mmc2.pdf.

[62] D. Schlachtberger, M. Greiner, and P. L. Sørensen, *Robust design of a future 100% renewable European energy supply*, *Energy*, vol. 207, 2020, Art. no. 118147. doi: 10.1016/j.energy.2020.118147.

[63] N. Mattsson, V. Verendel, F. Hedenus, and L. Reichenberg, *An autopilot for energy models—Automatic generation of renewable supply curves, hourly capacity factors and hourly synthetic electricity demand for arbitrary world regions*, *Energy Strategy Reviews*, vol. 33, 2021, Art. no. 100606. doi: 10.1016/j.esr.2020.100606.

[64] Gurobi Optimization, LLC, *Gurobi Optimizer Reference Manual*, 2025. Available at: https://www.gurobi.com.

[65] M. Welsch, P. Deane, M. Howells, B. Ó Gallachóir, F. Rogan, M. Bazilian, and U. Malmgren Persson, *Including flexibility options in a large-scale long-term energy model: Case study for Europe*, International Journal of Energy Research, vol. 39, no. 3, pp. 336–356, 2015, doi: 10.1002/er.3250.

[66] S. Collins, P. Deane, B. Ó Gallachóir, S. Pfenninger, and I. Staffell, *Impacts of inter-annual wind and solar variations on the European power system*, *Joule*, vol. 2, no. 10, pp. 2076–2090, 2018. doi: 10.1016/j.joule.2018.06.020.

[67] O. Ruhnau and S. Qvist, *Storage requirements in a 100% renewable electricity system: extreme events and inter-annual variability*, *Environmental Research Letters*, vol. 17, no. 4, p. 044018, 2022. doi: 10.1088/1748-9326/ac4dc8.

[68] S. Höltinger, C. Mikovits, J. Schmidt, J. Baumgartner, B. Arheimer, G. Lindström, and E. Wetterlund, *The impact of climatic extreme events on the feasibility of fully renewable power systems: A case study for Sweden*, *Energy*, vol. 178, pp. 695–713, 2019. doi: 10.1016/j.energy.2019.04.128.

[69] P. Hsia, J. Samuel, J. Gao, D. Kung, Y. Toyoshima, and C. Chen, *Formal approach to scenario analysis*, *IEEE Software*, vol. 11, no. 2, pp. 33–41, 1994. doi: 10.1109/52.268953.

[70] A. T. D. Perera, V. M. Nik, D. Chen, J.-L. Scartezzini, and T. Hong, *Quantifying the impacts of climate change and extreme climate events on energy systems*, *Nature Energy*, vol. 5, no. 2, pp. 150–159, 2020. doi: 10.1038/s41560-020-0558-0.

[71] F. Verástegui, Á. Lorca, D. E. Olivares, M. Negrete-Pincetic, and P. Gazmuri, *An adaptive robust optimization model for power systems planning with operational uncertainty*, *IEEE Transactions on Power Systems*, vol. 34, no. 6, pp. 4606–4616, 2019. doi: 10.1109/TPWRS.2019.2917854.

[72] Copernicus Climate Change Service (C3S), *Climate Data Store (CDS)*, European Union, 2025. Available at: `https://cds.climate.copernicus.eu/`. Accessed: April 2025.

A

Correlation Analysis of Wind, Solar and Offshore Wind

The correlation matrix, shown in Figure A.1, displays the correlations for wind capacity factors. It shows that no clear negative correlations are present. The lowest correlation is –0.05 between Norway and Portugal, while the highest—excluding the perfect correlation of 1—is 0.89 between Latvia and Lithuania.

Initial clustering of countries based on these correlations reveals several groups: The Nordic countries; the Netherlands, Belgium, Luxembourg, and Germany; Estonia, Lithuania, and Latvia; Czechia, Austria, Slovakia, and Hungary; Central European group including France, Switzerland, Italy, Slovenia, and Croatia; Southeast European group comprising Romania, Bulgaria, and Greece; And a distinct cluster of Spain and Portugal, which show strong mutual correlations. Additional notable correlations are observed between Estonia and the Nordic countries, as well as between France and Germany.
Solar capacity factors exhibit higher overall correlations compared to onshore wind which is shown in Figure A.2. While the correlation patterns for solar capacity factors are generally similar to those observed for wind, they show less variation across countries and consistently higher correlation values. This is due to the more uniform nature of solar irradiance, which is largely driven by the daily and seasonal cycle of sunlight that affects large regions in a relatively consistent way—especially compared to wind, which is more influenced by localized and highly variable weather patterns. The lowest observed Pearson correlation for solar is 0.58, between Estonia and Portugal, while the highest is 0.97 between Latvia and Lithuania.
Offshore wind capacity factors correlations are here presented in Figure A.3 and analyzed among countries with access to offshore wind resources. Strong correlations are observed within several regional groups: the Nordic countries; Ireland and the United Kingdom; the Netherlands, Belgium, and Germany; Latvia, Estonia, and Lithuania; as well as southern and southeastern European countries such as Italy, Slovenia, Croatia, Romania, Bulgaria, and Greece. These groupings reflect the shared exposure to similar offshore wind regimes within each region.
Although the overall correlation patterns are broadly similar to those observed for onshore wind, the clustering in offshore wind data is more distinct. This is due to the more homogeneous and stable wind conditions over open sea areas, which lead to stronger spatial correlations among countries with comparable offshore environments. In contrast, onshore wind is more affected by local terrain and weather systems, leading to greater variability in correlations. The lowest observed Pearson correlation

for offshore wind is –0.09 between Norway and Portugal, indicating virtually no relationship in their offshore wind patterns. The highest correlation is 0.89 between Latvia and Estonia, reflecting the shared characteristics of their adjacent offshore areas.

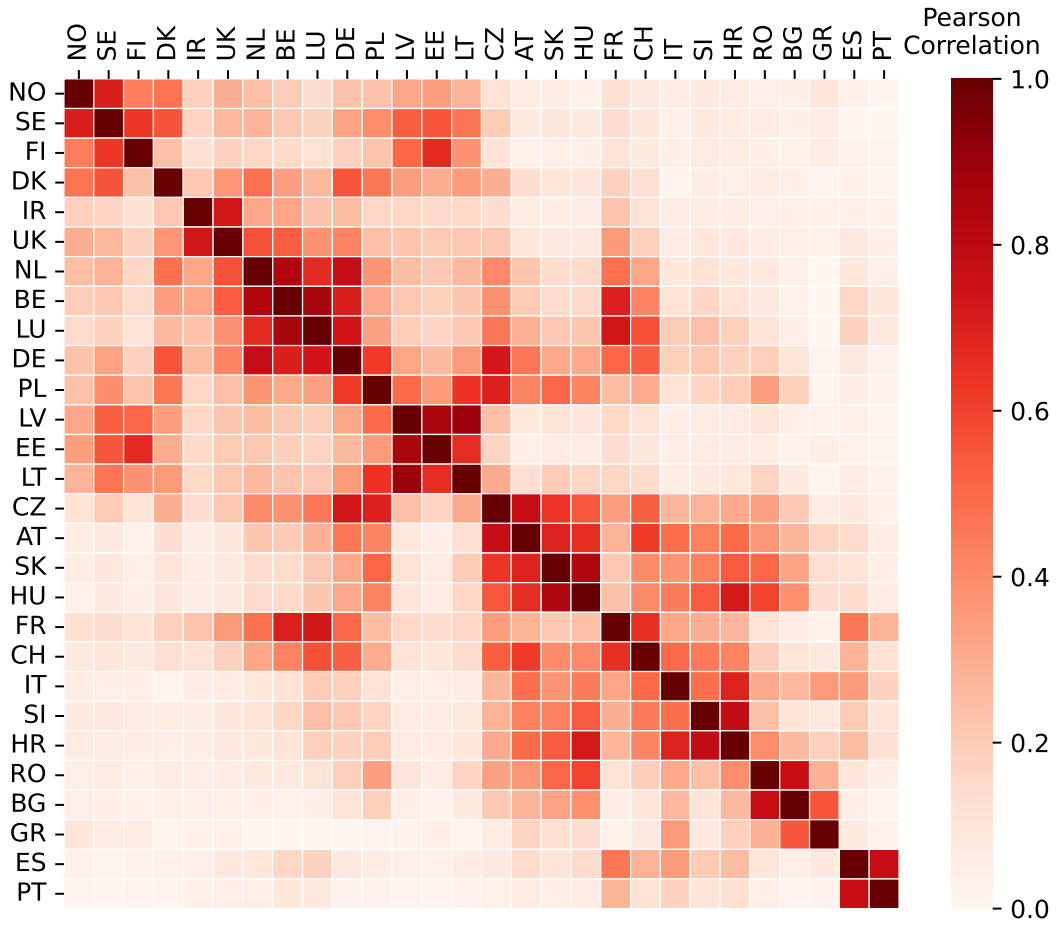

Figure A.1: Wind Capacity Factor Correlation Matrix for EU Countries, based on hourly data over one year.

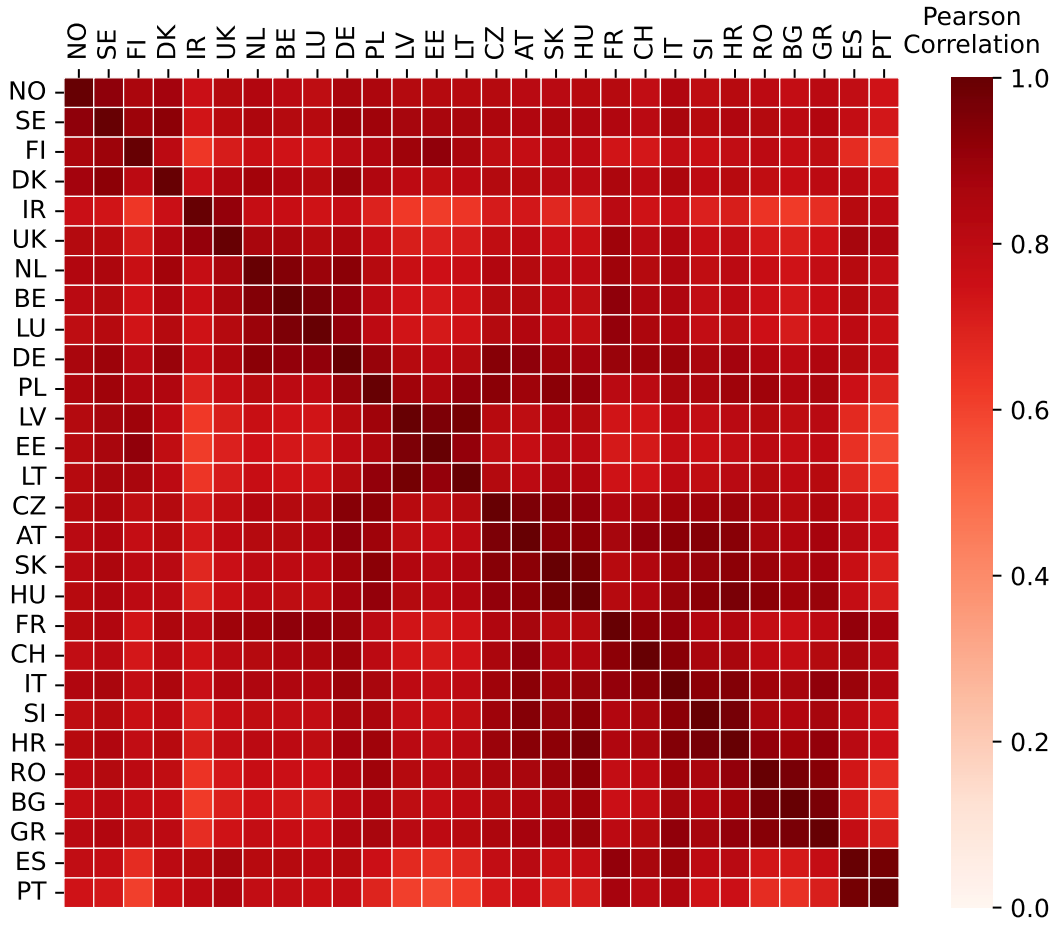

Figure A.2: Solar Capacity Factor Correlation Matrix for EU Countries, based on hourly data over one year.

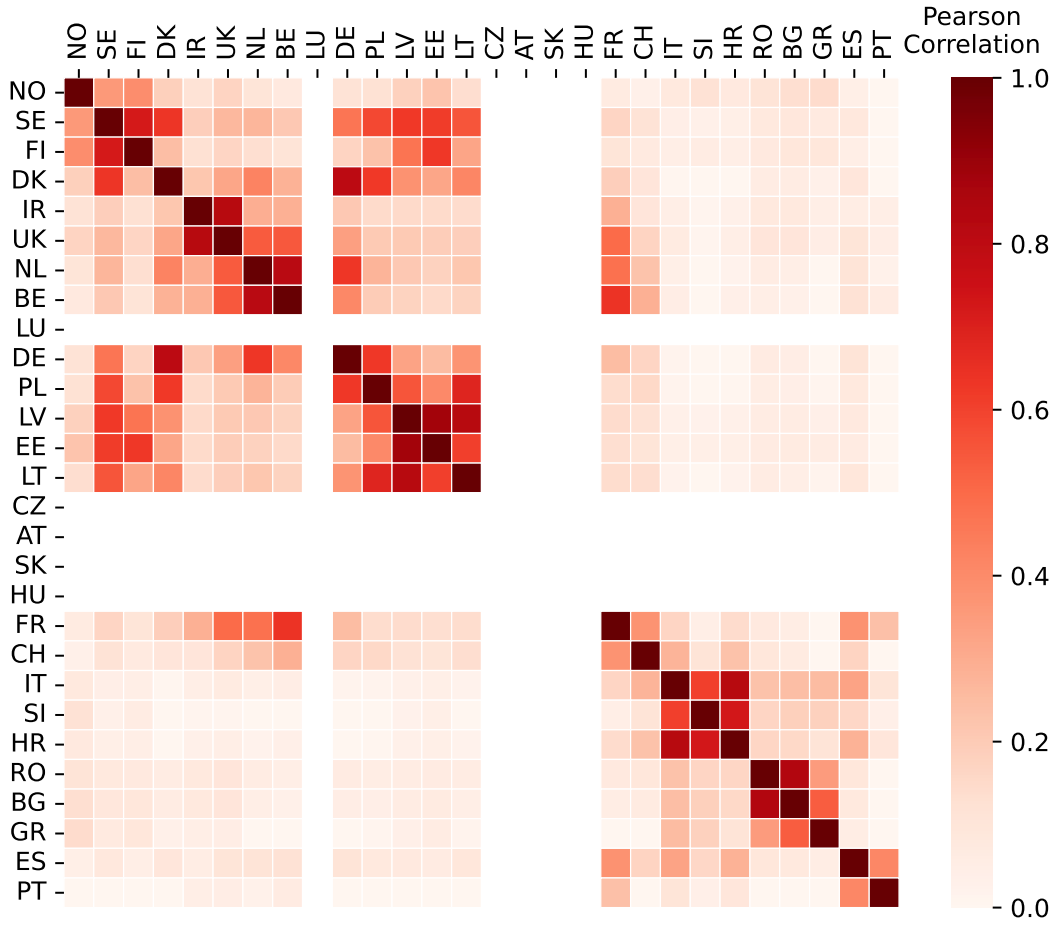

Figure A.3: Offshore-Wind Capacity Factor Correlation Matrix for EU Countries, based on hourly data over one year.

B

Wind and Solar Installed Capacities Derived from the Average Weather Year

The average weather year used to determine the shares of installed wind and solar capacity for each country, required for Section 3.1.2, was identified through a dedicated analysis. A simplified version of the energy system model (differing from the configuration described in Section 3.4) was employed to perform a deterministic optimization for each weather year and rank them based on the resulting total system cost. In particular, in this alternative setup, the nuclear investment cost was increased to enhance the deployment of wind and solar technologies. Additionally, a carbon tax was applied instead of the carbon cap, and standard winter-to-winter years were considered instead of summer-to-summer periods. The 2025 Reference Grid scenario (see Section 3.7) was used to perform this analysis.
The ranking results are presented in Figure B.1, with 2006 identified as the average weather year for this purpose. The wind and solar installed capacities resulting from the energy system optimized using the average weather year 2006 are presented in Table B.1.

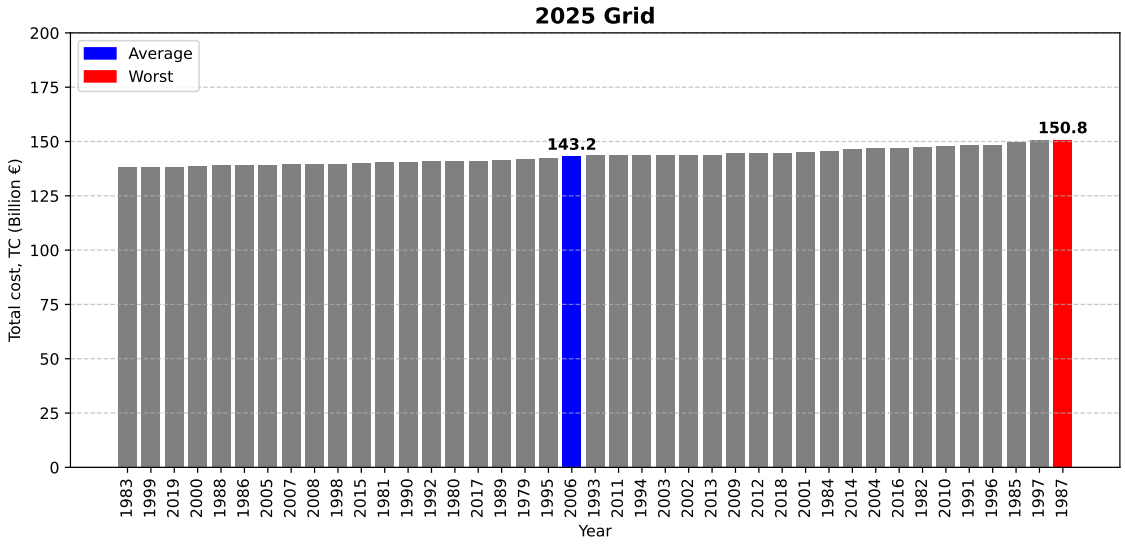

Figure B.1: Ranked total system costs (in billion of €) resulting from deterministic optimizations performed for each weather years, using a simplified version of the energy model under the 2025 Grid scenario.

Table B.1: Installed wind and solar capacities (in GW) by country, based on the system optimized using the average weather year (2006).

Country	Onshore Wind	Offshore Wind	Solar PV	Rooftop Solar PV
NO	30.88	0	0	0
SE	27.37	0	15.80	0
FI	6.89	5.99	8.77	0
DK	18.59	0	0	0
IE	8.77	0	4.86	0
UK	63.32	0	29.88	0
NL	11.80	0	0.18	0
BE	9.64	0	17.56	0
LU	0	0	1.03	0
DE	112.13	0	104.77	0
PL	55.71	0	40.90	0
LV	0.52	0	2.94	0
EE	2.76	0	0.03	0
LT	4.37	0	1.86	0
CZ	0.12	0	9.24	0
AT	0	0	32.93	0
SK	0	0	7.09	0
HU	6.00	0	8.82	0
FR	119.14	0	86.73	0
CH	0	0	34.89	0
IT	0	0	187.94	0
SI	0	0	0	0
HR	0	0	17.27	0
RO	1.21	0	7.32	0
BG	0	0	6.37	0
GR	0	3.02	27.51	0
ES	16.34	0	111.16	0
PT	5.31	0	24.12	0

C
Notation

This appendix provides a comprehensive list of sets, indices, parameters, and variables used in the energy system model.

Sets

$\mathcal{H}$	Set of hours in a year ($\mathcal{H} = \{1, 2, \ldots, 8760\}$)
$\mathcal{T}$	Set of all time steps ($\mathcal{T} = \{t \in \mathcal{H} \mid h = 1 + k \cdot \text{ts},\ k \in \mathbb{N}_0\}$)
$\mathcal{S}$	Set of scenarios used in the stochastic models
$\mathcal{S}'$	Set of scenarios used for simulations
$\mathcal{R}$	Set of regions
$\mathcal{P}'$	Set of power generation plants ($\mathcal{P}' = \{\mathbf{P}, \mathbf{RP}, \mathbf{W}, \mathbf{OW}, \mathbf{H2}, \mathbf{H}, \mathbf{R}, \mathbf{N}, \mathbf{G}\}$)
$\mathcal{P}$	Set of technologies ($\mathcal{P} = \mathcal{P}' \cup \{\mathbf{PSoP}, \mathbf{PSoT}, \mathbf{PScP}, \mathbf{PScT}, \mathbf{B}, \mathbf{I}, \mathbf{E}\}$)
$\mathcal{L}$	Set of valid transmission power lines that connect regions

Indices

$s \in \mathcal{S}$	Index for scenarios
$p \in \mathcal{P}$	Index for technologies
$t \in \mathcal{T}$	Index for hours and time steps
$r, r' \in \mathcal{R}$	Index for regions

Parameters

$\text{cap}_{p,r}^{\max}$	Maximum potential capacity of technology p in region r	MW
ts	Duration of each time period	h
$\text{cf}_{s,r,p,t}$	Capacity factor of plant p in region r under scenario s at time step t	
β	Planned outage rate for nuclear plants	
$\text{rl}_r^{\max}$	Maximum hydro reservoir level in region r	MWh
$\text{PSoL}_r^{\max}$	Maximum reservoir level of open-loop pumped storage hydropower in region r	MWh
$\text{PScL}_r^{\max}$	Maximum reservoir level of closed-loop pumped storage hydropower in region r	MWh
$\text{cap}_{r,r'}^{\text{T},\max}$	Maximum transmission capacity between regions r and r'	MW
$\text{rl}_r^{\min}$	Fraction of minimum hydro reservoir level in region r	
$\text{res\_i}_{r,t}$	Water inflow to reservoir in region r at time step t	MWh
$\text{ror\_i}_{r,t}$	Water inflow to run-of-river reservoir in region r at time step t	MWh
$\text{PS\_i}_{r,t}$	Water inflow to pumped storage reservoir in region r at time step t	MWh

$\text{dist}_{r,r'}$	Distance between regions r and r'	km
$\text{load}_{r,t}$	Electricity demand in region r at time step t	MW
$\eta^{\text{T}}_{r,r'}$	Transmission efficiency of electricity between r and r'	
sr	Maximum fraction of electricity demand that can be shed per each time step	
ef_p	Emission factor of plant p	$\text{t}_{\text{CO}_2}\,\text{MWh}^{-1}$
η_p	Efficiency of technology p	
c^{FL}_p	Fuel cost of technology p	$€\,\text{MWh}^{-1}$
c^{V}_p	Variable cost of technology p	$€\,\text{MWh}^{-1}$
c^{F}_p	Fixed cost of technology p	$€\,\text{MW}^{-1}\,\text{y}^{-1}$
c^{I}_p	Investment cost of technology p	$€\,\text{MWh}^{-1}$
c^{T}	Investment cost for constructing transmission lines between regions	$€\,\text{MWh}^{-1}\,\text{km}^{-1}$
c^{S}	Load shedding cost	$€\,\text{MWh}^{-1}$
crf_p	Capital recovery factor for technology p	
crf^{T}	Capital recovery factor of transmission lines p	
dt	Battery full discharge time	h
c^{cap}	Carbon cap	$\text{t}_{\text{CO}_2}\,\text{MWh}^{-1}$
π_s	Probability of scenario s	
OC_s	Operational cost under scenario s	$€\,\text{y}^{-1}$
TE_s	Annual CO_2 emissions under scenario s	$\text{t}_{\text{CO}_2}\,\text{y}^{-1}$
TS_s	Annual shed load under scenario s	MWh
FC	Annual fixed cost	$€\,\text{y}^{-1}$
IC	Levelized investment on technologies	$€\,\text{y}^{-1}$
SC	Levelized total costs	$€\,\text{y}^{-1}$

Decision Variables

$\text{E}_{s,r,p,t}$	Electricity generated by technology p in region r under scenario s at time step t	MWh
$\text{Cap}_{r,p}$	Capacity of technology p in region r	MW
$\text{Cap}^{\text{T}}_{r,r'}$	Transmission capacity between regions r and r'	MW
$\text{PO}_{s,r,t}$	Planned outage for nuclear plants in region r under scenario s at time step t	MWh
$\text{RL}_{s,r,t}$	Hydro reservoir level in region r for scenario s and time step t	MWh
$\text{T}_{s,r,r',t}$	Electricity transmitted from region r to region r' under scenario s at time step t	MWh
$\text{ES}_{s,r,t}$	Shed load in region r under scenario s at time step t	MWh
$\text{BL}_{s,r,t}$	Charge stored in the battery in region r under scenario s at time step t	MWh
$\text{PSoL}_{s,r,t}$	Reservoir level of open-loop pumped storage hydropower in region r for scenario s and time step t	MWh
$\text{PScL}_{s,r,t}$	Reservoir level of closed-loop pumped storage hydropower in region r for scenario s and time step t	MWh
$\text{H2L}_{s,r,t}$	Hydrogen stored in the hydrogen tank in region r under scenario s at time step t	MWh

D

Stochastic Optimization Model

The mathematical model of the *Stochastic Optimization Model* is detailed below.

Stochastic Optimization Model:

$$\min \mathrm{SC} = \mathrm{IC} + \mathrm{FC} + \sum_{s \in \mathcal{S}} \pi_s \left(\mathrm{OC}_s + \mathrm{c}^{\mathrm{S}} \cdot \mathrm{TS}_s \right) \tag{D.1}$$

Subject to:

$$\mathrm{Cap}_{r,p} \leq \mathrm{cap}_{r,p}^{\max}, \quad \forall r \in \mathcal{R},\ p \in \mathcal{P} \tag{D.2}$$

$$\begin{aligned} \sum_{p \in \mathcal{P}'} \mathrm{E}_{s,r,p,t} - \mathrm{E}_{s,r,\mathbf{B},t} - \mathrm{E}_{s,r,\mathbf{PSoP},t} - \mathrm{E}_{s,r,\mathbf{PScP},t} - \mathrm{E}_{s,r,\mathbf{E},t} + \mathrm{E}_{s,r,\mathbf{I},t} + \mathrm{E}_{s,r,\mathbf{PSoT},t} + \\ + \mathrm{E}_{s,r,\mathbf{PScT},t} + \mathrm{E}_{s,r,\mathbf{H2},t} + \sum_{\substack{r' \in \mathcal{R} \\ (r,r') \in \mathcal{L}}} \left(\eta_{r',r}^{\mathrm{T}} \cdot \mathrm{T}_{s,r',r,t} - \mathrm{T}_{s,r,r',t} \right) \\ \geq \mathrm{ts} \cdot \mathrm{load}_{r,t} - \mathrm{ES}_{s,r,t}, \quad \forall s \in \mathcal{S},\ r \in \mathcal{R},\ t \in \mathcal{T} \end{aligned} \tag{D.3}$$

$$\mathrm{ES}_{s,r,t} \leq \mathrm{sr} \cdot \mathrm{ts} \cdot \mathrm{load}_{r,t}, \quad \forall s \in \mathcal{S},\ r \in \mathcal{R},\ t \in \mathcal{T} \tag{D.4}$$

$$\sum_{t \in \mathcal{T}} \mathrm{PO}_{s,r,t} = \beta \cdot |\mathcal{T}| \cdot \mathrm{ts} \cdot \mathrm{Cap}_{r,\mathbf{N}}, \quad \forall s \in \mathcal{S},\ r \in \mathcal{R} \tag{D.5}$$

$$\begin{aligned} \mathrm{RL}_{s,r,t} \leq \left\{ \mathrm{RL}_{s,r,\mathrm{ts}\cdot|\mathcal{T}|},\ \text{if } h = 1;\ \mathrm{RL}_{s,r,h-\mathrm{ts}},\ \text{otherwise} \right\} + \mathrm{ts} \cdot \mathrm{res\_i}_{r,t} - \frac{\mathrm{E}_{s,r,\mathbf{H},t}}{\eta_{\mathbf{H}}}, \\ \forall s \in \mathcal{S},\ r \in \mathcal{R},\ t \in \mathcal{T} \end{aligned} \tag{D.6}$$

$$\begin{aligned} \mathrm{PSoL}_{s,r,t} \leq \left\{ \mathrm{PSoL}_{s,r,\mathrm{ts}\cdot|\mathcal{T}|},\ \text{if } h = 1;\ \mathrm{PSoL}_{s,r,h-\mathrm{ts}},\ \text{otherwise} \right\} + \mathrm{E}_{s,r,\mathbf{PSoP},t} \cdot \eta_{\mathbf{PSoP}} + \\ - \frac{\mathrm{E}_{s,r,\mathbf{PSoT},t}}{\eta_{\mathbf{PSoT}}} + \mathrm{ts} \cdot \mathrm{PS\_i}_{r,t}, \quad \forall s \in \mathcal{S},\ r \in \mathcal{R},\ t \in \mathcal{T} \end{aligned} \tag{D.7}$$

$$\begin{aligned} \mathrm{PScL}_{s,r,t} \leq \left\{ \mathrm{PScL}_{s,r,\mathrm{ts}\cdot|\mathcal{T}|},\ \text{if } h = 1;\ \mathrm{PScL}_{s,r,h-\mathrm{ts}},\ \text{otherwise} \right\} + \mathrm{E}_{s,r,\mathbf{PScP},t} \cdot \eta_{\mathbf{PScP}} + \\ - \frac{\mathrm{E}_{s,r,\mathbf{PScT},t}}{\eta_{\mathbf{PScT}}}, \quad \forall s \in \mathcal{S},\ r \in \mathcal{R},\ t \in \mathcal{T} \end{aligned} \tag{D.8}$$

$$\begin{aligned} \mathrm{BL}_{s,r,t} \leq \left\{ \mathrm{BL}_{s,r,\mathrm{ts}\cdot|\mathcal{T}|},\ \text{if } h = 1;\ \mathrm{BL}_{s,r,h-\mathrm{ts}},\ \text{otherwise} \right\} + \eta_{\mathbf{I}} \cdot \mathrm{E}_{s,r,\mathbf{B},t} - \frac{\mathrm{E}_{s,r,\mathbf{I},t}}{\eta_{\mathbf{I}}}, \\ \forall s \in \mathcal{S},\ r \in \mathcal{R},\ t \in \mathcal{T} \end{aligned} \tag{D.9}$$

$$\mathrm{H2L}_{s,r,t} \leq \left\{\mathrm{H2L}_{s,r,\mathrm{ts}\cdot|\mathcal{T}|},\ \text{if } h=1;\mathrm{H2L}_{s,r,h-\mathrm{ts}},\ \text{otherwise}\right\} + \eta_{\mathbf{E}} \cdot \mathrm{E}_{s,r,\mathbf{E},t} - \frac{\mathrm{E}_{s,r,\mathbf{H2},t}}{\eta_{\mathbf{H2}}}, \quad \forall s \in \mathcal{S},\ r \in \mathcal{R},\ t \in \mathcal{T} \tag{D.10}$$

$$\mathrm{E}_{s,r,\mathbf{N},t} \leq \mathrm{ts} \cdot \mathrm{Cap}_{r,\mathbf{N}} - \mathrm{PO}_{s,r,t}, \quad \forall s \in \mathcal{S},\ r \in \mathcal{R},\ t \in \mathcal{T} \tag{D.11}$$

$$\mathrm{E}_{s,r,p,t} \leq \mathrm{ts} \cdot \mathrm{cf}_{s,r,p,t} \cdot \mathrm{Cap}_{r,p}, \quad \forall s \in \mathcal{S},\ r \in \mathcal{R},\ p \in \{\mathbf{P},\mathbf{RP},\mathbf{W},\mathbf{OW}\},\ t \in \mathcal{T} \tag{D.12}$$

$$\mathrm{E}_{s,r,p,t} \leq \mathrm{ts} \cdot \mathrm{Cap}_{r,p}, \quad \forall s \in \mathcal{S},\ r \in \mathcal{R},\ p \in \{\mathbf{H2},\mathbf{H},\mathbf{R},\mathbf{G},\mathbf{PSoP},\mathbf{PSoT},\mathbf{PScP},\mathbf{PScT}\},\ t \in \mathcal{T} \tag{D.13}$$

$$\mathrm{E}_{s,r,\mathbf{I},t} + \mathrm{E}_{s,r,\mathbf{B},t} \leq \mathrm{ts} \cdot \mathrm{Cap}_{r,\mathbf{I}}, \quad \forall s \in \mathcal{S},\ r \in \mathcal{R},\ t \in \mathcal{T} \tag{D.14}$$

$$\mathrm{E}_{s,r,\mathbf{E},t} \cdot \eta_{\mathbf{E}} \leq \mathrm{ts} \cdot \mathrm{Cap}_{r,\mathbf{E}}, \quad \forall s \in \mathcal{S},\ r \in \mathcal{R},\ t \in \mathcal{T} \tag{D.15}$$

$$\mathrm{dt} \cdot \mathrm{Cap}_{r,\mathbf{I}} \leq \mathrm{Cap}_{r,\mathbf{B}}, \quad \forall r \in \mathcal{R},\ t \in \mathcal{T} \tag{D.16}$$

$$\mathrm{E}_{s,r,\mathbf{R},t} \leq \mathrm{ts} \cdot \mathrm{ror\_i}_{r,t}, \quad \forall s \in \mathcal{S},\ r \in \mathcal{R},\ t \in \mathcal{T} \tag{D.17}$$

$$\mathrm{T}_{s,r,r',t} + \mathrm{T}_{s,r',r,t} \leq \mathrm{ts} \cdot \mathrm{Cap}^{\mathrm{T}}_{r,r'}, \quad \forall s \in \mathcal{S},\ r,r' \in \mathcal{R},\ r' > r,\ (r,r') \in \mathcal{L},\ t \in \mathcal{T} \tag{D.18}$$

$$\mathrm{Cap}^{\mathrm{T}}_{r,r'} \leq \mathrm{cap}^{\mathrm{T,max}}_{r,r'}, \quad \forall r,r' \in \mathcal{R},\ r' > r,\ (r,r') \in \mathcal{L} \tag{D.19}$$

$$\mathrm{RL}_{s,r,t} \leq \mathrm{rl}^{\max}_{r}, \quad \forall s \in \mathcal{S},\ r \in \mathcal{R},\ t \in \mathcal{T} \tag{D.20}$$

$$\mathrm{PSoL}_{s,r,t} \leq \mathrm{PSoL}^{\max}_{r}, \quad \forall s \in \mathcal{S},\ r \in \mathcal{R},\ t \in \mathcal{T} \tag{D.21}$$

$$\mathrm{PScL}_{s,r,t} \leq \mathrm{PScL}^{\max}_{r}, \quad \forall s \in \mathcal{S},\ r \in \mathcal{R},\ t \in \mathcal{T} \tag{D.22}$$

$$\mathrm{BL}_{s,r,t} \leq \mathrm{Cap}_{r,\mathbf{B}}, \quad \forall s \in \mathcal{S},\ r \in \mathcal{R},\ t \in \mathcal{T} \tag{D.23}$$

$$\mathrm{H2L}_{s,r,t} \leq \mathrm{Cap}_{r,\mathbf{H2S}}, \quad \forall s \in \mathcal{S},\ r \in \mathcal{R},\ t \in \mathcal{T} \tag{D.24}$$

$$\mathrm{RL}_{s,r,t} \geq \mathrm{rl}^{\min}_{r} \cdot \mathrm{rl}^{\max}_{r}, \quad \forall s \in \mathcal{S},\ r \in \mathcal{R},\ t \in \mathcal{T} \tag{D.25}$$

$$\mathrm{PSoL}_{s,r,t} \geq \mathrm{rl}^{\min}_{r} \cdot \mathrm{PSoL}^{\max}_{r}, \quad \forall s \in \mathcal{S},\ r \in \mathcal{R},\ t \in \mathcal{T} \tag{D.26}$$

$$\mathrm{TE}_{s} \leq \mathrm{c}^{\mathrm{cap}} \cdot \sum_{r \in \mathcal{R}} \sum_{t \in \mathcal{T}} \left(\mathrm{ts} \cdot \mathrm{load}_{r,t} - \mathrm{ES}_{s,r,t}\right), \quad \forall s \in \mathcal{S} \tag{D.27}$$

$$\mathrm{TS}_{s} = \sum_{r \in \mathcal{R}} \sum_{t \in \mathcal{T}} \mathrm{ES}_{s,r,t}, \quad \forall s \in \mathcal{S} \tag{D.28}$$

$$\mathrm{TE}_{s} = \sum_{r \in \mathcal{R}} \sum_{p \in \mathcal{P} \setminus \{\mathbf{B}\}} \sum_{t \in \mathcal{T}} \mathrm{ef}_{p} \cdot \frac{\mathrm{E}_{s,r,p,t}}{\eta_{p}}, \quad \forall s \in \mathcal{S} \tag{D.29}$$

$$\mathrm{OC}_{s} = \sum_{r \in \mathcal{R}} \sum_{p \in \mathcal{P} \setminus \{\mathbf{B}\}} \sum_{t \in \mathcal{T}} \left(\frac{\mathrm{c}^{\mathrm{FL}}_{p}}{\eta_{p}} + \mathrm{c}^{\mathrm{V}}_{p}\right) \mathrm{E}_{s,r,p,t}, \quad \forall s \in \mathcal{S} \tag{D.30}$$

$$\mathrm{FC} = \sum_{r \in \mathcal{R}} \sum_{p \in \mathcal{P}} \mathrm{c}^{\mathrm{F}}_{p} \cdot \mathrm{Cap}_{r,p} \tag{D.31}$$

$$\mathrm{IC} = \sum_{r \in \mathcal{R}} \sum_{p \in \mathcal{P}} \mathrm{c}^{\mathrm{I}}_{p} \cdot \mathrm{crf}_{p} \cdot \mathrm{Cap}_{r,p} + \sum_{\substack{r,r' \in \mathcal{R} \\ r' > r}} \mathrm{c}^{\mathrm{T}} \cdot \mathrm{crf}^{\mathrm{T}} \cdot \mathrm{dist}_{r,r'} \cdot \mathrm{Cap}^{\mathrm{T}}_{r,r'} \tag{D.32}$$

$$\mathrm{PO}_{s,r,t}, \mathrm{RL}_{s,r,t}, \mathrm{T}_{s,r,r',t}, \mathrm{ES}_{s,r,t}, \mathrm{BL}_{s,r,t}, \mathrm{PSoL}_{s,r,t}, \mathrm{PScL}_{s,r,t}, \mathrm{H2L}_{s,r,t} \geq 0, \quad \forall s \in \mathcal{S},\ r,r' \in \mathcal{R},\ (r,r') \in \mathcal{L},\ t \in \mathcal{T} \tag{D.33}$$

$$\mathrm{Cap}^{\mathrm{T}}_{r,r'} \geq 0, \quad \forall r,r' \in \mathcal{R},\ r' > r,\ (r,r') \in \mathcal{L} \tag{D.34}$$

$$\mathrm{Cap}_{r,p} \geq 0, \quad \forall r \in \mathcal{R},\ p \in \mathcal{P} \tag{D.35}$$

$$\mathrm{E}_{s,r,p,t} \geq 0, \quad \forall s \in \mathcal{S},\ r \in \mathcal{R},\ p \in \mathcal{P} \setminus \{\mathbf{B}\},\ t \in \mathcal{T} \tag{D.36}$$

The objective function (D.1) minimizes the levelized total cost, which comprises levelized investment costs and the average operational, fixed, and load-shedding costs across different scenarios. Constraint (D.2) limits the capacity of each technology in a region to not exceed the region-specific maximum potential. Constraint (D.3) ensures electricity demand is met at all time steps through a combination of generation, storage, and transmission, accounting for any shed load. Constraint (D.4) restricts the amount of load shedding to a certain fraction of the electricity demand. Constraint (D.5) imposes that planned outages for nuclear power correspond to a certain fraction of the yearly time horizon. Constraint D.6 governs the energy balance of hydropower reservoirs, requiring that the stored energy at the end of each time step equals that of the previous step, plus water inflows (in energy terms), minus the energy generated. Constraints D.7 and D.8 describe the energy balance for open-loop and closed-loop pumped storage hydropower (PSH), respectively, considering energy added through pumping, withdrawn through generation, and natural water inflows (only for open-loop systems). Similarly, constraint (D.9) ensures that the amount of electrical energy stored in batteries at the end of each time step equals that of the previous time step plus the added charge minus the discharged amount. Constraint (D.10) guarantees that the amount of hydrogen (in energy terms) stored in hydrogen tanks at the end of each time step equals that of the previous time step plus the added hydrogen (from the electrolyzer) minus the discharged amount. All storage balance constraints (D.6–D.10) implement a cyclical time structure, linking the last time step to the first time step to ensure temporal consistency. Constraint (D.11) restricts the electricity produced by nuclear plants to be less than or equal to their available capacity. Constraint (D.12) ensures that the wind (onshore and offshore) and solar (utility-scale and rooftop) generation does not exceed their capacity, adjusted by the corresponding capacity factor for each time step. Constraint (D.13)–(D.16) ensures that the electricity generated by hydrogen gas turbines, hydropower plants (reservoir, run-of-river and PSH), gas turbines, the electricity used for battery charging, the electricity discharged from batteries, and the electricity used for the electrolizer, do not exceed their respective capacities. Constraint (D.17) limits run-of-river hydropower generation to inflow availability (in energy terms). Constraint (D.18) states that the electricity transmitted between regions does not exceed the transmission line capacity. Constraint (D.19) limits the transmission capacity between regions to the maximum transmission capacity value. Constraints (D.20)–(D.22) restrict the stored electricity in the hydro reservoir (for reservoir and PSH plants) to its maximum storage capacity in each region. Constraint (D.23) ensures that the electricity stored in the batteries does not exceed storage capacity in each region, and constraint (D.24) guarantees that the hydrogen stored in the hydrogen tanks does not exceed their storage capacity. Constraints (D.25) and (D.26) assure a minimum storage level for both hydro reservoir and PSH plants. Constraint (D.27) limits the total CO_2 emissions to the carbon cap value. Constraints (D.28)–(D.32) respectively compute the annual load shedding, CO_2 emissions, operating and fixed costs, and levelized investment costs. Finally, the non-negativity requirement of the decision variables is stated in constraints (D.33)–(D.36).

E

Simulation Model

For a given solution $\overline{\mathbf{Cap}}$, which represents the capacity mix of various technologies, the *Simulation problem* is solved independently for each year $s \in \mathcal{S}'$, where $\mathcal{S}'$ denotes the set of simulation years. The mathematical formulation of the *Simulation Model* is as follows.

Simulation problem($\overline{\mathbf{Cap}}, s$):

$$\mathrm{SC}_s = \mathrm{IC} + \mathrm{FC} + \min\left\{\mathrm{OC}_s + \mathrm{c}^{\mathrm{S}} \cdot \mathrm{TS}_s + \mathrm{BM} \cdot \mathrm{LoL}_s\right\} \tag{E.1}$$

subject to: (D.4)–(D.15), (D.17)–(D.18), (D.20)–(D.36)

$$\sum_{p \in \mathcal{P}'} \mathrm{E}_{s,r,p,t} - \mathrm{E}_{s,r,\mathbf{B},t} - \mathrm{E}_{s,r,\mathbf{PSoP},t} - \mathrm{E}_{s,r,\mathbf{PScP},t} - \mathrm{E}_{s,r,\mathbf{E},t} + \mathrm{E}_{s,r,\mathbf{I},t} + \mathrm{E}_{s,r,\mathbf{PSoT},t} + \\ + \mathrm{E}_{s,r,\mathbf{PScT},t} + \mathrm{E}_{s,r,\mathbf{H2},t} + \sum_{\substack{r' \in \mathcal{R} \\ (r,r') \in \mathcal{L}}} \left(\eta^{\mathrm{T}}_{r',r} \cdot \mathrm{T}_{s,r',r,t} - \mathrm{T}_{s,r,r',t}\right) \\ \geq \mathrm{ts} \cdot \mathrm{load}_{r,t} - \mathrm{ES}_{s,r,t} - \mathrm{EL}_{s,r,t}, \quad \forall r \in \mathcal{R},\ t \in \mathcal{T} \tag{E.2}$$

$$\mathrm{Cap}_{r,p} = \overline{\mathrm{Cap}}_{r,p}, \quad \forall r \in \mathcal{R},\ p \in \mathcal{P} \tag{E.3}$$

$$\mathrm{LoL}_s = \sum_{r \in \mathcal{R}} \sum_{t \in \mathcal{T}} \mathrm{EL}_{s,r,t} \tag{E.4}$$

$$\mathrm{EL}_{s,r,t} \geq 0, \quad \forall r \in \mathcal{R},\ t \in \mathcal{T} \tag{E.5}$$

The objective function (E.1) minimizes the total system cost, including a penalty associated with the Loss of Load (LoL). It is important to note that the investment and fixed costs (IC and FC) are determined only by the given capacity mix and can therefore be pre-computed. As a result, these components are excluded from the optimization. Constraint (E.2) is analogous to Constraint (D.3) but includes the loss of load variable. Constraint (E.3) ensures that the capacity mix remains fixed throughout the simulation. Constraint (E.4) calculates the annual loss of load for the simulated year, and Constraint (E.5) enforces the non-negativity of the loss of load variable.

F

Description of additional parameters in the case study

The minimum storage level for both the hydro reservoir and open-loop PSH plants was derived from ENTSO-E [51], by analyzing historical stored energy values from 2020 to 2024. The resulting minimum reservoir level ($\mathrm{rl}_r^{\min}$) is expressed as the ratio of the minimum observed stored energy to the hydro reservoir capacity of each country. The maximum transmission capacity between each pair of connected regions r and r' ($\mathrm{cap}_{r,r'}^{\mathrm{T,max}}$) is obtained from Ember's Europe Electricity Interconnection Data Tool [52]. The carbon cap ($\mathrm{c}^{\mathrm{cap}}$) is set to $0.01\,\mathrm{t_{CO_2}\,MWh^{-1}}$, corresponding to 10 g_{CO_2} per kWh of satisfied load.

Other parameters were adopted from the mathematical formulation presented by Forghani et al. [46] and are detailed below. The investment cost, fixed cost, variable cost, fuel cost, efficiency, lifetime, and emission factor of each technology are given in Table G.1, which are mainly derived from the Danish Energy Agency [56]. For the transmission grids, the investment cost, c^{T}, is $0.4\,€\,\mathrm{kW^{-1}\,km^{-1}}$ with a lifetime equal to 40 years [58]. The transmission efficiency between the regions, $\eta_{r,r'}^{\mathrm{T}}$, is calculated by $(1-\alpha^{\mathrm{Loss}})^{\mathrm{dist}_{r,r'}/1000}$ where α^{Loss} is the electricity loss per kilometer and is assumed to be 0.016. A discharge time of four hours is assumed for the batteries, i.e., dt = 4h [59].
The capital recovery factor of each technology is calculated by $\frac{\mathrm{i}}{1-(1+\mathrm{i})^{-\mathrm{T}}}$, where i is the discount rate and is assumed to be 0.05, and T is the life of the technology. It is assumed that the total shed load at each time step should not exceed 5% of the electricity demand, i.e., sr = 0.05 [60]. Additionally, the load shedding cost c^{S}, and penalty cost for loss of load (in the *Simulation Model*) BM are set to $150\,€\,{\mathrm{t_{CO_2}}}^{-1}$, $1000\,€\,\mathrm{MWh^{-1}}$, and $10\,000\,€\,\mathrm{MWh^{-1}}$, respectively. The planned outage rate, β, is also assumed to be 15%. Each region has some requirements to ensure that investment in solar and wind technologies does not exceed certain limits, due to the limited land availability. Additionally, the hydropower and reservoir capacity are assumed to be fixed in each region due to environmental regulations. The limitations on solar and wind capacities, along with the existing capacity of the hydropower technologies and reservoirs in the countries, are given in Tables G.2 and G.3.

G
Tables

Table G.1: Cost parameters, operational characteristics, and environmental impacts of the technologies considered in the case study. Hydropower values are taken from [61], the hydrogen gas turbine parameters from [62], and the remaining cost assumptions are drawn from the Danish Energy Agency [56, 57].

Plant	Investment Cost €$\,kW^{-1}$	Fixed Cost €$\,MW^{-1}\,y^{-1}$	Variable Cost €$\,MWh^{-1}$	Fuel Cost €$\,MWh^{-1}$	Efficiency –	Lifetime y	Emission Factor $t_{CO_2}\,MWh^{-1}$
H	0	22082	0	0	0.9	80	0
R	0	66245	0	0	0.9	80	0
PSoT	0	11041[b]	0	0	0.87	80	0
PSoP	0	11041	0	0	0.87	80	0
PScT	0	11041	0	0	0.87	80	0
PScP	0	11041	0	0	0.87	80	0
G	436	7893	4.79	22	0.43	25	0.202
W	1090	15602	1.85	0	1	30	0
OW	1640	33000	3.25	0	1	30	0
P	290	9900	0	0	1	40	0
RP	410	7500	0	0	1	40	0
B	65[a]	0	0	0	1	15	0
I	200	38000	0	0	0.85	15	0
N	5000	126000	3.5	2.6	0.33	40	0
E	300	12000	0	0	0.7	25	0
H2S	22[a]	425	0	0	0.9	30	0
H2	760	11000	2.4	0	0.6	25	0

[a] The unit for battery storage capacity and hydrogen storage capacity is €$\,kWh^{-1}$.
[b] The fixed cost of PSH is split between turbine and pumping mode (for both open-loop and closed-loop systems).

Table G.2: Hydropower capacity (reservoir, run-of-river and PSH systems) [51] and maximum wind and solar potential [63] in GW for each country.

Country	$cap^{max}_{r,\mathbf{H}}$	$cap^{max}_{r,\mathbf{R}}$	$cap^{max}_{r,\mathbf{PSoT}}$	$cap^{max}_{r,\mathbf{PSoP}}$	$cap^{max}_{r,\mathbf{PScT}}$	$cap^{max}_{r,\mathbf{PScP}}$	$cap^{max}_{r,\mathbf{W}}$	$cap^{max}_{r,\mathbf{OW}}$	$cap^{max}_{r,\mathbf{P}}$	$cap^{max}_{r,\mathbf{RP}}$
NO	27.65	7.47	0.71	0.76	0	0	93.28	13.19	179.43	11.37
SE	15.62	0	0	0	0	0	116.51	41.26	49.56	14.36
FI	3.24	0	0	0	0	0	83.49	20.93	28.79	9.7
DK	0	0	0	0	0	0	18.59	32.92	59.26	11.83
IE	0	0.22	0	0	0.59	0.59	29.41	9.98	113.29	6.61
UK	0	2.22	0	0	2.74	2.68	87.39	80.44	281.48	110.31
NL	0	0.04	0	0	0	0	11.80	31.54	33.80	34.23
BE	0	0.15	0	0	1.31	1.23	9.64	3.11	23.85	28.13
LU	0	0.04	0	0	1.31	1.03	0.47	0	1.03	1.39
DE	0.82	3.93	2.14	1.86	7.01	7.17	130.44	13.30	375.54	132.91
PL	0.43	0.37	0.22	0.17	1.33	1.49	127.83	8.37	431.76	43.23
LV	0	1.59	0	0	0	0	26.00	9.26	62.23	2.52
EE	0	0	0	0	0	0	17.90	13.03	31.29	1.36
LT	0	0.13	0	0	0.94	0.90	27.36	1.58	98.37	2.34
CZ	0.52	0.43	0.65	0.60	0.69	0.66	30.88	0	93.19	22.48
AT	2.79	6.38	5.61	5.53	0.45	0.45	33.24	0	64.16	11.66
SK	0.02	1.63	0.28	0.18	0.76	0.69	16.43	0	44.85	10.5
HU	0	0.06	0	0	0	0	34.29	0	140.70	14.54
FR	10.03	13.61	1.85	1.85	1.95	1.95	223.77	23.62	773.16	106.64
CH	8.53	4.22	2.46	1.89	1.90	1.90	16.29	0.02	41.62	20.14
IT	8.80	7.05	3.62	2.14	4.17	4.17	102.72	23.54	265.80	128.85
SI	0.02	1.18	0	0	0.18	0.19	6.05	0.07	9.15	3.93
HR	1.95	0.38	0.28	0.25	0	0	17.38	7.17	50.93	5.61
RO	2.56	3.37	0.81	0.09	0	0	88.15	4.63	315.14	26.2
BG	1.28	0.54	0.54	0.15	0.86	0.78	37.28	3.04	133.47	10.05
GR	2.74	0.38	0.70	0.74	0.68	0.71	44.98	3.02	91.82	9.06
ES	11.41	3.42	4.22	3.96	5.30	5.20	176.42	7.21	590	64.77
PT	3.77	0.77	3.84	3.59	0	0	34.32	1.45	66.00	17.96

Table G.3: Reservoir storage capacity in TWh and minimum reservoir level (ratio of reservoir capacity) for each country [51].

Country	rl_r^{max}(TWh)	$PSoL_r^{max}$(TWh)	$PScL_r^{max}$(TWh)	rl_r^{min}(-)
NO	71.875	15.453	0	0.217
SE	31.931	0	0	0.165
FI	5.530	0	0	0.284
DK	0	0	0	0
IE	0	0	0.004	0
UK	0	0	0.026	0.165
NL	0	0	0	0
BE	0	0	0.012	0
LU	0	0	0.005	0
DE	0.237	0.438	0.276	0.165
PL	0.001	0.001	0.006	0.165
LV	0	0	0	0.165
EE	0	0	0	0
LT	0	0	0.011	0.025
CZ	0.002	0.003	0.004	0
AT	0.769	1.747	0.004	0.084
SK	0.017	0.048	0.008	0.165
HU	0	0	0	0
FR	10.057	0.090	0.010	0.089
CH	7.912	1.194	0.056	0.053
IT	5.488	0.299	0.061	0.233
SI	0	0	0.004	0.165
HR	2.046	0.018	0	0.087
RO	2.340	1.033	0	0.115
BG	0.843	0.042	0.228	0.265
GR	4.044	0.005	0.004	0.466
ES	14.775	5.764	0.101	0.259
PT	1.290	2.018	0	0.264

H

Total Installed Capacity Tables

Table H.1: Comparison of total installed capacity for generation technologies (in GW) and storage technologies (in GWh) across the four cases and the benchmark case, under the 2025 Reference Grid scenario.

Total Installed Capacity - 2025 Grid					
Technology	**Benchmark**	**Case 1**	**Case 2**	**Case 3**	**Case 4**
Generation (GW)					
Gas	112.3	99.0	95.4	96.0	95.3
Wind	517.4	506.2	516.6	516.3	517.4
PV	617.5	540.6	566.0	596.1	613.0
Nuclear	32.6	58.4	54.1	47.9	44.4
Hydrogen GT	8.8	5.2	5.8	5.8	5.9
Storage (GWh)					
Hydrogen Storage	294.6	185.3	189.9	177.9	169.6
Battery	398.9	275.4	312.9	402.9	447.7

Table H.2: Comparison of total installed capacity for generation technologies (in GW) and storage technologies (in GWh) across the four cases and the benchmark case, under the 2040 Reference Grid scenario.

Total Installed Capacity - 2040 Grid					
Technology	**Benchmark**	**Case 1**	**Case 2**	**Case 3**	**Case 4**
Generation (GW)					
Gas	108.5	100.3	99.5	97.6	99.7
Wind	539.2	548.8	554.5	559.0	557.7
PV	624.3	527.2	558.6	581.3	602.1
Nuclear	13.5	38.3	33.7	28.4	23.8
Hydrogen GT	7.1	1.4	2.1	3.2	4.5
Storage (GWh)					
Hydrogen Storage	174.8	32.3	48.2	73.7	104.0
Battery	438.3	300.6	372.3	435.1	454.0

Table H.3: Comparison of total installed capacity for generation technologies (in GW), storage technologies (in GWh), and transmission grid (in GW) across the four cases and the benchmark case, under the Unconstrained Grid scenario.

Total Installed Capacity - Unconstrained Grid					
Technology	**Benchmark**	**Case 1**	**Case 2**	**Case 3**	**Case 4**
Generation (GW)					
Gas	103.1	122.7	120.0	120.2	117.3
Wind	572.1	624.0	598.5	624.6	605.2
PV	452.8	395.8	506.6	475.4	491.0
Nuclear	0	0	0	0	0
Hydrogen GT	0	0	0	0	0
Storage (GWh)					
Hydrogen Storage	0	0	0	0	0
Battery	120.6	100.2	263.3	226.6	279.0
Transmission (GW)					
Transmission	446.2	484.2	439.3	421.9	420.3